2D NMR Characterization of Cellobiose Sulfate Hydrolyzed from Cellulose Nanocrystals

by

Daihui Zhang

A thesis submitted to the Graduate Faculty of
Auburn University
in partial fulfillment of the
requirements for the Degree of
Master of Science

Auburn, Alabama
August 2, 2014

Keywords: Cellulose Nanocrystals; Characterization; Cellulase; Enzymatic Hydrolysis; Cellobiose Sulfate; NMR;

Approved by

Maobing Tu, Chair, Associate Professor of Forestry and Wildlife Sciences
Sushil Adhikari, Associate Professor of Biosystems Engineering
Brian Via, Associate Professor of Forestry and Wildlife Sciences
Xinyu Zhang, Associate Professor of Polymer and Fiber Engineering

Abstract

There has been growing interest in the study of Cellulose nanocrystals (CNC) and the development of CNC-based new materials due to its renewable nature, unique aspect ratio and high elastic moduli. Characterization of CNC physiochemical properties, especially its surface chemistry, is essential for the CNC-based materials development. Two types of CNC have been produced and characterized in this study, they are sulfuric acid hydrolyzed CNC (CNC-S) and hydrochloric acid hydrolyzed CNC (CNC-H). The approach of enzymatic hydrolysis was used to characterize the physiochemical properties difference between CNC-S and CNC-H. We determined the Langmuir adsorption isotherm of cellulase on CNC-S, CNC-H and Avicel, and observed higher adsorption capacity (Γ_{max}=240 mg/g) and higher affinity (R= 0.159 L/g) of enzyme on CNC-S than those (Γ_{max}=50.17 mg/g, R= 0.124 L/g) on CNC-H. Correspondingly, the hydrolysis yield was higher (55 %) in CNC-H than that (20 %) in CNC-S. Interestingly, we also observed a small peak presented in the HPLC analysis of CNC-S hydrolysis samples. The peak compound was analyzed and confirmed as cellobiose sulfate by LC-MS and NMR.

The structural elucidation of cellobiose sulfate was analyzed by 2D NMR (COSY, HSQC, TOSCY and HMBC). The NMR analysis indicated the sulfation occurred on the C6 (primary alcohol) of non-reducing end. In addition, we used XRD to determine the CNC crystallinity and observed no considerable difference between CNC-S and CNC-H. FT-IR has been used to characterize the functional groups on CNC-H and CNC-S. Zeta potential has been compared

between CNC-S and CNC-H, which has a potential effect on electrostatic interaction between enzyme and CNC. The significance of this work provides a better understand of sulfate groups on CNC and their potential effects on enzymatic hydrolysis of cellulose and surface modification of CNC.

Acknowledgments

Firstly, I would like to express my appreciation to my supervisor Dr. Maobing Tu for his guidance of my research work in the past two years. Also, thanks my committee members, Dr. Xinyu Zhang, Dr. Brian Via and Dr. Sushil Adhikari, for their valuable advices on my thesis. I also wish to extend my thanks to all the members in our research groups. Finally, appreciate the encouragement and support from my friends and parents.

Table of Contents

List of Tables

List of Figures

List of Abbreviations

CNC-S Nanocrystalline Cellulose Hydrolyzed by Sulfuric Acid

CNC-H Nanocrystalline Cellulose Hydrolyzed by Hydrochloric Acid

NMR Nuclear Magnetic Resonance

SEM Scanning Electron Microscope

FT-IR Fourier Transform Infrared Spectroscopy

SDS-PAGE Sodium Dodecyl Sulfate Polyacrylamide Gel Electrophoresis

LC-MS Liquid Chromatography–Mass Spectrometry

DEPT-135 Distortionless Enhancement by Polarization Transfer-135

DQF-COSY 2H Double Quantum Filtered-Correlation Spectroscopy

HSQC Heteronuclear Single Quantum Coherence Spectroscopy

HMBC Heteronuclear Multiple Bond Correlation

TOSCY Total Correlation Spectroscopy

NOESY Nuclear Overhauser Enhancement Spectroscopy

ROESY Rotating-frame Overhauser Spectroscop

Chapter 1 Introduction

Cellulose nanocrystals (CNC) are typically prepared from cellulose fibers by acid hydrolysis (HCl and H_2SO_4). The resulting CNCs are generally in the nanoscale with a length of 100-300 nm and diameter of 3-5 nm. The aspect ratio of CNCs is ~20-100, and the elastic moduli are in the range of 100-170 GPa. Due to its small size, renewable nature, high elastic moduli, growing interests have been focused on the development of CNC-based new engineering materials. Characterization of CNC physiochemical properties, especially its surface chemistry, is essential for the CNC-based materials development. In this thesis, I used Langmuir adsorption and cellulase enzymatic hydrolysis to characterize the physiochemical properties of CNCs hydrolyzed by HCl and H_2SO_4. Subsequently, I isolated a special compound from enzymatic hydrolysis CNC-H_2SO_4, which was identified as cellobiose sulfate by Mass Spectrometry and NMR. 1D NMR (^{1}H and ^{13}C-NMR) and 2D NMR (Correlation spectroscopy (COSY), Heteronuclear single-quantum correlation spectroscopy (HSQC), Total correlation spectroscopy (TOSCY), Heteronuclear multiple-bond correlation spectroscopy (HMBC)) were used to elucidate the structure of cellobiose sulfate. The results from this study advanced the surface chemistry knowledge of CNCs and provided some insights on the surface modification of CNCs in the future.

Chapter 2 Literature Review

2.1 Cellulose Chemistry

2.1.1 Structure and Morphology of Cellulose

Cellulose is one of the most abundant polymers linked by β-1, 4 glucosidic bonds (Habibi 2014). Its basic unit is cellobiose. Inter and intra hydrogen bonds between hydroxyl groups assemble individual cellulose chain together to form elementary fibers. These elementary fibers could be packed into microfibers, and cellulose fibers are finally formed by grouping those microfibers. Due to strong hydrogen bonding interactions, cellulose is insoluble in water and most organic solvents, which leads to the difficulties in structural elucidation (O'Dell 2009). Up to now, several descriptions of the cellulose structure have been presented (Astbury and Davies 1944; Larsson, Hult et al. 1999). One is widely accepted that cellulose consists of crystalline and amorphous regions, and the crystalline parts are much more resistant to the acid degradation and enzymatic hydrolysis (Ahola, Turon et al. 2008) (Figure 2.1). The crystalline structure of cellulose has been classified into four allomorphs, cellulose I, II, III and IV (Moon, Martini et al. 2011). Cellulose I is the most abundant form in nature, and solid-state ^{13}C NMR has verified that cellulose I is a mixture of cellulose Iα and cellulose Iβ (Atalla and Vanderhart 1984), and ratio of Iα and Iβ varies with the source. Cellulose II can be prepared by either mercerization or regeneration (Park, Baker et al. 2010). Cellulose III can be obtained by the liquid ammonia treatment of cellulose I and cellulose II, respectively (Lewin and Roldan 1971).

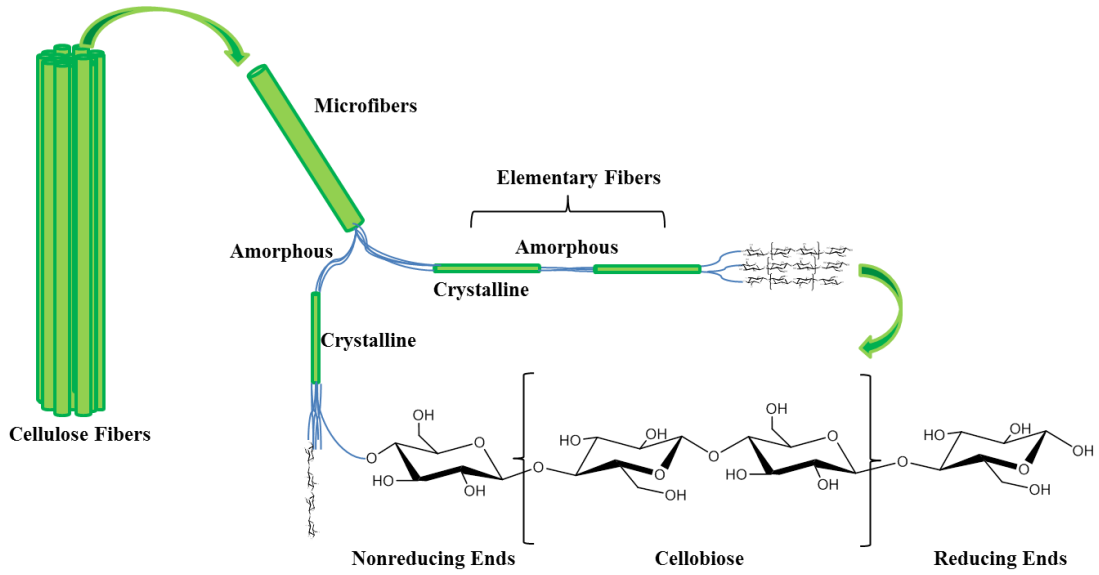

Figure 2.1 Schematic of the Structure of Cellulose Fibers

2.1.2 Application of Cellulose and its Derivatives

Cellulose structure is responsible for cellulose properties such as hydrophilicity, biodegradability and other unique functionality (Bisaria and Ghose 1981; Grundke, Bogumil et al. 1996). Cellulose and its derivatives have been applied in food science as viscosity modifier (Okiyama, Motoki et al. 1993), paper production and biomaterials industries (Kalia, Kaith et al. 2009). Li et al. have prepared cellulose-based biofilm with good mechanical properties, increased hydrophobicity and gas barrier properties (Li, Wu et al. 2014). It was also reported that cellulose-based modifier have been successfully used to increase the viscosity of cement-based materials, and therefore improving the convenience of transport of cement (Saric-Coric, Khayat et al. 2003).

2.2 Cellulose Nanocrystals

2.2.1 Preparation, Structure and Properties

Cellulose nanocrystals (CNC) are produced from cellulose fibers by selectively hydrolyzing amorphous regions (Habibi, Lucia et al. 2010). The strong acid hydrolysis follows strictly controlled conditions. Acid types, reaction temperature and acid concentration appear to affect

the properties of CNC significantly (Dong, Revol et al. 1998). After hydrolysis, the reaction is terminated by dilution with DI water and subsequently with continuous centrifugation. The remaining free acid in CNC is completely removed by dialysis against DI water. Additional steps such as filtration and ultrasonic treatment have been suggested to obtain homogeneously dispersed CNC suspension. Sulfuric acid has been extensively used for CNC preparation due to stable suspension after introducing sulfate groups on the cellulose (Dong, Revol et al. 1998) (Figure 2.2).

The length and width of CNC highly depend on the source of cellulosic material and hydrolysis condition (Moon, Martini et al. 2011). Transmission electron microscope (TEM), scanning electron microscope (SEM) and atomic force microscopy (AFM) have already been used to characterize the morphology of CNC (Elazzouzi-Hafraoui, Nishiyama et al. 2007; Morán, Alvarez et al. 2008). The dimensions of CNC isolated from different sources have been summarized in Table 2.1.Another important property for CNC is its crystallinity index (CI), which dramatically increased after acid hydrolysis of amorphous parts of cellulose (Jiang, Esker et al. 2010). Although it has been found that CI varied significantly on the measurement methods, X-ray diffraction is still a useful tool providing a relatively more accurate measurement (Park, Baker et al. 2010). Since CNC produced by sulfuric acid hydrolysis is electrostatically stabilized in aqueous suspension due to repulsive force of sulfate groups, the amount of surface charge also need to be determined. Titration methods have been used to determine the surface charge of CNC (Klemm, Kramer et al. 2011). The zeta potential can also be measured and correlated to surface charge on CNC (Jiang and Hsieh 2013).

The thermal, mechanical, rheological and optical properties of CNC have also been characterized. Thermogravimetirc analysis (TGA) has been used to measure the thermal chemical degradation

of CNC. The degradation takes place between 200-300 ℃ depending on heating rate and surface modification (Moon, Martini et al. 2011). CNC forms liquid crystals at low concentration, which properties between conventional liquid and solid crystal. There are several different types of liquid crystal phases, which can be indicated by their optical properties (Kresge, Leonowicz et al. 1992). Various factors such as shape, size and charge could influence the liquid crystal properties (Drzaic 1995). CNC suspension has potential to show separation into a chiral nematic and isotropic phase under certain concentration (Dong, Revol et al. 1998). The mechanical properties of CNC reinforced composites have been studied, and it generally shows a good mechanical property with higher modulus and higher thermal stability (Lee, Mohan et al. 2009).

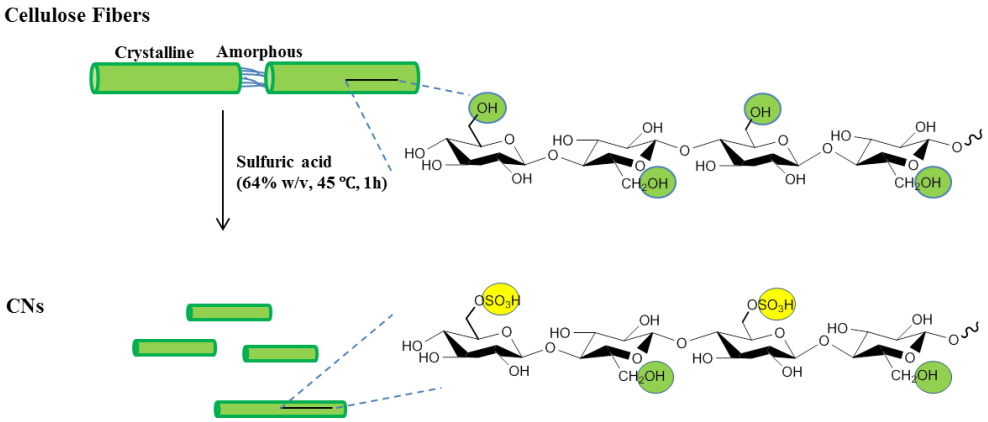

Figure 2.2 Schematic of the Acid Hydrolysis of Cellulose Fibers and Chemical Modification of Cellulose Chain during the Process of Hydrolysis

Table 2.1 Dimensions of CNC Isolated from Different Sources

Cellulose Source	Length (nm)	Width(nm)	Reference
Bacterial	100-1000	10-50	(Araki and Kuga 2001)
Tunicate	1000-3000	10-30	(Kimura, Kimura et al. 2005)
Cotton	100-300	5-10	(Araki, Wada et al. 2000)
Wood	100-200	3-5	(Beck-Candanedo, Roman et al. 2005)

2.2.2 Study of Cellulose Nanocrystals and its Derivatives

Considerable attention has been focused on the development of CNC-based materials due to its good mechanical properties, high aspect ratio and biodegradability (Auad, Contos et al. 2008; Wu, Saito et al. 2012). It has been studied as fillers in polymer composites (Meng and Hu 2009), barrier membrane in food packaging (Liimatainen, Ezekiel et al. 2013), antimicrobial films (Dehnad, Mirzaei et al. 2014) and electronic engineering materials (Zhou, Fuentes-Hernandez et al. 2013). Surface chemical modification of CNC is typically required for its better dispersion of modified-CNC in composites (Li, Wu et al. 2014). Current researches on CNC have been summarized in Figure 2.3.

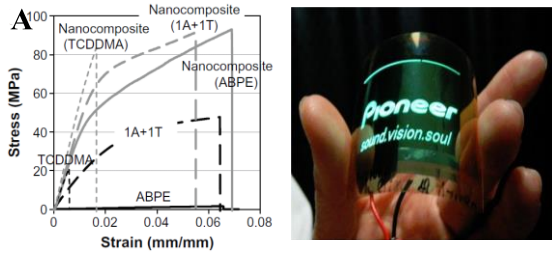

Optically Transparent Wood-cellulose Nanocomposite as a Base Substrate for Flexible Organic Light-emitting Diode Displays

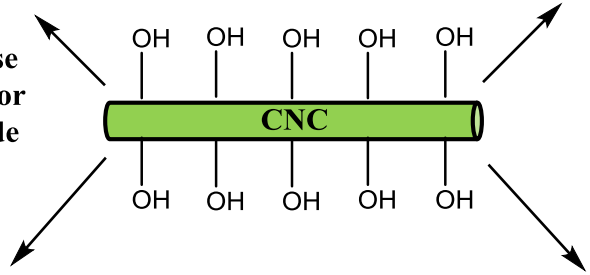

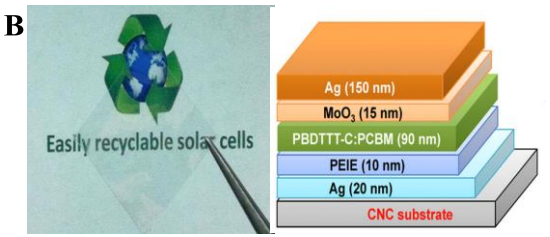

Recyclable Organic Solar Cells on Cellulose Nanocrystal Substrates

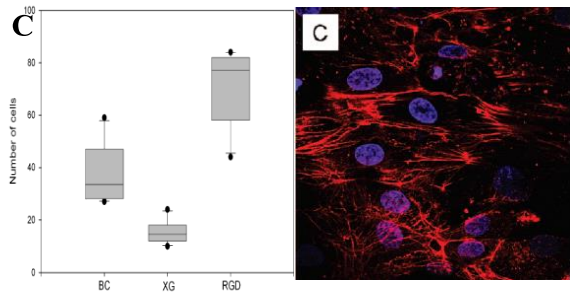

Modification of NCC with a Xyloglucan-RGD Conjugate Enhances Adhension and Proliferation of Endothelial Cells: Implications for Tissue Engineering

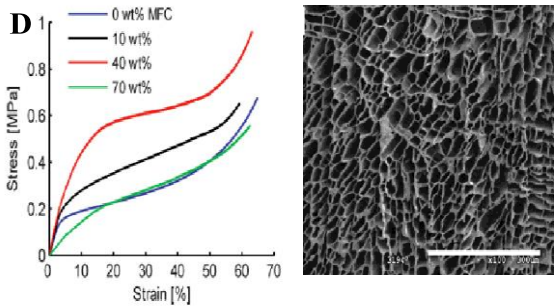

Biomimetic Foams of High Mechanical Performance Based on Nanostructured Cell Walls Reinforced by Native Cellulose Nanofibrils

Figure 2.3 Potential Application of CNC; (A) (Okahisa, Yoshida et al. 2009) (B) (Zhou, Fuentes-Hernandez et al. 2013) (C) (Bodin, Ahrenstedt et al. 2007) (D) (Svagan, Samir et al. 2008)

2.3 Enzymatic Hydrolysis of Lignocelluloses

2.3.1 Properties of Cellulase and Hydrolysis Mechanism

Cellulase, produced by microorganisms (bacteria and fungi), is a group of enzymes that hydrolyze cellulose to glucose. They are composed of endo-glucanases (EG), cellobiohydrolases (CBH) and β-glucosidases (β-G). CBH is composed of two components (CBH I and CBH II), acting on insoluble cellulose and the main products are cellobiose and glucose. Table 2.2 presents the properties of main cellulase components from *Trichoderma reesei* (Nakagame 2010). CBH I is a dominant component accounting for 60% in cellulase, attacking the cellulose chain from reducing ends. Oppositely, CBH II mainly works on the non-reducing ends (Goyal, Ghosh et al. 1991). Igarashi et al. monitored CBH I on algal crystalline cellulose fibers using AFM, and results showed CBH I was unidirectional possessive enzyme which even could halt or slow down when facing obstacles (Igarashi, Uchihashi et al. 2011). Endo-glucanases preferentially act on amorphous regions of cellulose fibers (Kleman-Leyer, SiiKa-Aho et al. 1996) in cooperation with CBH. β-G is capable of hydrolyzing cellobiose to glucose.

Typical action of cellulase is explained as an initial attack by EG, then by the combined action of CBH and EG, and finally hydrolyzing cellobiose to glucose by β-G (Fox, Levine et al. 2011). Figure 2.4 showed the synergy of individual components in cellulase to hydrolyze cellulose (Medie, Davies et al. 2012).

Table 2.2 The Properties of Cellulase from *T. reesei.*

Enzyme	Molecular Weight (kDa)	Isoelectric Point
CBHI	59-68	3.5-4.2
CBHII	50-58	5.1-6.3
EGI	50-55	3.9-6.0
EGII	48	4.2-5.5
EGIII	25	6.8-7.5
EGV	23	
β-GI	75	7.4-7.8

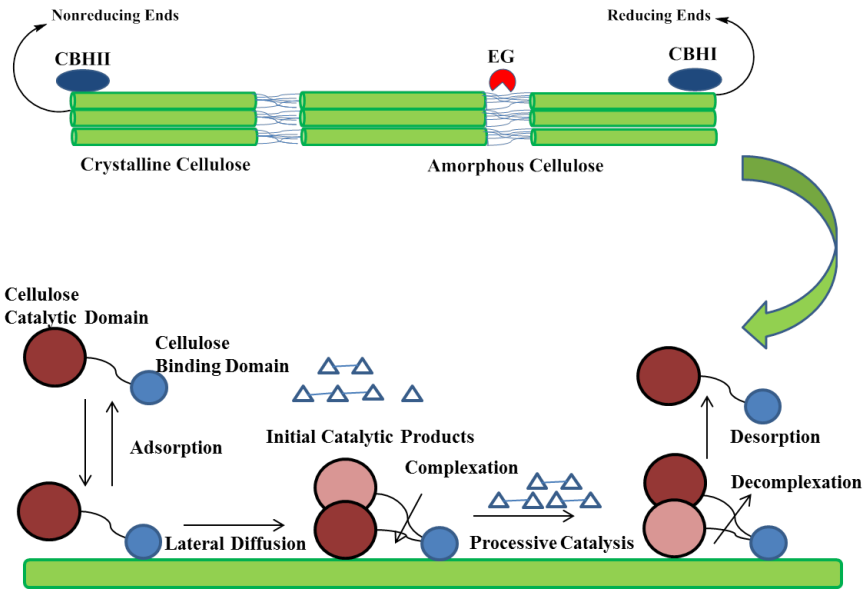

Figure 2.4 General Conceptual Picture of Enzymatic Hydrolysis of Insoluble Cellulose (Fox, Levine et al. 2011)

2.3.2 Characteristics of Cellulose Affecting Enzymatic Hydrolysis

Enzymatic hydrolysis is affected not only by the structural features of cellulose, but also the cooperation of enzyme. Although detailed investigations of several aspects of substrates properties, such as crystallinity, assessable surface area, degree of polymerization and porosity, have been investigated (Yang, Dai et al. 2011), it's still hard to figure out which factor is the dominant one due to the difficulties in controlling other factors. For example, cellulose crystallinity has been reported as a key predictor for the enzymatic hydrolysis rate, and a continuous decrease in enzymatic hydrolysis rate as crystallinity increases was observed (Hall,

Bansal et al. 2010). However, after phosphoric acid treatment on Avicel to prepare controlled degrees of crystallinity, other properties including porosity and surface area which contributed to enzymatic hydrolysis rate were also changed. Many pretreatment methods have been proposed to fractionate lignocellulosic biomass efficiently. Several researchers have reported lignocellulosic fibers could carry negative charges due to the existence of acidic groups after pretreatment (Hsu, Ladisch et al. 1980; Bhardwaj, Kumar et al. 2004) (Figure 2.5). However, the effect of negative surface charge on enzymatic hydrolysis is still unknown. In this thesis, we mainly focus on surface charge to see its role in enzymatic hydrolysis.

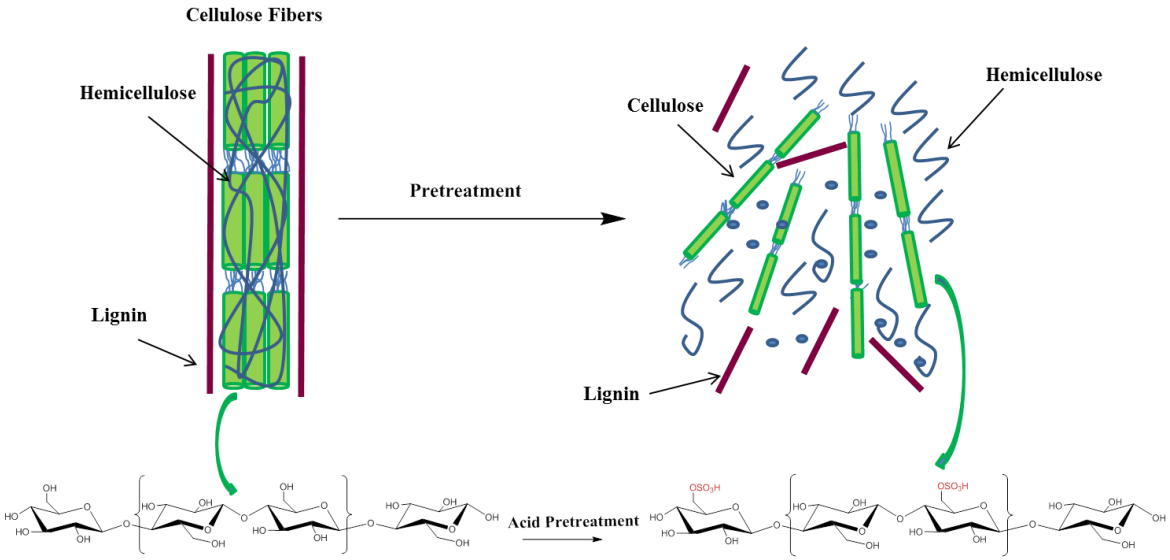

Figure 2.5 Schematic of Goals of Pretreatment on Lignocellulosic Materials (Mosier, Wyman et al. 2005) and Potential Effect of Acid Pretreatment on Cellulose Structure (Jiang, Kittle et al. 2013)

2.3.3 Cellulase Interactions with Cellulose

Enzyme binding onto solid surface is important in biological process. Enzyme-surface interactions can be non-covalent, and the driving forces mostly involve hydrophobic and electrostatic interactions (Claesson, Blomberg et al. 1995). Hydrophobic interactions usually govern enzyme adsorption on solid surface due to entropy gain, even though there was a repulsively electrostatic interaction. Shikiya reported that 30% of BSA (negatively charged) was

adsorbed on negatively charged polystyrene particles at pH=7. This indicated a hydrophobic interaction could overcome the unfavorable free-energy barrier (Shikiya, Tomita et al. 2013). However, Haupt et al. thought that the secondary structure of BSA which desorbed from the particles was not disturbed (Haupt, Neumann et al. 2005), and the main driving force should be the interaction between negative polyelectrolytes chains and positive patches on the surface of protein. Fungal cellulase typically consisted of a catalytic domain which attached to a cellulose binding domain (CBD) through a flexible peptide linker (Gilkes, Henrissat et al. 1991). The role of CBD is generally considered to enhance the hydrolysis of cellulose by increasing enzyme adsorption through van der Waals and aromatic ring polarization interactions (Reinikainen, Teleman et al. 1995). Igarashi et al. suggested that CBD of CBHI could increase the concentration of enzyme molecules on the substrates, but have no contribution to possessive action of the enzyme (Igarashi, Koivula et al. 2009). Up to now, few studies were focused on the interaction between cellulase and charged cellulose. We think it is important to evaluate it, as well as the effect of surface charge on enzymatic hydrolysis. Several aspects which need to be solved have been indicated in Figure 2.6.

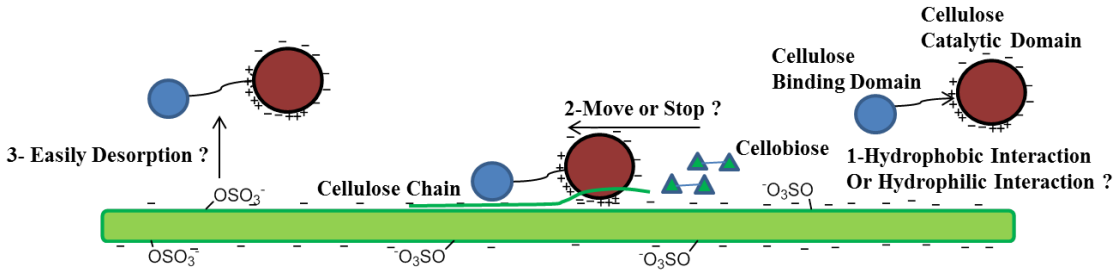

Figure 2.6 Potential Explanation of Enzymatic Hydrolysis of Charged Cellulose Substrates

2.4 Biomass Characterization by NMR Spectroscopy

2.4.1 Introduction to NMR Spectroscopy

NMR has been considered as a powerfully analytical tool for the study of structural elucidation (Agrawal 1992), hydrogen bonding interaction (Liu, Hu et al. 2000), molecular dynamics (Graf, Nguyen et al. 2007), drug screening (Hajduk, Meadows et al. 1999) and protein folding (Balbach, Forge et al. 1995). As the developments in both instrumentation and methodology, it has become one of the most useful technologies for biomacromolecules structural determination with the assistance of X-ray crystallography (Yamakawa, Jiang et al. 2009; Jenkins, Sampath et al. 2013). Partial 1D and 2D NMR were shown in Figure 2.7. DEPT-135 was emphasized here since we can use it to specially differentiate CH_2 and CH_3/CH groups, due to negative signals for CH_2 while positive signals for CH and CH_3. Additionally, 2D NMR provides much more information than 1D NMR, and it is especially useful to determine the molecular structure when too many overlapped peaks in 1D NMR spectra. H-H correlation and C-H correlation of 2D NMR have been shown in Figure 2.7 as well.

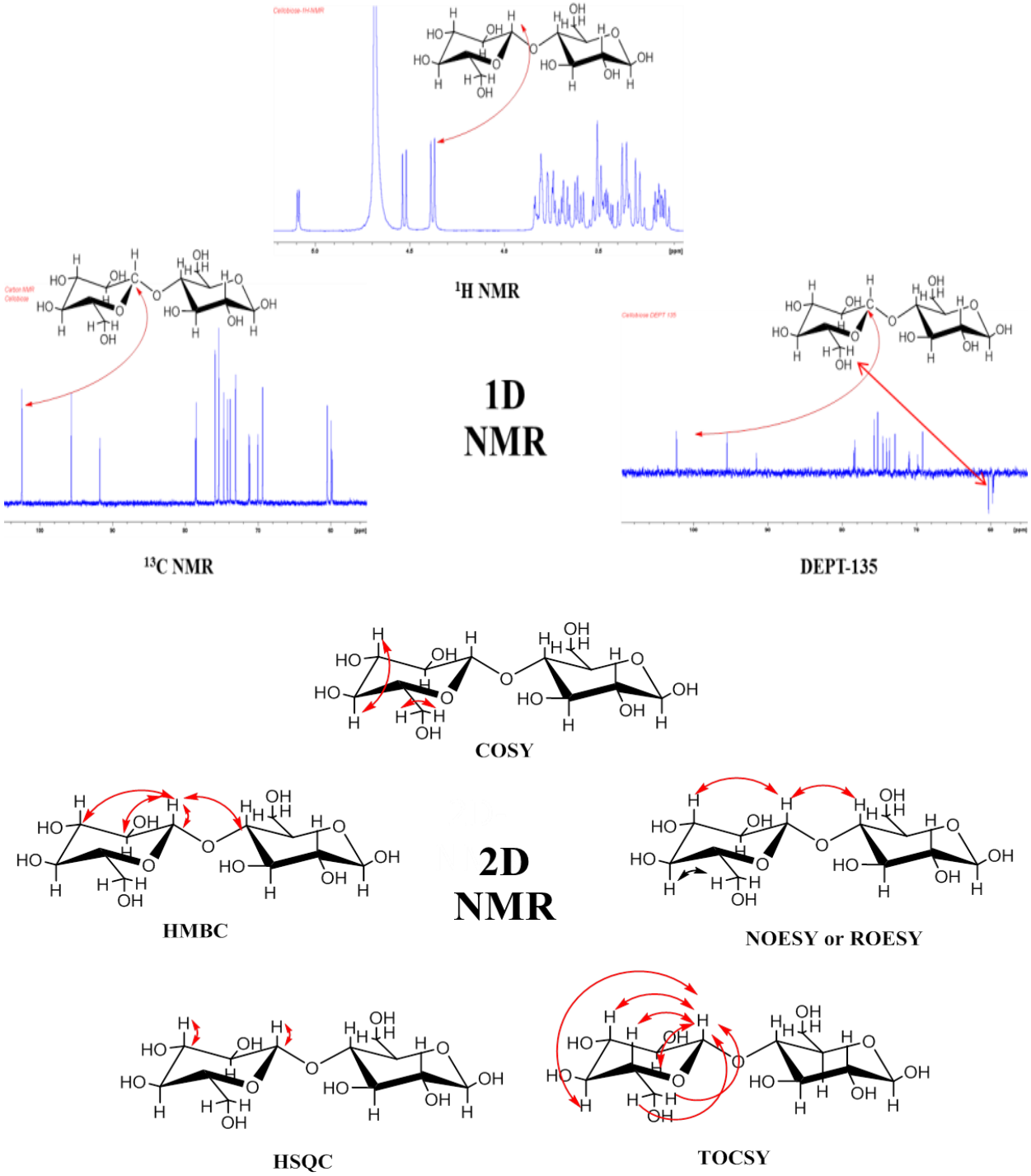

Figure 2.7 Introductions to 1D NMR and 2D NMR

2.4.2 Application of NMR Spectroscopy

Several detailed NMR applications in different fields were shown in Figure 2.8. Shawn et al. have successfully utilized 2D NMR to analyze lignin extracted from biological plant tissue, and

the approach they established can be used to obtain whole cell wall information and improve our understanding of cell wall structure (Mansfield, Kim et al. 2012). Cellulose acetate (CA) is one of the most important polymers applied in the industries, and which structure with a degree of substitution of 2.33 recently was elucidated by a combination of 2D NMR (Kono 2013). Additionally, structure of polysaccharide with biological activity was also successfully identified, and this work is useful to evaluate the relationship between structure and activity (Zhang, Wang et al. 2013).

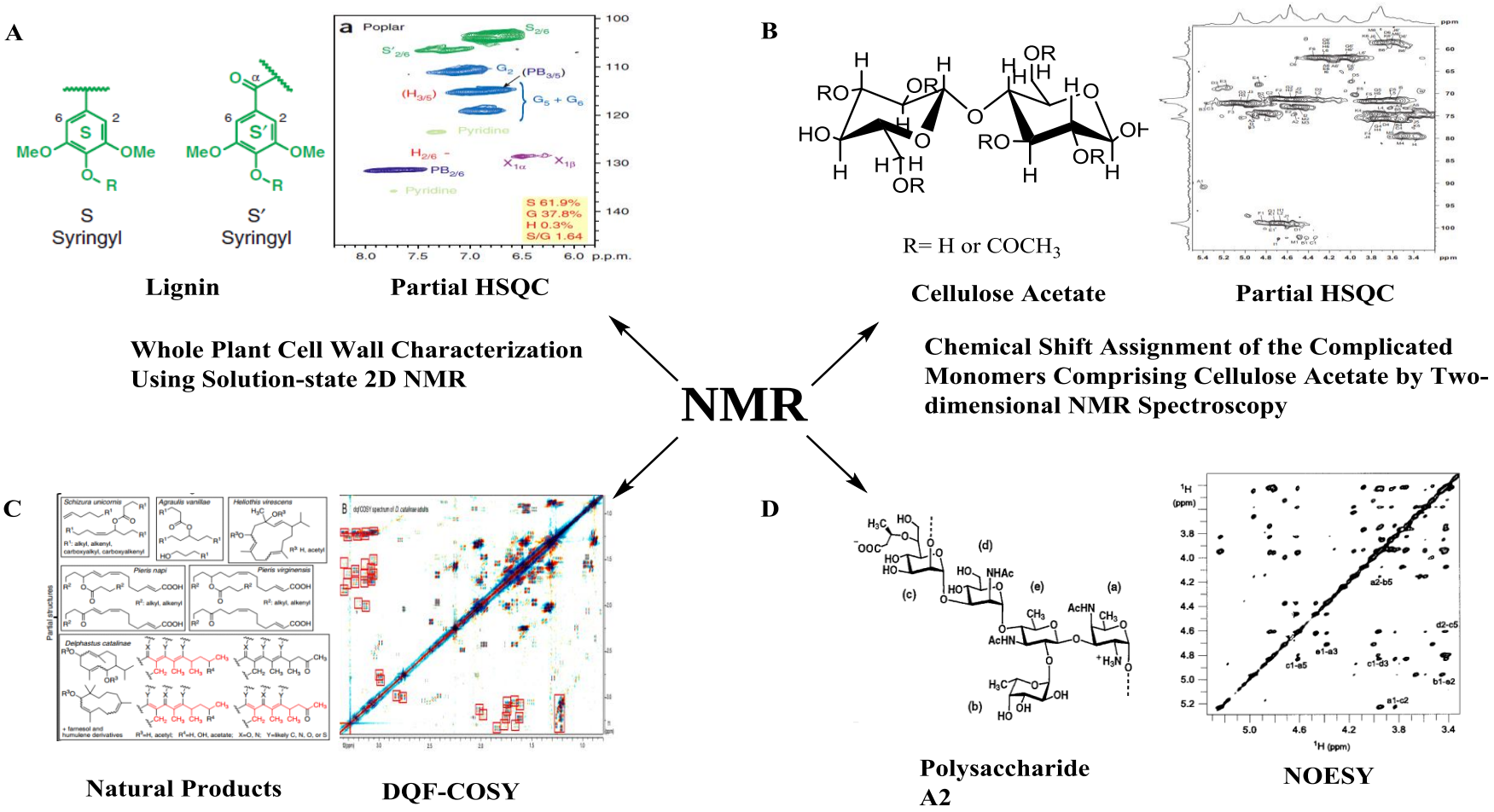

Figure 2.8 Application of 2D NMR (A) (Mansfield, Kim et al. 2012) (B) (Kono 2013) (C) (Deyrup, Eckman et al. 2011) (D) (Wang, Kalka-Moll et al. 2000)

Chapter 3 Materials and Methods

3.1 Materials

Commercial cellulase, Novozym 22C, obtained from Novozymes (Franklinton, NC) was used in the enzymatic hydrolysis of substrates. Its activity was 100 FPU/mL, which was determined using Whatman # 1 filter paper as the substrate. β-glucosidase activity was 343 IU/mL using *p*-nitrophenyl-β-D-glucoside (PNPG) as a substrate. Cellulase C2730 from *Trichoderma reesei* ATCC 26921, which used for enzyme adsorption isotherms determination, was purchased from Sigma-Aldrich (St. Louis, MO). Sulfuric acid and hydrochloric acid were analytical grade and purchased from VWR. Avicel ® PH 101 and commercial cellobiose were purchased from Sigma-Aldrich (St. Louis, MO). Deuterium oxide (99.95 +%) were purchased from Alfa Aesar (Ward Hill, MA).

3.2 Preparation and Characterization of Cellulose Nanocrystals

3.2.1 Preparation of CNC

H_2SO_4-hydrolyzed CNC (CNC-S) was prepared based on the previous method with minor modification (Jiang, Esker et al. 2010). Sulfuric acid (500 mL, 64% w/v) was preheated to 45 °C, and then 40 g Avicel was added into the solution with the solid-solution ratio 1: 12.5. The reaction was carried out under mechanical stirring at 45 °C for 60 min until obtaining stable suspension. 6 L of DI water was used to dilute the highly concentrated sulfuric acid to terminate the reaction. The remaining acid was removed by repeated centrifugation from CNC-S suspension until supernatant started to become turbid. Then it was transferred to dialysis bag to be dialyzed against DI water for two or three days until the pH of DI water stayed constant. The final suspension was sonificated for at least 5 min for disruption of potential CNC aggregates.

HCl-hydrolyzed CNC (CNC-H) was prepared according to the methods of Araki with minor modification (Araki, Wada et al. 1998). Avicel (10 g) was added into preheated hydrochloric acid (300 mL, 4 M, 80 °C), and then the reaction was conducted under mechanical stirring at 80 °C for 240 min. We terminated the reaction by immerse the flask into an ice bath for 10 min. Repeated centrifugation was utilized to get rid of free acid from suspension. Dialysis is an essential step to remove residual acid. After sonification, the samples were collected and freeze-dried.

3.2.2 Acid-Catalyzed Desulfation of CNC-S

The acid-catalyzed desulfation of CNC-S was carried out according to the method of Jiang (Jiang, Esker et al. 2010) with minor modification. Briefly, original CNC-S (100ml, 2.1 wt. %) suspension was acidified to 0.025 M by the addition of HCl (0.5 ml, 5M, BHA) and reacted at 80 °C for 5 h with stirring. After desulfation, the reaction was quenched by immersion in an ice bath and then dialyzed against DI water.

3.2.3 SEM Analysis of CNC

SEM analysis of CNC was performed with a field emission SEM, JEOL 7000F operated at 20.0 KV. For imaging, 0.001wt% suspension was deposited on cleaned holder and then air dried. It was subsequently coated with a very thin gold layer (50 nm) using a PELCO SC-6 Sputter Coater.

3.2.4 FT-IR Analysis of CNC

FT-IR spectra of CNC were obtained from PerkinElmer ATR-FTIR spectrometer. The spectra were collected at room temperature in the transmittance mode from an accumulation of 64 scans at 4 cm^{-1} resolution over the regions of 4000-400 cm^{-1}.

3.2.5 Zeta Potential Determination

Zeta potential (ζ , mv) of 0.1 wt% aqueous CNC was measured at pH=4.8 (citrate buffer) with 10 mM ionic strength using a Zetasizer Nano (Malvern Instruments, Ltd) at 25 °C. Two minutes equilibration is necessary. The ζ value was calculated from the electrophoresis mobility using Henry equation. Three measurements were conducted for each suspension (Jiang and Hsieh 2013).

3.2.6 Dynamic Light Scattering (DLS)

DLS experiments were performed with a Zetasizer Nano (Malvern Instruments, Ltd.). Reported values are mean intensity diameters obtained from Zetasizer Nano software. Measurements were finished in triplicate at 25 °C with 0.01 wt% CNC without added electrolytes. The CNC suspension was sonicated for 10 min prior to measurement in order to disrupt the potential aggregates.

3.2.7 Elemental Analysis of CNC

Samples were lyophilized and further dried under vacuum at room temperature for a while prior to elemental analysis. Sulfur analysis was completed by combusting solid to SO_2, and then it was measured and calculated according to the standard.

3.2.8 Crystallinity Measurement

X-ray diffraction spectroscopy (D8 Discover, Bruker, USA) with Cu Kα radiation generated at 40 kv and 40 mA was employed to investigate the crystallinity index and crystalline dimensions in different plans of samples. 5-60° 2θ was recorded. Peaks were analyzed using Peakfit software (www.systat.com), and Voigt function was used to fit the peaks (Okita, Saito et al. 2010). Crystallinity index was calculated according to the Segal equation: (Segal, Creely et al. 1959)

$$\text{CI} = \frac{I_{200} - I_{am}}{I_{200}} \times 100\%$$

Where I_{200} is the intensity of the peak at 2θ around 22.6°, and I_{am} is the intensity of baseline at 2θ about 18.0°.

Crystalline size of different planes was evaluated by using Scherrer's expression.

$$D_{hkl} = \frac{0.9 \times \lambda}{\beta_{1/2} \times \cos\theta}$$

Where θ is the diffraction angle, λ is the X-ray wavelength (0.15418 nm) and $\beta_{1/2}$ represents the full width at half maximum (FWHM) of the reflection peak.

3.2.9 CNC Reducing Ends Determination

The DNS assay was applied to quantification of insoluble reducing ends (Kongruang, Han et al. 2004). DNS reagent (3 mL) was mixed with 0.4 mL DI water containing 10 mg solid CNC, which was capped with aluminum foil and then incubated in boiling water for 15 min. After heating, tubes were cooled down using ice water. The supernatant was collected after 13,000 rpm centrifugation for 5 min. The absorbance of the resulting cellulose-free supernatant was measured at 600 nm. The micromole of reducing ends per milligrams of cellulose was calculated from cellobiose standard.

3.3 Effect of CNC Characteristics on Cellulase Adsorption and Hydrolysis

3.3.1 Enzymatic Hydrolysis of CNC

Enzymatic hydrolysis was performed in 10 mL of 50 mM sodium citrate buffer (pH=4.8) at 2% substrates mixed with commercial enzyme (Novozym 22C) (Li, Tu et al. 2012). Briefly, enzymatic hydrolysis reaction was incubated at 50 °C with shaking at 150 rpm for 72 h. The

cellulase loading was 5 FPU/g glucan. No extra β-glucosidase was added since Novozym 22C was a mixture of cellulase and β-glucosidase. Certain samples were taken from the hydrolysis solution at 0, 3, 6, 12, 24, 48, 72 h time intervals, respectively. After centrifugation, the supernatant was diluted and the glucose content was quantified by HPLC with Aminex HPX-87P column. The cellulose conversion (%) was calculated from the released glucose content divided initial substrates content. The hydrolysis reaction was performed in duplicated.

3.3.2 Cellulase Adsorption and Desorption

Cellulase adsorption was performed at 4 °C with 150 rpm in 50 mM citrate buffer (pH=4.8) for 2 h (Lai, Tu et al. 2014). Cellulase C2730 from *T. reeesei* ATCC 26921 with protein content 44 mg/mL was employed to determine the adsorption isotherm. A range of enzyme concentration from 0.01 to 2.0 mg/mL was mixed with substrates (2% w/t). After 2 h to reach equilibrium, the sample was centrifuged to collect supernatant. The protein concentration was investigated by Bradford methods using BSA as the protein standard. The adsorbed enzyme was accurately calculated from the difference between the initial enzyme content and the free enzyme content. Following Langmuir adsorption isotherm equation was applied to determine the cellulase adsorption. In this case, the surface concentration of adsorbed enzyme (Γ) was calculated by

$$\Gamma = \frac{\Gamma_{\max} KC}{1 + KC}$$

Where Γ_{max} is the surface concentration of protein at full coverage (mg/g substrate); K is the Langmuir constant (mL/mg); C is the free enzyme in solution (mg/mL). The distribution coefficient (*R*) which can be used to estimate the relative affinity of protein are expressed as

$$R = \Gamma_{\max} \times K$$

Cellulase desorption experiment was performed as following procedure in Figure 2.9.

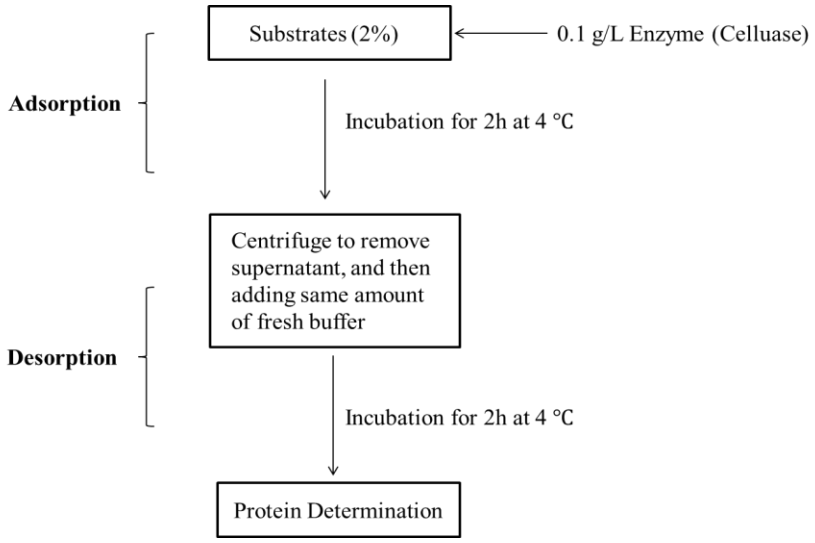

Figure 2.9 Flowchart of Cellulase Desorption Experiment

3.3.3 Effect of pH on Enzyme Adsorption and Enzymatic Hydrolysis

Citrate buffer was used to adjust pH of the solution, ranging from 4.4 to 6.0. Final ionic strength is 50 mM for each solution. Cellulase was added into 5 mL solution containing 0.1 g CNC (2% w/t) at 4 °C for 2 h to reach equilibrium, and the final enzyme concentration was 0.1g /L. The supernatant was collected after centrifugation (13,000 rpm) for 5min. The protein concentration was determined by Branford G-250 method. For enzymatic hydrolysis, we followed the procedure mentioned in 3.3.1, and one more step was adjusting pH of the solution from 4.4 to 6.0 using citrate buffer before enzymatic hydrolysis.

3.3.4 Effect of Ionic Strength on Enzyme Adsorption and Enzymatic Hydrolysis

0mM, 50mM, 100mM and 200mM NaCl was prepared in the 5mL solution containing 0.1 g CNC (2% w/t) and 50 mM citrate buffer. After incubation at 4 °C for 2 h to reach equilibrium, the protein concentration in supernatant was then determined by Branford G-250 method. For

enzymatic hydrolysis, the same procedure was followed as mentioned above after controlling the addition of sodium chloride.

3.3.5 SDS-PAGE

The preparation of SDS-PAGE follows the standard protocol. The concentration of stacking and separating gel was 5% and 12%, respectively. After cellulase adsorption, the supernatant was collected by centrifugation, and then 100 µL was mixed with 20 µL of loading buffer. Hydrophobic regions of enzymes were denatured, and then enzymes were linearized by SDS in the process of heating (Yu, Jameel et al. 2013). Also, the color in reducing buffer can be used to indicate the protein position. After heating for 5 min in boiling water to denature the enzyme, 20 µL of the supernatant was loaded into wells. Protein maker was placed into the first well. The gel was run at 180 V (constant voltage), and the time was set for 52min. Longer time was not recommended since the loading buffer could contaminate the running buffer. After running, the gel was gently peeled off from glass plates, and then stained by imperial blue stain for 30 min under heating. The stained gel was again immersed into DI water, and then microwave was used to heat the water up in order to reduce the background. By exchanging the DI water and heating it up again for several rounds, obvious bands could be observed for analysis.

3.4 Structural Elucidation of Disaccharide by NMR Spectra

Solution state ^{1}H and ^{13}C NMR measurements were obtained on a Bruker 400 MHz spectrometer which equipped with a Quad probe dedicated to ^{31}P, ^{13}C, ^{19}F, and ^{1}H acquisition. Samples (10-15 mg) was dissolved in 600 µL D_2O. The distortionless enhancement by polarization transfer experiment (DEPT-135) was set following the pulse sequence provided by Bruker. 2D double quantum filter correlated spectroscopy (DQF-COSY), heteronuclear single quantum coherence (HSQC) and hetero-nuclear multiple bond connectivity (HMBC) spectra of water soluble

products were also recorded on a Bruker 400 MHz spectrometer. NMR data were processed and analyzed using Topspin 3.0 software (Bruker Biospin AG, Switzerland).

Chapter 4 Results and Discussions

4.1 Preparation and Characterization of Cellulose Nanocrystals

4.1.1 Preparation of CNC

The properties of cellulose nanocrystals (CNC) could be affected by temperature, hydrolysis time and concentration of acid in the preparation process. Dong et al. have investigated the effect of preparation conditions on the particle properties of the CNC suspensions (Dong, Revol et al. 1998). They suggested longer hydrolysis time increased the total sulfur content which corresponded to the surface charges, but reduced the particle length. However, the length showed no changes after reaching a certain time (100 min). As the increase of hydrolysis temperature and hydrolysis time, the yield of CNC decreased from 89.8% w/v (26 °C, 1h) to 43.5% w/v (45 °C, 1h) and to 34.4% w/v (26 °C, 18 h), respectively. It could be explained that more cellulose was hydrolyzed. Additionally, acid-to-pulp ratio has been examined during the preparation of CNC by acid hydrolysis of two different pulps (Beck-Candanedo, Roman et al. 2005) The increase of acid-to-pulp from 8.75 mL/g to 17.5 mL/g slightly shorted the length and diameter of CNC.

In this thesis, we successfully prepared sulfuric acid hydrolyzed CNC (CNC-S) and hydrochloric acid hydrolyzed CNC (CNC-H), respectively, according to the previous methods with modifications (Rusli, Shanmuganathan et al. 2011). The resulting CNC-S could be well dispersed in water for one week due to strong surface repulsive interaction. Conversely, CNC-H initially formed stable colloidal suspension, but precipitated after one week (Figure 2.10). The hydrolysis yield of CNC-S was 25% w/w, and 1.5 times lower than that of CNC-H (89% w/w). Furthermore, we determined the water content of each samples after extended freeze-dry. The water content of CNC-S and CNC-H was 1.5 % and 0.1 %, respectively. The higher water

content of CNC-S may be explained that there must be an interaction between sulfate groups and adsorbed water molecules, which prevented water to be removed from the CNC surface (Huang, Li et al. 2013).

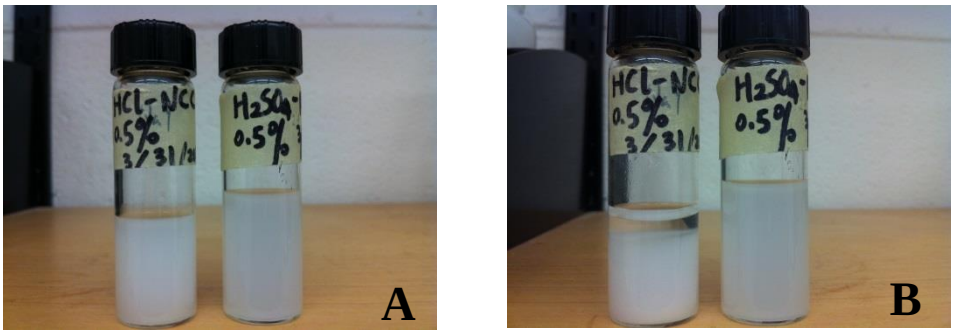

Figure 2.10 Dispersion of CNC-S and CNC-H in the Water (A), One Week Later (B)

4.1.2 Morphology of Cellulose Nanocrystals

Microscopy technologies such as TEM, AFM and SEM, have been widely used to investigate the dimensions of CNC (Morán, Alvarez et al. 2008) (Elazzouzi-Hafraoui, Nishiyama et al. 2007). Therefore, we utilized SEM to study the lengths and diameters of CNC-S and CNC-H, respectively (Figure 2.11). It's easier to find individual CNC-S particles due to better dispersion in contrast to the obvious aggregation of CNC-H. The distribution of particle lengths and diameters in CNC-S suspension was obtained from 30 pieces of images analysis, and shown in Figure 2.12. It revealed CNC-S have diameters (*d*) of 8 nm ± 1 nm and lengths (*L*) of 210 ± 10 nm, giving an aspect ratio (L/d) of 26.3. Samira et al. have prepared CNC with the length of around 120 nm using 64% w/v sulfuric acid to hydrolyze Avicel (Elazzouzi-Hafraoui, Nishiyama et al. 2007). The significant length difference was probably caused by hydrolysis temperature. They controlled the hydrolysis temperature to 72 °C which is much higher than our conditions (45 °C).

For CNC-H, We failed to obtain reliable results from SEM analysis since it was difficult to distinguish one from others. Dynamic light scattering (DLS) has been employed to study the precise morphology of nanoparticles (De Souza Lima, Wong et al. 2002). Therefore, we utilized DLS to measure the length of CNC-H, as well as CNC-S. For CNC-S, it was in accordance with SEM analysis and the length of main parts was 220-290 nm. For CNC-H, the length of main parts was 550-750 nm and 2.5 times longer than that of CNC-S.

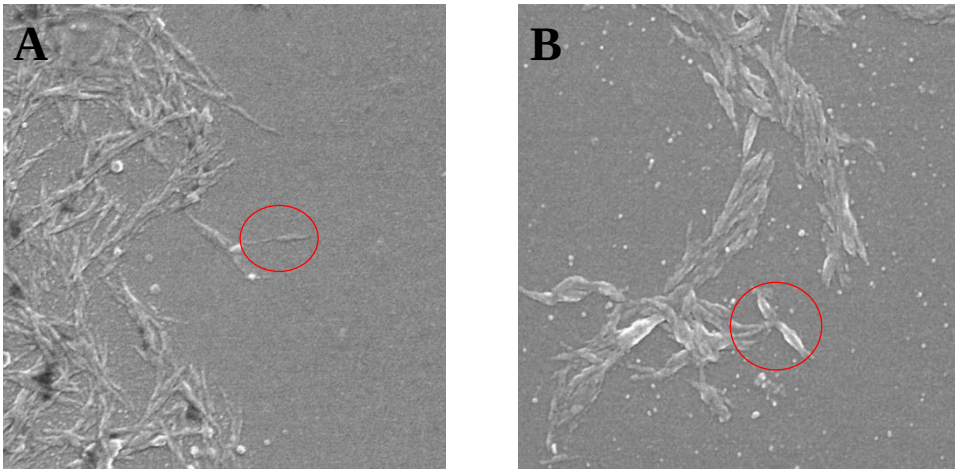

Figure 2.11 SEM Images of CNC-S (A) and CNC-H (B)

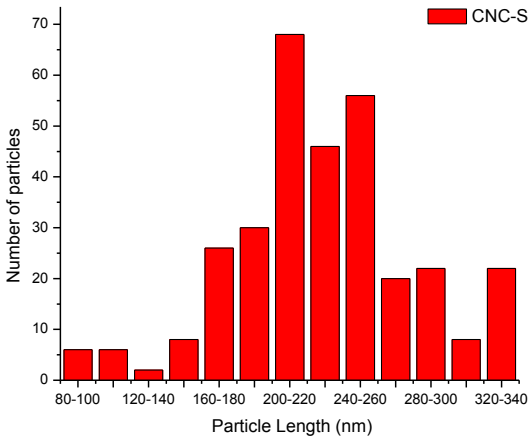

Figure 2.12 Distribution of Particle Length of CNC-S from Suspension

4.1.3 FT-IR Analysis of Cellulose Nanocrystals

FT-IR is a useful analytical instrument to analyze liquids, powders and films. It has been used to determine super-molecular structure and to analyze chemical compositions (Kokot, Czarnik-Matusewicz et al. 2002; Guo and Wu 2008). Morais et al. have used FT-IR to characterize CNC produced from cotton linters, and number of peaks increased in CNC in comparison to the original cotton linters(Morais, Rosa et al. 2013).

The FT-IR spectra of CNC-S, CNC-H and Avicel were shown in Figure 2.13. Absorption at ~3400 cm^{-1} and 2900 cm^{-1} were assigned to stretching of -OH and C-H symmetrical stretching of CH_2 groups, respectively, which are typically characteristic absorptions of cellulose (Zhang, Wang et al. 2013). Comparing the FT-IR spectra of three samples, no significant change at the main cellulose adsorptions bands could be found, which indicated CNC were the derivative of cellulose. However, two new FT-IR adsorption bands of CNC-S appeared at 1250 cm^{-1} from asymmetrical S=O vibration and at 833 cm^{-1} from symmetrical C-O-S vibration, respectively, which typically were attributed to sulfate groups on carbohydrate polymers (Gu, Catchmark et al. 2013). Furthermore, FT-IR has been utilized to investigate the crystal structure of cellulose I. O-H stretching at 3270 cm^{-1} and out of plane bending at 710 cm^{-1} for Iβ has been reported (Lu and Hsieh 2010). Therefore, CNC-S and CNC-H remained their original crystalline structure (Iβ) after the acid hydrolysis of Avicel. Other FT-IR bands have been summarized in Table 2.3 mainly referring to Fan's et al. work (Fan, Dai et al. 2012).

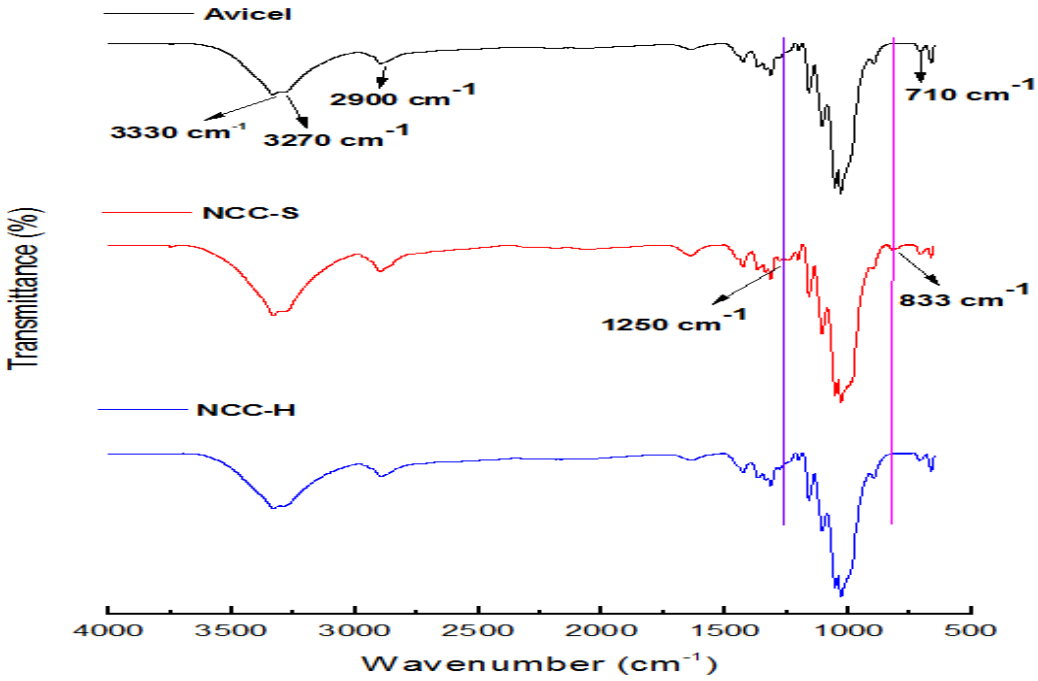

Figure 2.13 FT-IR Results of CNC-S, CNC-H and Avicel

Table 2.3 FT-IR Absorption of CNC-S, CNC-H and Avicel

Wavenumber (cm^{-1})	Assignment
1640	OH bending of absorbed water
1425	HCH and OCH in plane bending vibration
1368	In the plane CH bending
1312	CH_2 rocking vibration at C6
1247	C-C plus C-O stretch
1204	C-O-C symmetric stretching, OH plane deformation
1160	C-O-C asymmetrical stretching
1053	C-C, C-OH, C-H ring vibration
1028	C-C, C-OH, C-H ring vibration
998	C-C, C-OH, C-H ring vibration
895	COC, CCO and CCH deformation and stretching
664	C-OH out of plane bending

4.1.4 Surface Charge Determination

As the most promising fundamental building blocks, surface charge of CNC served as an important parameter for its application. Composites, for example, the surface charge content

directly influenced CNC dispersion when mixed with others polymers, which in turn affected composites properties (Abitbol, Palermo et al. 2013). Several methods have been developed to determine the surface charge, such as conductometric titration (Abitbol, Palermo et al. 2013), elemental analysis (Abitbol, Kloser et al. 2013), zeta potential determination (Tantra, Schulze et al. 2010) and methylene blue adsorption test (Karaaslan, Gao et al. 2013).

Jiang et al. previously produced CNC from sulfite pulp by using sulfuric acid and hydrochloric acid. The sulfur content of CNC-S was 0.57%, and there was no detectable sulfur in CNC-H (Jiang, Esker et al. 2010). In this thesis, we utilized elemental analysis and Zetasizer Nano to investigate the sulfur content and surface charge of CNC-S and CNC-H, respectively. The sulfur content of CNC-S and CNC-H determined by elemental analysis was 0.69 % ± 0.02, and 0.29 % ± 0.02, respectively. From zeta potential determination, CNC-S had a mean value of -30.9 ± 10.2 mV which was lower than that of CNC hydrolyzed from cotton linter (-45 ± 1.4 mV) (Morais, Rosa et al. 2013). Generally, when the absolute value of zeta potential was higher than 25 mV, it was considered as a stable suspension. For CNC-H, the zeta potential was -15 ± 7.41 mV, which showed rapid aggregation.

4.1.5 Crystallinity Measurement

Crystallinity structure of cellulose has been widely studied by different techniques incorporating X-ray diffraction, solid-state ^{13}C NMR, FT-IR and Raman spectroscopy (Moon, Martini et al. 2011). In this thesis, X-ray diffraction technique was used to investigate the crystallinity, as well as crystal sizes of cellulose I structure. The comparison of diffraction diagrams of three samples was shown in Figure 2.14. Typical cellulose I characteristic peaks at round $2\theta=14.7°$ (1-10), 16.5° (110), 20,4° (012), 22.6° (200) and 34.4° (004) have been observed in three samples indicating no change of crystalline structure of cellulose after acid hydrolysis. Several crystallinity index (CI)

calculation methods based on XRD have been proposed, and height method is widely used along with amorphous subtraction or peak deconvolution methods (Park, Baker et al. 2010). The CI was 89.42%, 92.61% and 91.69% for Avicel, CNC-S and CNC-H, respectively, calculated according to Segal methods (Segal, Creely et al. 1959). Avicel is defined as purified and partially depolymerized cellulose (Ohwoavworhua and Adelakun 2007), and thus it showed relatively high crystallinity index (89.42%). The CI of CNC-S and CNC-H would increase as a result of hydrolyzing the amorphous parts of avicel during the CNC preparation.

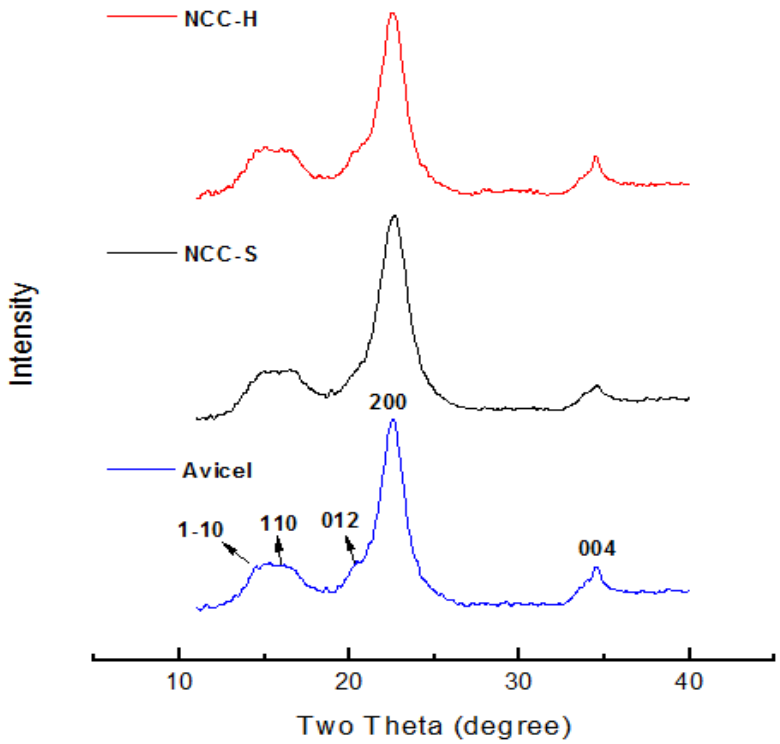

Figure 2.14 X-ray Diffractions of Avicel, CNC-S and CNC-H

4.1.6 CNC Reducing End Determination

The quantification of reducing ends on cellulose substrate is highly relevant to enzyme-catalyzed cellulose degradation (Kongruang, Han et al. 2004). DNS method was used to determine the

reducing ends of CNC-S, CNC-H and Avicel. Results were summarized in Table 2.4. CNC-H exposed more accessible reducing ends with 0.65 mmol/mg, and then CNC-S with 0.55 mmol/mg. The reducing ends of Avicel were 0.5 mmol/mg.

Table 2.4 Reducing Ends Determination of CNC-S, CNC-H and Avicel

Cellulose Preparation	Reducing Ends (mmol/mg)
CNC-S	0.55 ± 0.01
CNC-H	0.65 ± 0.02
Avicel	0.50 ± 0.01

4.2 Effect of Cellulose Nanocrystals Characteristics on Cellulase Hydrolysis and Adsorption

4.2.1 Enzymatic Hydrolysis of Three Different Substrates

Several cellulose characteristics have been identified to affect enzymatic hydrolysis, such as degree of polymerization (Sinitsyn, Gusakov et al. 1991), available surface area (Mansfield, Mooney et al. 1999), particle size (Dasari and Eric Berson 2007) and crystallinity (Hall, Bansal et al. 2010). However, due to the difficulties of controlling one substrates parameter without changing others, it's still unconvincing to conclude which factor plays the dominant role in enzymatic hydrolysis.

As mentioned in Chapter 2, cellulose fibers would carry negative charges after acid pretreatments. Currently, few attentions were focused the effect of surface charge on the enzyme adsorption and enzymatic hydrolysis. Increasing the carboxylic acid content of the associated lignin has been reported to enhance the enzymatic hydrolysis of lignocellulosic biomass. Surface charge on lignin could significantly decrease the non-productive binding of cellulase (Nakagame, Chandra et al. 2011). Therefore, it's interesting to investigate the effect of surface charge of cellulose on cellulase adsorption and hydrolysis. In Figure 2.15, enzymatic hydrolysis of CNC-S,

CNC-H and Avicel was determined. Under 5 FPU/g glucan of cellulase loading, 72h hydrolysis yields of CNC-S, CNC-H and Avicel were 20%, 47.5% and 55%, respectively.

CNC-H was prepared from Avicel hydrolysis by hydrochloric acid, and there should be an increase of crystallinity index since the amorphous parts of Avicel were easily attacked by acid. It was confirmed by X-ray diffraction analysis. Hydrolysis rates have been found to slow down as the increase of crystallinity of cellulose (Sinitsyn, Gusakov et al. 1991). However, others proposed the opposite effect and they found no significant change in crystallinity during enzymatic hydrolysis of cellulose (Puls and Wood 1991). Consequently, crystallinity of substrates failed to be employed as a factor to evaluate the cellulase performance in this case. For CNC-S, there was two times lower cellulose conversion than that of CNC-H. Actually, comparing the characteristics of CNC-S and CNC-H, no obvious difference was observed except for the surface charge. So we believe that there was a correlation between surface charge and enzymatic hydrolysis. Since enzymatic hydrolysis is highly related to cellulase adsorption, we firstly used Langmuir isotherm to investigate the enzyme adsorption and then explain the different cellulose hydrolysis.

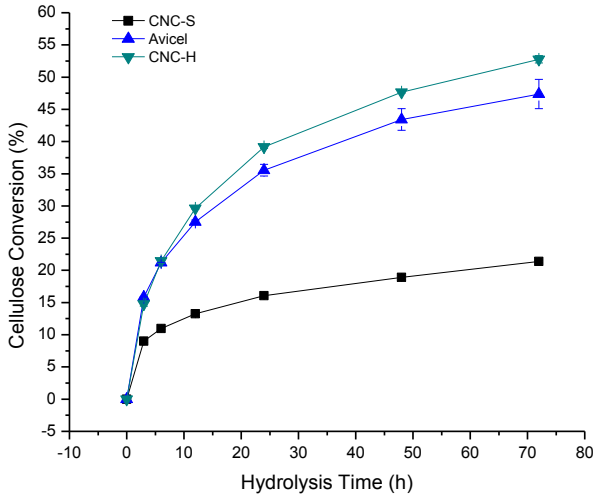

Figure 2.15 Enzymatic Hydrolysis of CNC-S, CNC-H and Avicel

4.2.2 Cellulase Adsorption on Three Different Substrates

Cellulase adsorption isotherm was widely used to evaluate the affinity of enzyme on solid substrates. In this thesis, Langmuir adsorption isotherm model was used to fit cellulase adsorption on CNC-S, CNC-H and Avicel, respectively (Figure 2.16 and Table 2.5). It was observed that the cellulase showed highest affinity (R) to CNC-S (0.159 L/g) than that to CNC-H (0.124 L/g) and Avicel (0.138 L/g). In the case of cellulase adsorption to CNC-S, the Langmuir constant (K) was 0.66 mL/mg and Γ_{max} was 240.65 mg/g which was 5-fold higher than that on CNC-H (50.17 mg/g). In the case of CNC-H, the Langmuir constant (K) was 2.47 mL/mg and Γ_{max} was 50.17 mg/g. For Avicel, it showed the lowest Γ_{max} (37.77 mg/g), but the highest K (3.68 mL/mg).

The difference of Γ_{max} for CNC-H (50.17 mg/g) and Avicel (37.77 mg/g) might be responsible for the higher cellulose conversion for CNC-H. The increase of enzyme adsorption on CNC-H actually resulted from more accessible surface area, due to shorter length of CNC-H, higher surface area. Meanwhile, the highest amounts of reducing ends were detected in CNC-H (0.65

mmol/mg), which means more reducing ends and non-reducing ends created by acid hydrolysis of amorphous parts were available for CBH to recognize and then effectively hydrolyze.

As for CNC-S, the hydrolysis yield was low (20%). The Γ_{max} of CNC-S was 240.65 mg/g which indicated that more cellulase was adsorbed onto it. But, its Langmuir constant was low (0.66 mL/mg). We need to investigate the reason for lower hydrolysis yield of CNC-S in the future.

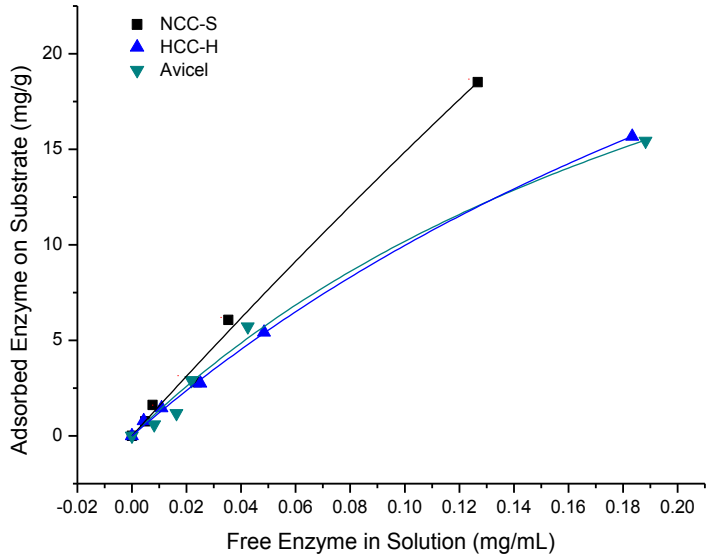

Figure 2.16 Langmuir Isotherm of Cellulase Adsorption on CNC-S, CNC-H and Avicel

Table 2.5 Langmuir Isotherm Parameters of Cellulase Adsorption on Three Substrates

Substrates	Γ_{max} (mg/g)	K(mL/mg)	R(L/g)
CNC-S	240.65	0.66	0.159
CNC-H	50.17	2.47	0.124
Avicel	37.77	3.68	0.139

4.2.3 Enzymatic Hydrolysis and Enzyme Adsorption of CNC-S and Desulfated CNC-S

Given that CNC-S was prepared by sulfuric acid hydrolysis of Avicel, presence of sulfate groups on CNC-S rather than CNC-H has been proved. It's reasonable to hypothesize the sulfate groups

might give rise to cellulase adsorption. Therefore, acid-catalyzed desulfation of CNC-S has been performed. We used ~ 0.025N hydrochloric acid to catalyze the desulfation of CNC-S at 80 °C for 5 h, and chemical analysis and crystallite dimensions determination showed no changes except for the decreased surface charge density (Jiang, Esker et al. 2010). Enzyme adsorption and enzymatic hydrolysis of CNC-S, desulfated CNC-S, CNC-H and Avicel were investigated. Results (Figure 2.17 and Figure 2.18) indicated 72 h hydrolysis yield of desulfated CNC-S was significantly enhanced by 25% in comparison with that of CNC-S, but it was still lower than that of CNC-H and Avicel. Γ_{max} for desulfated CNC-S significantly decreased to 70.98 mg/g, over three-fold lower than that of CNC-S (240.65 mg/g). Therefore, we believe that sulfate groups on CNC-S led to the increased enzyme adsorption. Similarly, Jiang et al. have investigated the effect of sulfate groups on cellulase adsorption and enzymatic hydrolysis by quartz crystal microbalance with dissipation monitoring (QCM-D) (Jiang, Kittle et al. 2013). They also suggested that sulfate groups on cellulose could promote the enzyme adsorption but hinder the enzymatic hydrolysis.

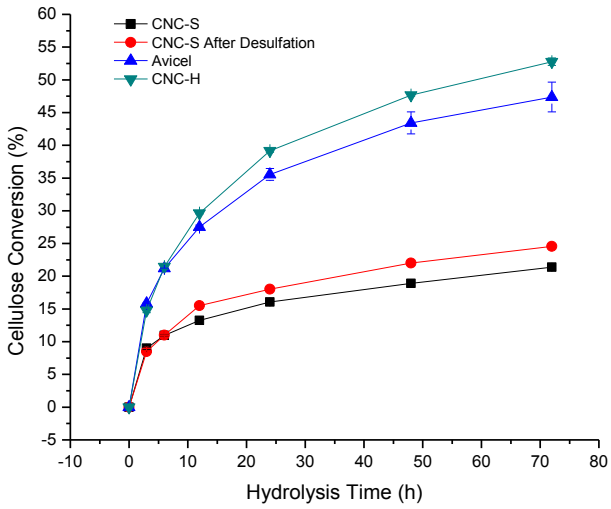

Figure 2.17 Enzymatic Hydrolysis of CNC-S, CNC-S after Desulfation, CNC-H and Avicel

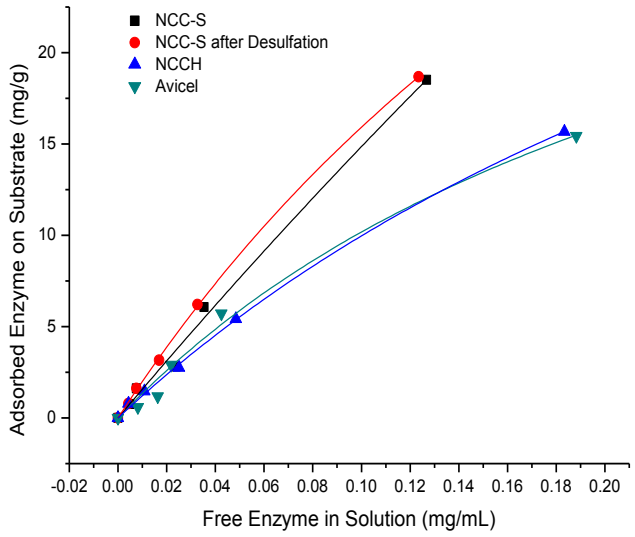

Figure 2.18 Langmuir Isotherm of Cellulase Adsorption on CNC-S, CNC-S after Desulfation, CNC-H and Avicel

Table 2.6 Langmuir Isotherm Parameters of Four Substrates

Substrates	Γ_{max} (mg/g)	K(ml/mg)	R(L/g)
CNC-S	240.65	0.66	0.158
CNC-S after Desulfation	70.98	2.89	0.205
CNC-H	50.17	2.47	0.123
Avicel	37.77	3.68	0.139

4.2.4 Effects of pH on Enzyme Adsorption and Enzymatic Hydrolysis

Generally, it is believed that hydrophobic interaction is responsible for the adsorption of cellulase on pure cellulose, while electrostatic interaction were not of key factor (Nakagame, Chandra et al. 2011). In this special case of CNC-S, we believe that electrostatic interaction might play important roles in enzyme adsorption since introduction of sulfate groups would decrease cellulose hydrophobicity. pH was one of important variables that was commonly utilized to examine the interaction between solid and enzyme (Wang and Somasundaran 2005). In Figure 2.19**,** the effect of pH on cellulase adsorption and enzymatic hydrolysis of CNC-S, CNC-H and Avicel were studied. Rahikainen et al. evaluated the binding of endoglucanase

(MaCel 45A) and MaCel 45A-CBM on microcrystalline cellulose, and it showed no pH-dependency (Rahikainen, Evans et al. 2013). This was in a good agreement with our observation that no obvious desorption occurred on CNC-H and Avicel as the pH increased. In other word, if hydrophobic force dominated the interaction between cellulase and cellulose, no pH effect on enzyme adsorption could be found. However, for CNC-S, free enzyme in the supernatant increased from 23.6% to 27.40% with pH variation from 4.4 to 5.6, and then almost kept constant, which confirmed the electrostatic interaction between CNC-S and enzyme. The surface charge of enzyme was dependent on the isoelectric-point of enzyme and the pH of solution. As the increase of pH from 4.4 to 6.0, carboxylic acid groups from amino acids in enzyme dissociated, which in turn increased the total amounts of negative charges. As a result, there was a stronger electrostatic repulsive interaction between sulfate groups on CNC-S and negative charge of enzyme. Time course of enzymatic hydrolysis of CNC-S, CNC-H and Avicel under different pH were shown in Figure 2.19. Figure 2.19 E was pH versus 72 h cellulose conversion. Similar trends for CNC-H and Avicel were observed, and optimal pH for Novozym 22C was around 5.0. When we changed pH from 4.8 to 6.0, cellulose conversion for Avicel and CNC-H significantly decreased from 47.5% to 27.5% and 55% to 42.5%, respectively, due to conformational change of enzyme (Mayans, Scott et al. 1997). Conversely, as the increase of pH from 4.8 to 6.0, cellulose conversion for CNC-S slowly decreased from 25% to 17.5%. Desorption of enzyme from CNC-S as the increase of pH seemed to promote the enzymatic hydrolysis in contrast to the widely acceptable ideas that increasing enzyme adsorption was favorable for enzymatic hydrolysis (Lu, Yang et al. 2002). Another possible reason is the enzyme conformation was stabilized due to its immobilization on charged CNC-S, which is

similar to enzyme immobilization between enzyme and support materials (Garcia-Galan, Berenguer-Murcia et al. 2011).

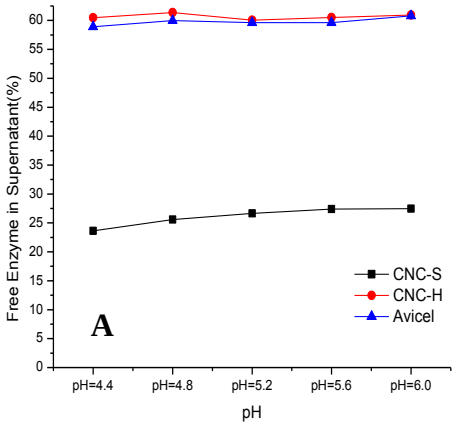

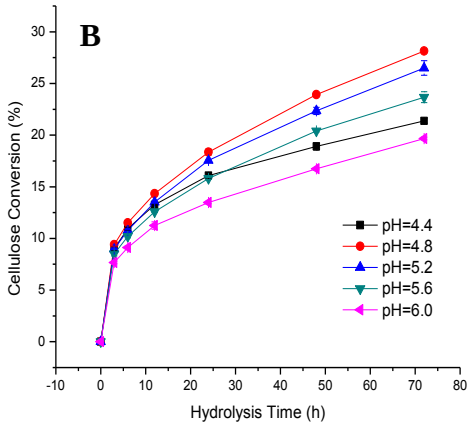

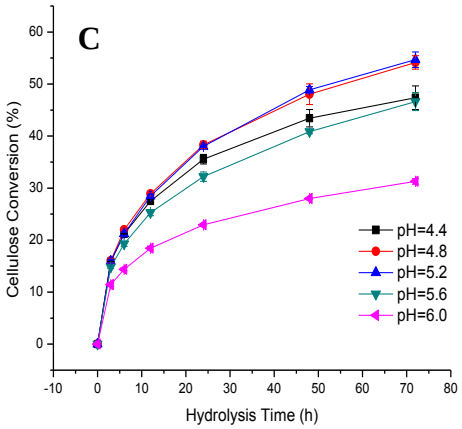

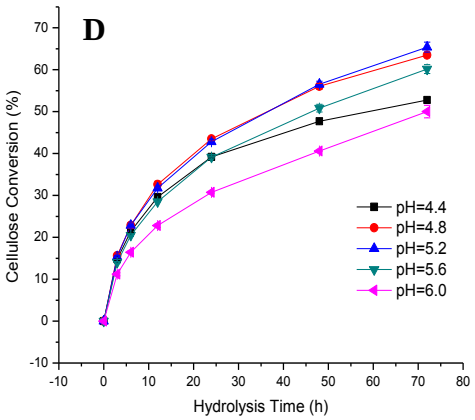

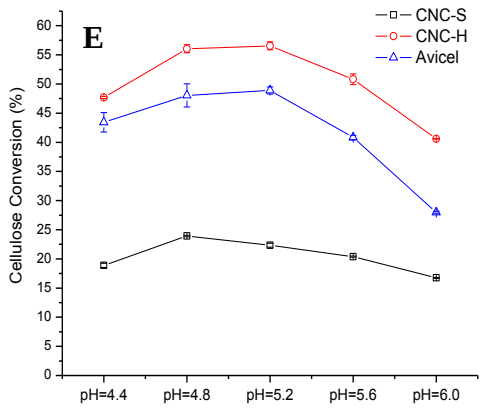

Figure 2.19 Effect of pH on Enzyme Adsorption (A) and Enzymatic Hydrolysis of CNC-S (B), Avicel (C) and CNC-H (D); Effect of pH on 72h Enzymatic Hydrolysis of Three Different Substrates (E)

4.2.5 Effects of Ionic Strength on Enzyme Adsorption and Enzymatic Hydrolysis

Ionic strength was another important variable for analyzing the interaction between solid and protein. NaCl was capable of suppressing electrostatic interactions, and increasing hydrophobic interaction because of its salting-out effectiveness (Shikiya, Tomita et al. 2013). Therefore, we evaluated the effect of NaCl concentration on enzyme adsorption and enzymatic hydrolysis in Figure 2.20. As the increase of NaCl concentration to 200 mM, 50% free enzyme in the supernatant was found for CNC-S, while only 25% free enzyme suspended in the supernatant without NaCl addition. Na^+ could combine with sulfate groups via ionic bonds, and hinder the electrostatic interaction between sulfate groups and positive patches on the surface of the protein. Additionally, we found that CNC-H and Avicel showed similar variation trends, and the percentage of free enzyme in the supernatant for CNC-H and Avicel increased from 57.5% to 65% and from 67.5% to 75%, respectively. The increase of free enzyme in the supernatant for CNC-S (25%) was much higher than that of CNC-H (7.5 %) and Avicel (7.5 %) with the addition of NaCl, which confirmed the electrostatic interaction between cellulase and charged cellulose. Kim and Hong found similar results that there was a decrease of CBHI adsorption on

microcrystalline cellulose as the increase of buffer concentration from 0.01 to 0.4 M (Kim and Hong 2000). The ions had the potential to compete for protein binding sites on cellulose, leading to the decrease of enzyme (Tu, Pan et al. 2009).

Time course of effect of ionic strength on enzymatic hydrolysis was shown in Figure 2.20. Similar to pH effect, as the increase of ionic strength, cellulose conversion of CNC-S showed slow decrease, while we observed obvious decrease of cellulose conversion for CNC-H and Avicel. Summarily, effect of pH and ionic strength on enzyme adsorption clearly indicated that it was electrostatic interaction that dominated the enzyme adsorption between enzyme and charged cellulose. Desorption of enzyme from CNC-S interestingly contributed to the improvement of enzymatic hydrolysis.

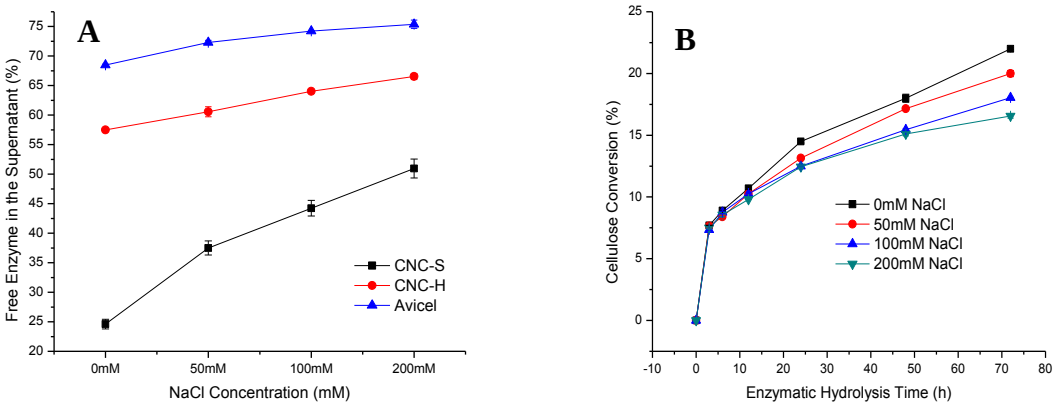

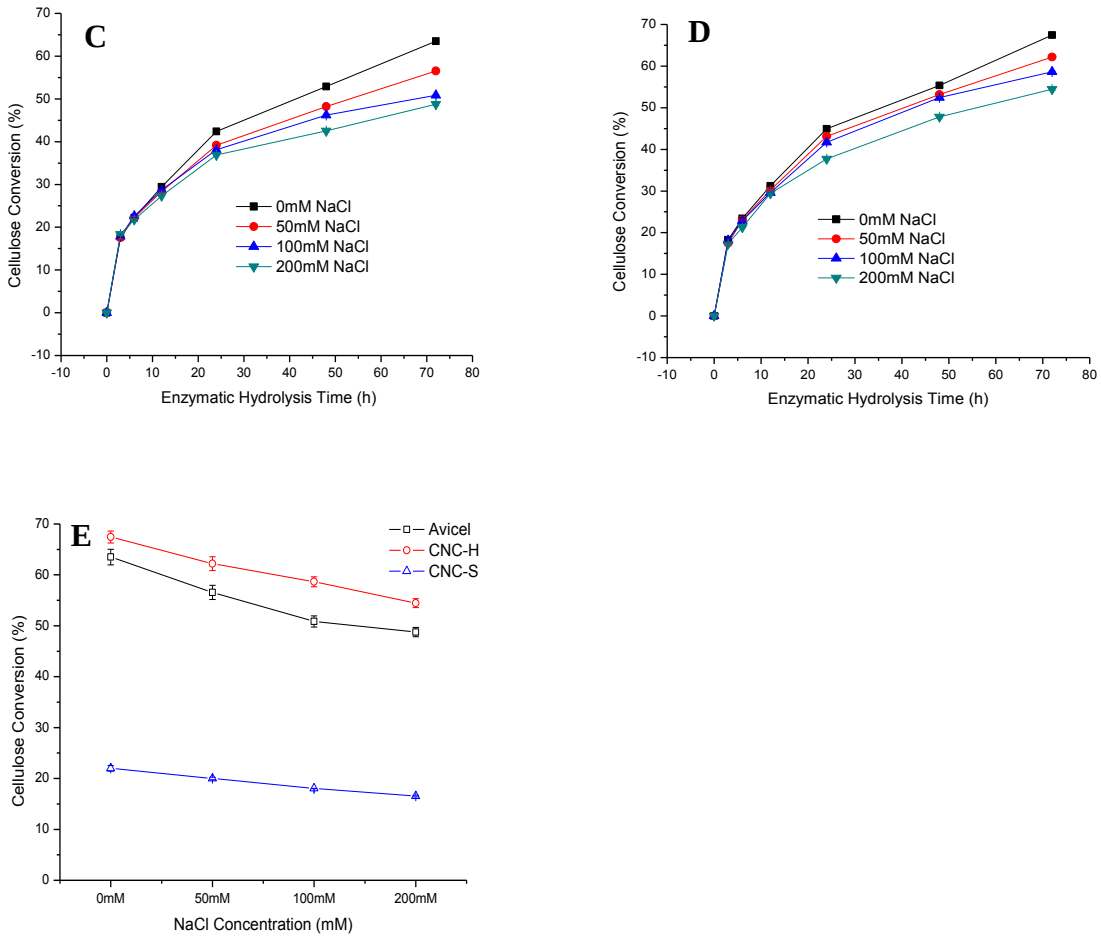

Figure 2.20 Effect of Ionic Strength on Enzyme Adsorption (A) and Enzymatic Hydrolysis of CNC-S (B), Avicel (C) and CNC-H (D); Effect of Ionic Strength on 72h Enzymatic Hydrolysis of Three Different Substrates (E)

4.2.6 Cellulase Adsorption and Desorption

In this thesis, we used SDS-PAGE to evaluate the enzyme adsorption on CNC-S, CNC-H and Avicel, respectively. The increase of enzyme adsorption on CNC-S have been suggested some enzymes, such as CBHII, EGII and EGIII, which have isoelectric point above 4.8, possessed positive charges that might be responsible for the more adsorption (Jiang, Kittle et al. 2013). However, we proposed another explanation for enzyme adsorption on CNC-S based on SDS-PAGE results. The molecular weight of marker has been displayed in the left lane (Figure 2.21). Apparently, after mixing cellulase with CNC-S, even CBHI (pI=3.5~4.2) could also be adsorbed

onto substrates judging from all decreased band intensity, although the net surface charges of CBHI was negative. For CNC-H and Avicel, they showed similar adsorption type, but all band intensity was stronger than that of CNC-S. It was reported that positive patches on the surface of protein could work as a counter ion of the negative charged polyelectrolyte chains (Haupt, Neumann et al. 2005). Therefore, we suggested no matter whether the enzyme showed a net negative or positive charge, it could be adsorbed onto CNC-S via the electrostatic interaction between sulfate groups and positive patches on the surface of cellulase.

In order to explain the decreased cellulose conversion of CNC-S, desorption experiments of CNC-S, CNC-H and Avicel were performed, and the result was shown in Figure 2.22. After adsorption of cellulase onto CNC-S, only 20% of adsorbed enzyme could be desorbed. This was three-fold and two-fold lower than that of CNC-H (80 %) and that of Avicel (65 %), respectively. CBH as the dominant components in cellulase could attack the cellulose chain from reducing and nonreducing ends, and it was unidirectional processive enzyme (Igarashi, Uchihashi et al. 2011). In other words, this processive mode of action is essential for its efficient performance of hydrolyzing cellulose (Kurašin and Väljamäe 2011). Consequently, the decreased cellulose conversion of CNC-S was probably caused by the tight binding of cellulase onto cellulose, which slowed down or limited the processivity of CBH.

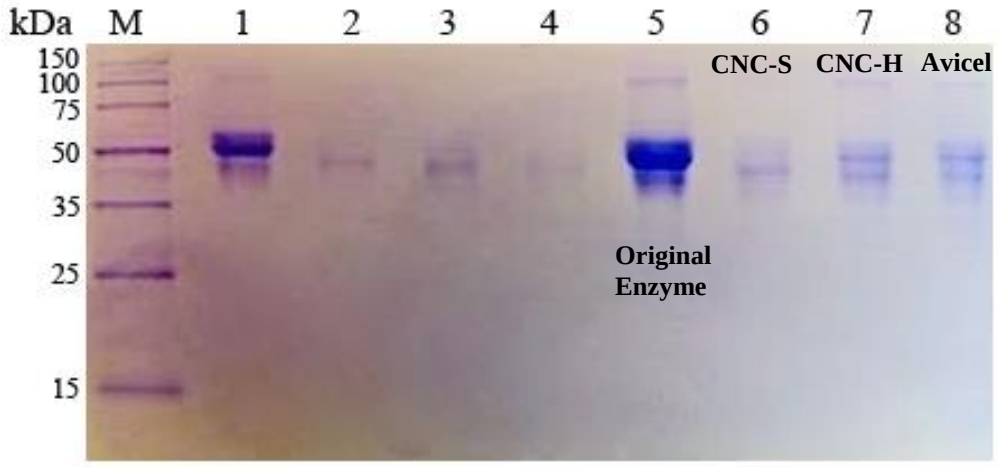

Figure 2.21 SDS-PAGE of Cellulase after Adsorption on CNC-S (Lane 6), CNC-H (Lane7) and Avicel (Lane 8); M (Maker); Original Enzyme (Lane 5)

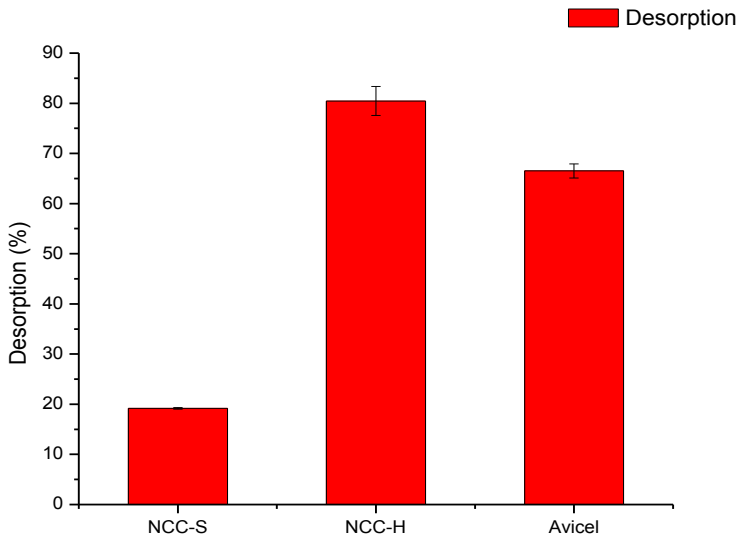

Figure 2.22 Desorption of Cellulase after Adsorption on CNC-S, CNC-H and Avicel

4.2.7 Analysis of Enzymatic Hydrolysate of CNC-S

Previous report suggested that the active site of CBHI contains three acidic residues, and it has a negative charge in the tunnel and the active site, which could prevent negatively charged cellulose chains entering the catalytic domain (Jiang, Kittle et al. 2013). However, we successfully identified one new sulfated disaccharide from the products of enzymatic hydrolysis

of CNC-S (Figure 2.23). This new compound was found in HPLC curve prior to the glucose peaks. After purification, we applied LC-MS to obtain its molecular weight of 422 g/mol, and it was regarded as the product from CBH hydrolysis (Figure 2.24).

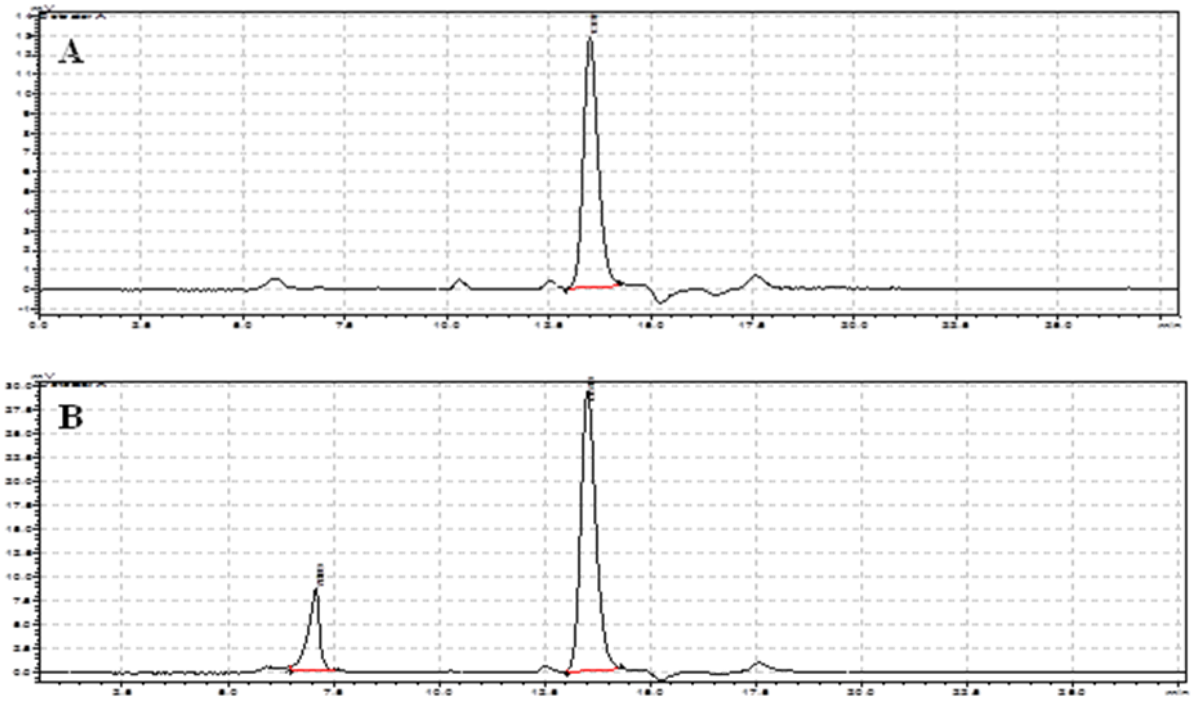

Figure 2.23 HPLC Curve of Enzymatic Hydrolysis of Avicel (A) and CNC-S (B)

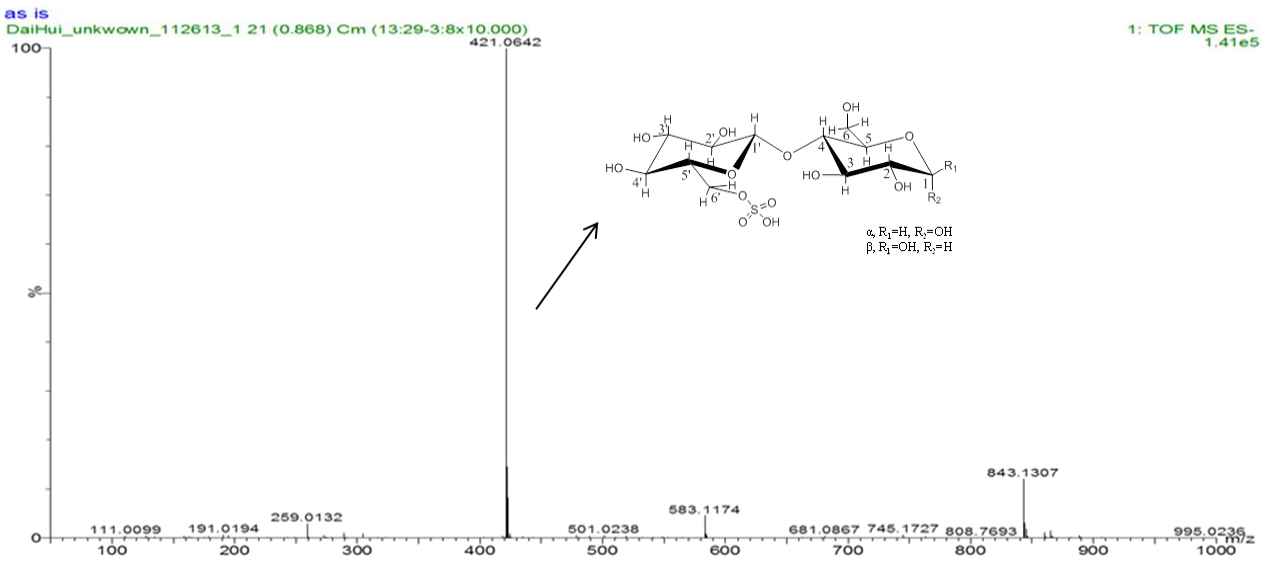

Figure 2.24 LC-MS Analysis of Product Purified from Hydrolyzate of Enzymatic Hydrolysis of CNC-S

4.3 Structural Elucidation of Cellobiose Sulfate

4.3.1 ^{1}H NMR Spectra

Several methods can be used to elucidate the structure of carbohydrates including X-ray diffraction (Jamal, Nurizzo et al. 2004), NMR (Duus, Gotfredsen et al. 2000) and MALDI-TOF-MS (Harvey 2012). NMR has been widely used to obtain conformational and dynamical information of sugars in water (Martin-Pastor and Bush 1999). Therefore, in this thesis, we used 1D and 2D NMR to analyze a new compound from enzymatic hydrolysate of CNC-S. Although complete ^{1}H and ^{13}C signals assignments of cellobiose have been reported (Roslund, Tähtinen et al. 2008), we still performed 1D and 2D NMR spectra of cellobiose to assist the analysis of new compound .

We hypothesize that new compound was cellobiose sulfate (S-cellobiose) based on its molecular weight of 422 g/mol (Section 4.2.7), and one of the hydroxyl groups of cellobiose was sulfated. ^{1}H NMR spectra of cellobiose and s-cellobiose were shown in Figure 2.25**,** respectively. Firstly, we started our peak assignments from four obvious signals appeared between 4.3 δ and 5.3 δ in ^{1}H NMR spectra of cellobiose. Signal displayed at around 4.7 δ is from solvent (D_2O). The rest three peaks are caused by protons (α H1, β H1 and H1') which connected to anomeric carbon that was directly connected to two oxygens, while the rest of protons connected to carbons which were only bonded to one oxygen. Furthermore, the relative areas of the signals in the ^{1}H NMR spectra represented the relative number of protons. After integration of ^{1}H NMR spectra, we suggested the signal at around 4.5 δ was caused by the proton which was bonded to the C1' since its integration value is 1.00 in comparison with 0.35 at 5.2 δ and 0.63 at around 4.6 δ. There was a doublet at 5.2 δ, and the coupling constant (*J*) for this doublet was 3.8 Hz. It was the result of a smaller axial-equatorial dihedral angle (approximately 60 °) (Gurst 1991). Therefore, we firmly

assigned this peak as α H1. Another doublet appears at 4.6 δ, and the J value was calculated as 7.9 Hz, which resulted from the larger axial-axial dihedral angle (approximately 180 °). Therefore, this peak was assigned as β H1. Another method to distinguish α H1 and β H1 is electronic shielding and/or deshielding effects. Generally, the electrons in a carbon-carbon bond will generate shielding and deshielding zones (Drake and Brown 1977). α H1 located in deshielding region, and thus we would expect a downfield chemical shift. Oppositely, β H1 was positioned in a shielding region. Correspondingly, there was an upfield chemical shift. It's impossible to assign the signals ranging from 4.0 δ to 3.0 δ due to their overlapping. Additionally, same strategies have been applied to the ^{1}H NMR of s-cellobiose, and α H1, β H1 and H1' have been clearly marked in Figure 2.25 A. After comparison ^{1}H NMR spectra of cellobiose and s-cellobiose, we found two signals appeared at 4.33 δ and 4.19 δ in the ^{1}H NMR of s-cellobiose. These obvious downfield shifts were possibly due to the proton which was bonded to the carbon that was sulfated during the process of CNC preparation. Therefore, we would combine 1D and 2D NMR spectra to elucidate these two signals in the following section.

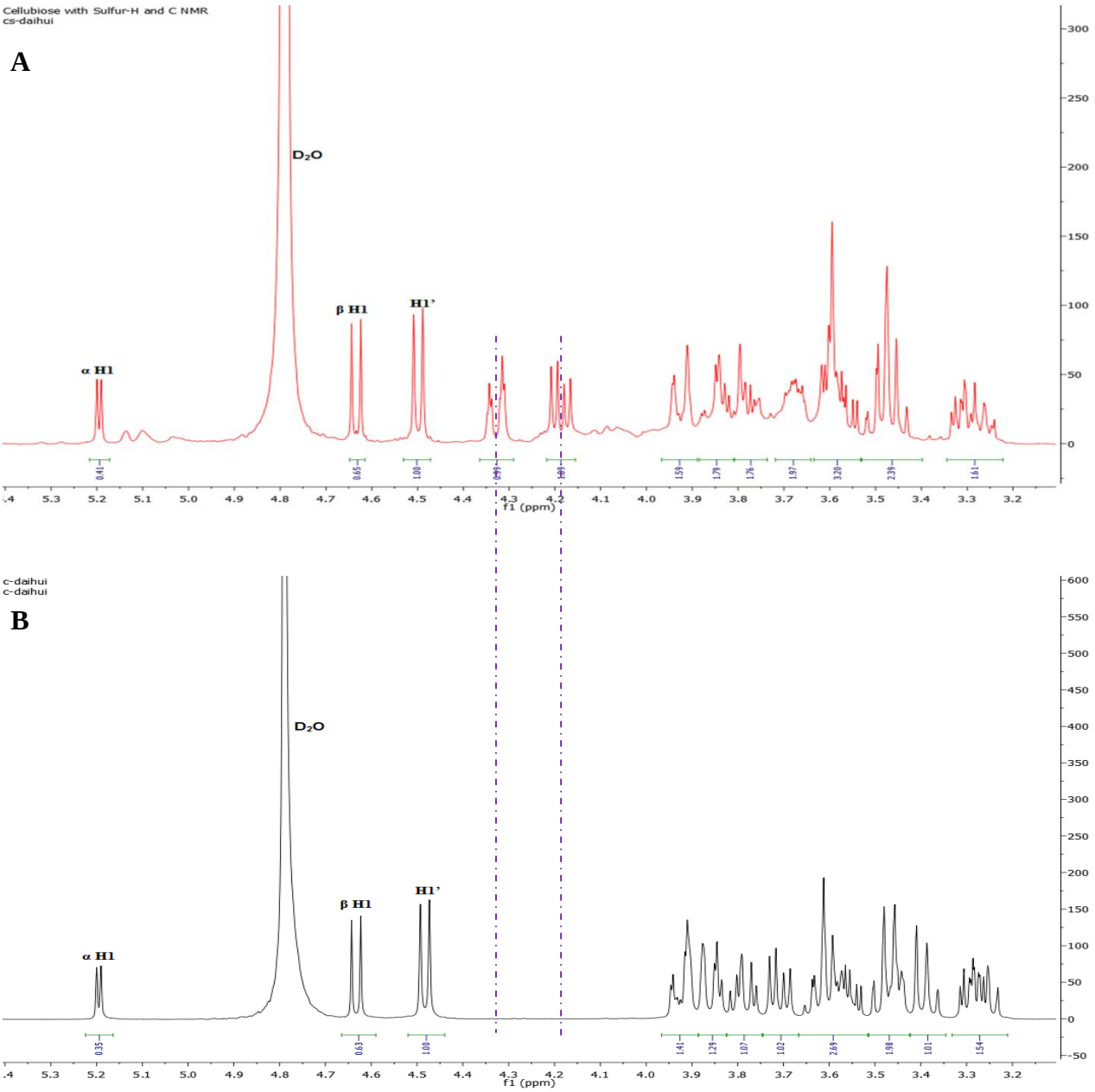

Figure 2.25 ^{1}H NMR Spectra of S-Cellobiose (A) and Cellobiose (B);

4.3.2 Determination of Sulfation Position

Although we have suggested this new compound was cellobiose sulfate, where the sulfate groups located was still unknown. Two different methods have been presented to determine the sulfation position. One is the combination of ^{1}H NMR, DQF-COSY and HSQC, and another is the combination of ^{1}H NMR, HSQC, DEPT-135 and TOSCY.

DQF-COSY and HSQC of s-cellobiose were shown in Figure 2.26. Starting from the known proton which has been assigned (H1'), theoretically, the signals of H2', H3', H4', H5', H6'1 and H6'2 could be found based on the cross peaks in DQF-COSY (Figure 2.26 A), respectively. For example, H1' (4.50 δ) showed a cross peak with a resonance at 3.30 δ, and the latter was assigned to H2' due to H1' and H2' coupling (Wang, Kalka-Moll et al. 2000). Similarly, H2' signal (3.30 δ) also displayed a cross peak at 3.48 δ, which was obviously from H3'. However, from H3' to H4', signals overlapped in ^{1}H NMR and cross peaks almost mixed with diagonal peaks, so it's difficult to identify each of them. After enlarging certain regions of DQF-COSY of s-cellobiose (Figure 2.26 C), we could recognize that there were two different proton signals which slightly overlapped to each other at 3.48 δ and 3.45 δ, and it's reasonable to draw a square which indicated the coupling of H3' and H4'. Furthermore, we confirmed it from HSQC in Figure 2.26 D. There were two carbon-proton cross peaks from 3.4 δ to 3.5 δ which suggested two different protons located in this region. Importantly, the integration value of this region (3.4 δ to 3.5 δ) is around 2.0. Therefore, these two protons were from H' rather than α H or β H. Same way could be applied to find H5', H6'1 and H6'2 based on cross peaks in Figure 2.26 B. Yamada et al. have reported that signals of protons which directly bound to an O-sulfated carbon were shifted downfield by 0.4-0.7 δ, but only 0.07-0.3 δ from the protons which bound to the first neighboring carbon (Yamada, Yoshida et al. 1992). Since two signals appeared at 4.33 δ and 4.19 δ, respectively, which already have been assigned to H6'1 and H6'2 (Figure 2.26 B), we concluded that these downfield shifts (approximately 0.4 δ from the closest signals on the right) resulted from the protons which was directly bonded to C6' that was sulfated during the process of CNC preparation.

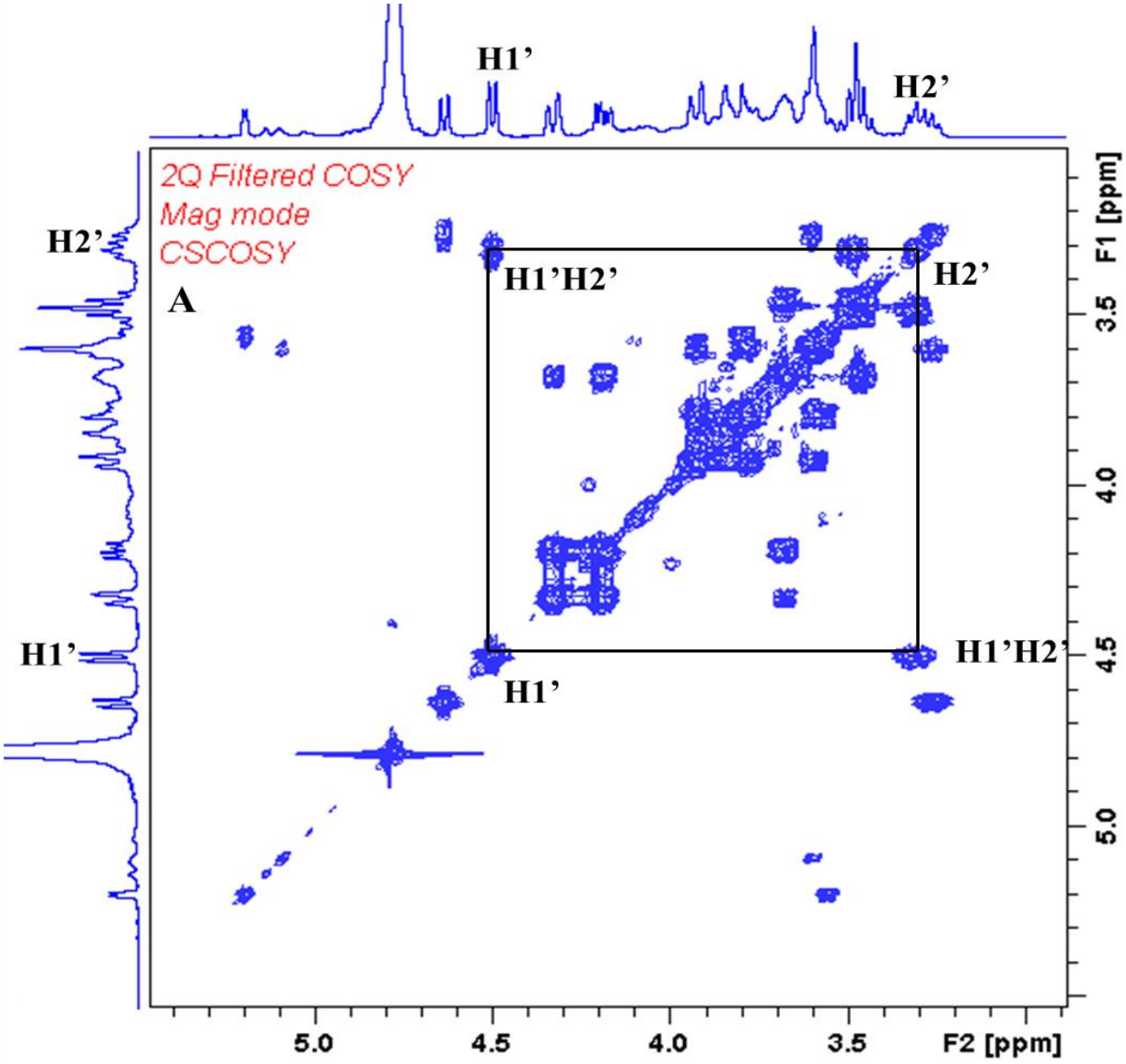
H1'
H2'
2Q Filtered COSY
Mag mode
CSCOSY
A
H2'
H1'H2'
H2'
H1'
H1'H2'
H1'
F1 [ppm]
3.5
4.0
4.5
5.0
5.0
4.5
4.0
3.5
F2 [ppm]

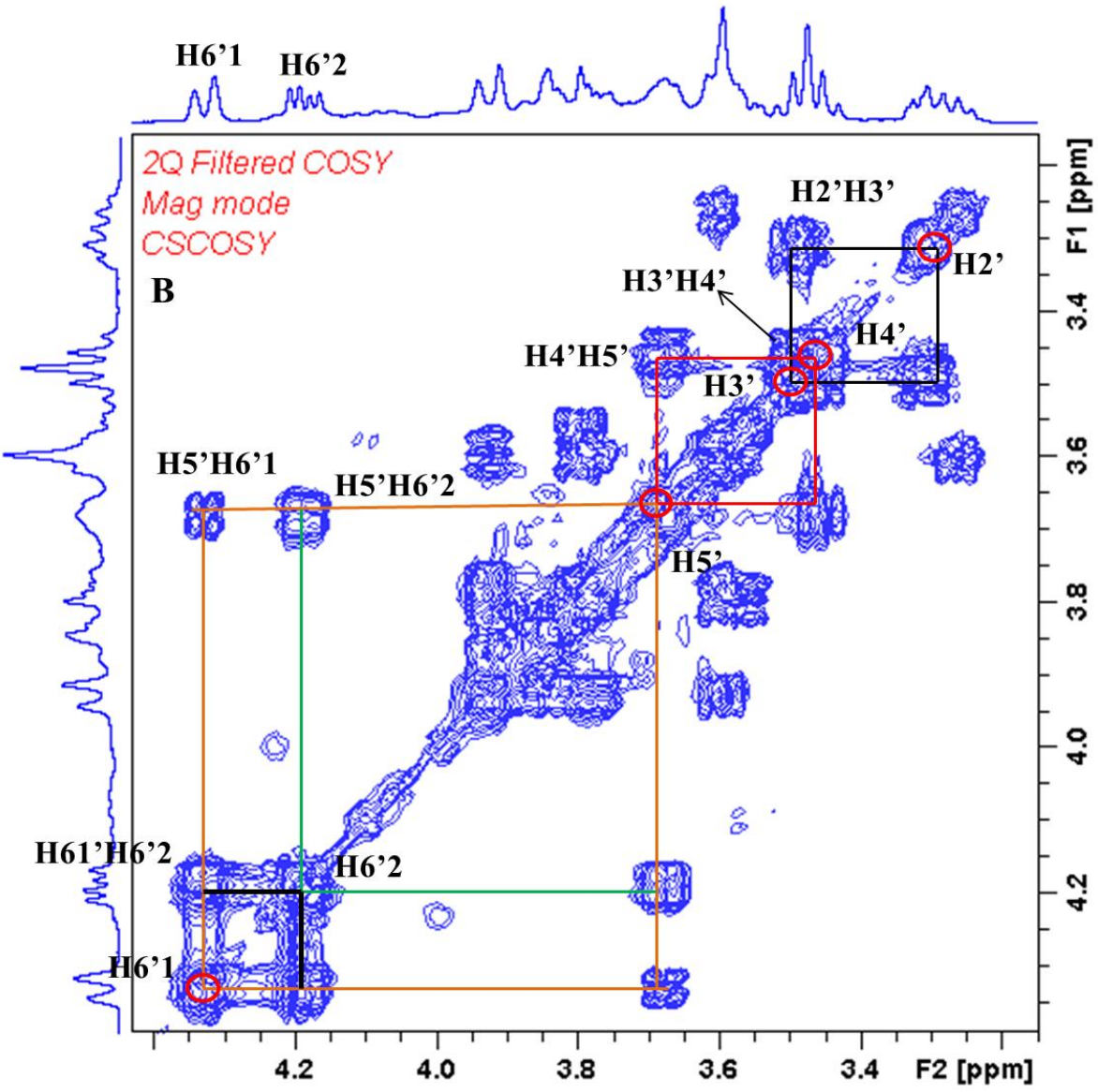
H6'1
H6'2
2Q Filtered COSY
Mag mode
CSCOSY
B
H2'H3'
H2'
H3'H4'
H4'
H4'H5'
H3'
H5'H6'1
H5'H6'2
H5'
H61'H6'2
H6'2
H6'1
F1 [ppm]
3.4
3.6
3.8
4.0
4.2
4.2
4.0
3.8
3.6
3.4
F2 [ppm]

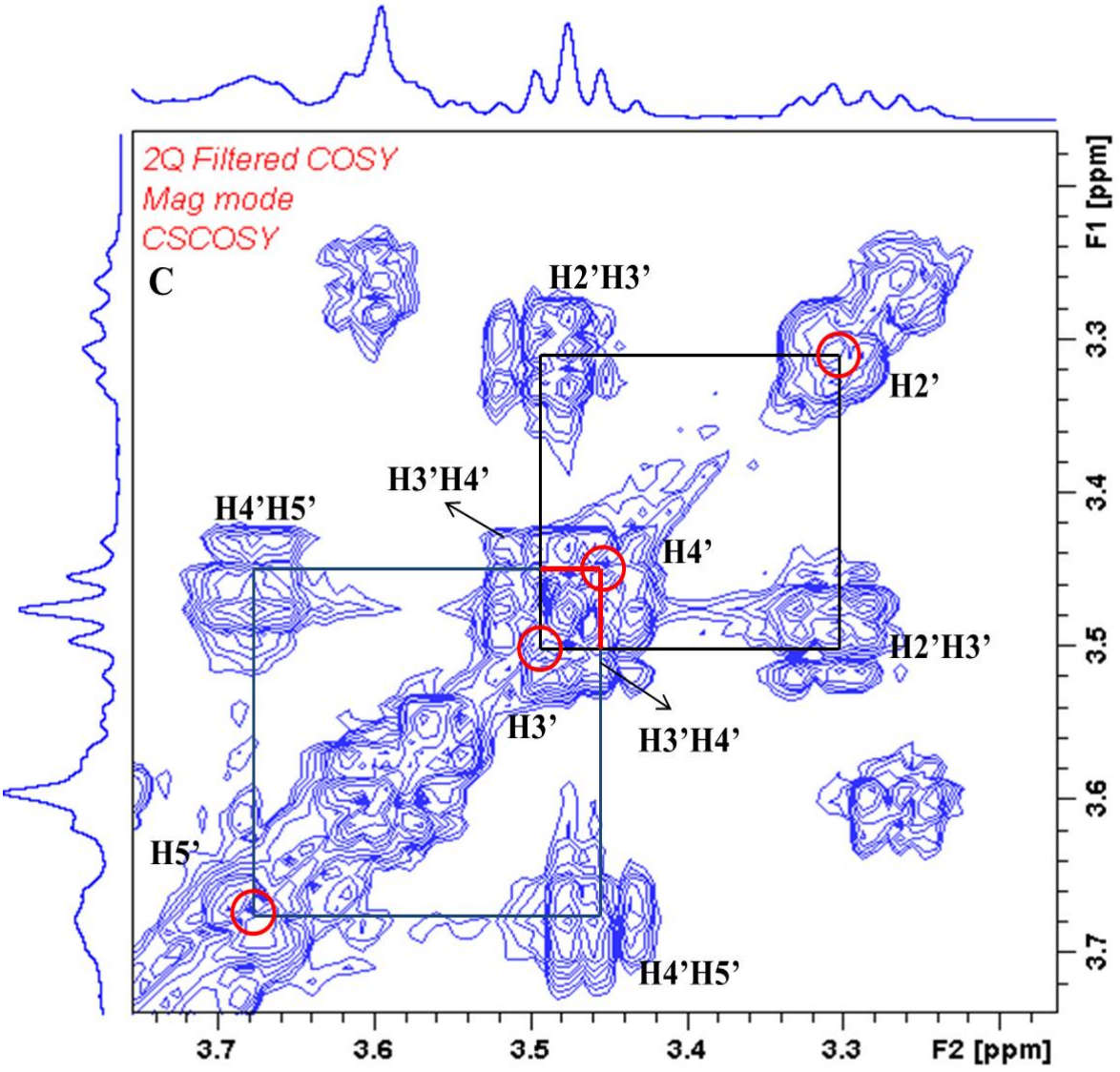
2Q Filtered COSY
Mag mode
CSCOSY
C
H2'H3'
H2'
H3'H4'
H4'H5'
H4'
H2'H3'
H3'
H3'H4'
H5'
H4'H5'
3.7
3.6
3.5
3.4
3.3
F2 [ppm]
F1 [ppm]
3.3
3.4
3.5
3.6
3.7

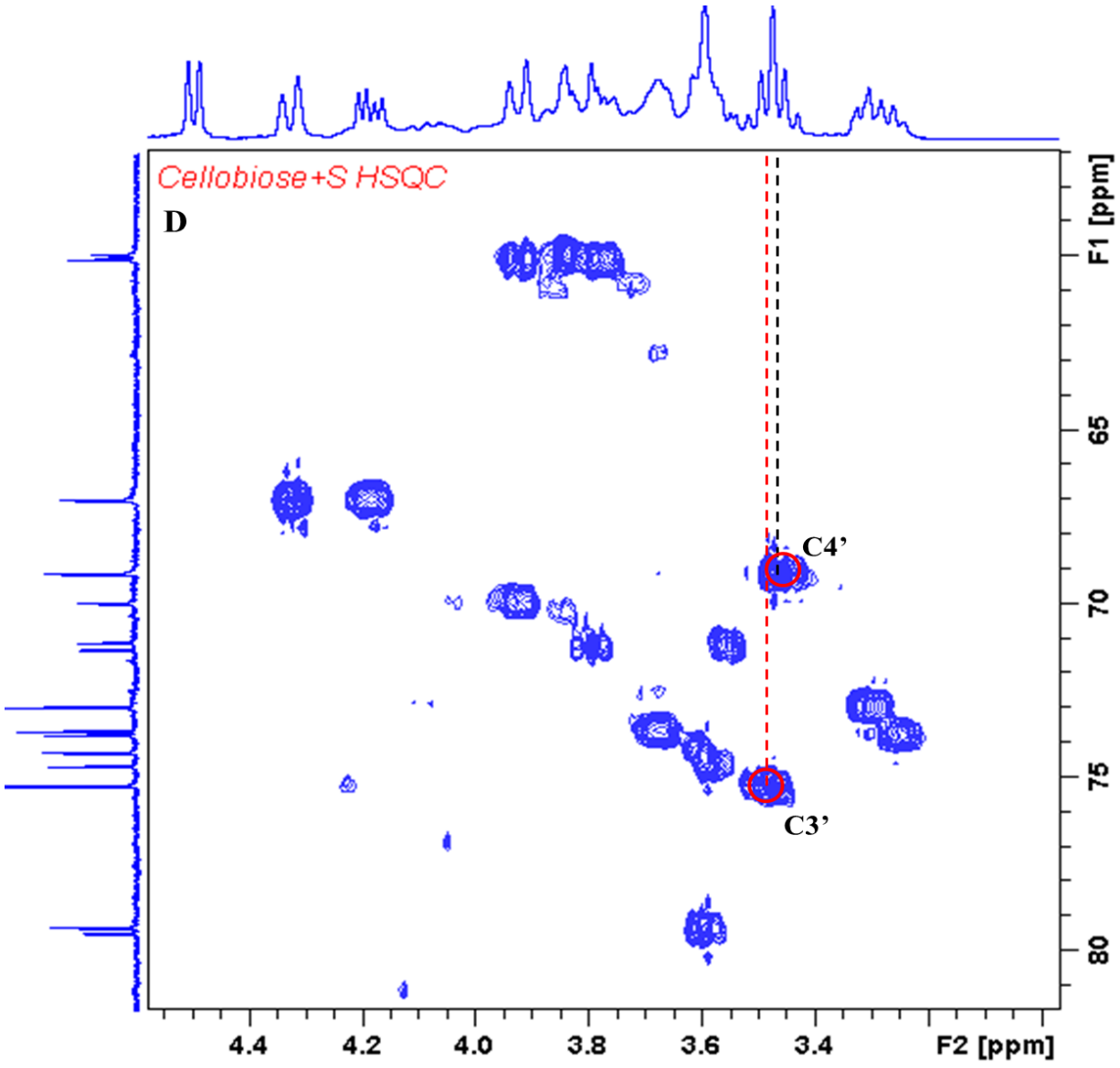

Figure 2.26 COSY of S-cellobiose (A), Partial Expansion of Contour Plots of COSY of S-cellobiose (B), Double-enlarged COSY (C) and HSQC of S-cellobiose (D)

The second method we used to locate the sulfate group was the combination of ^{1}H NMR, DEPT-135, HSQC and TOSCY. DEPT is kind of NMR technique used to distinguish multiplicity of carbon substitution with protons. DEPT-135, HSQC and TOSCY of s-cellobiose were shown in Figure 2.27. Four carbon signals were turned from positive to negative (Figure 2.27 A), which indicated the peaks at 66.95 δ, 66.98 δ, 60.04 δ and 59.89 δ were from the carbon of CH_2 of s-cellobiose. We observed that only α, β C6 and α, β C6' connected to two protons. Therefore,

signals at 4.33 δ and 4.19 δ were identified either from H6 or H6’ which directly bound to C6 or C6’ based on HSQC in Figure 2.27 B. Currently we believed sulfation happened on carbon six but failed to distinguish it on either reducing end or non-reducing end. In TOSCY spectra, there were two cross peaks from coupling of H1’ and H6’1 and coupling of H1’ and H6’2 (Figure 2.27 C), which indicated that they were in same coupling system. Therefore, these downfield shifts in ^{1}H NMR spectra of s-cellobiose were from H6’1 and H6’2 instead of H6-1 and H6-2. As we discussed above, sulfation occurred on C6’ during the process of CNC preparation.

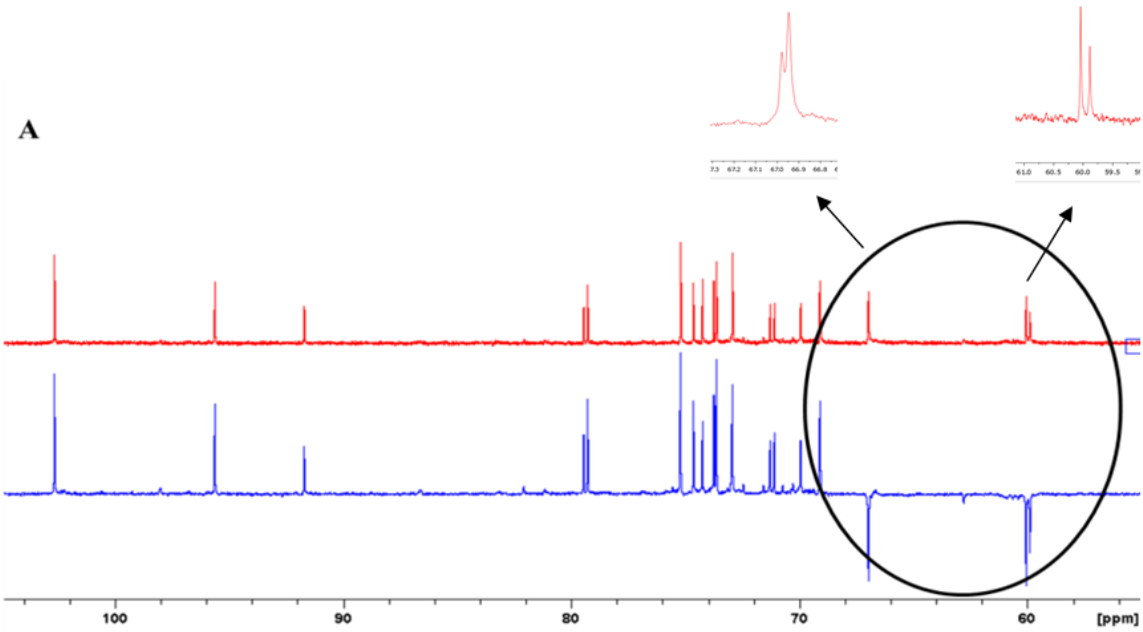

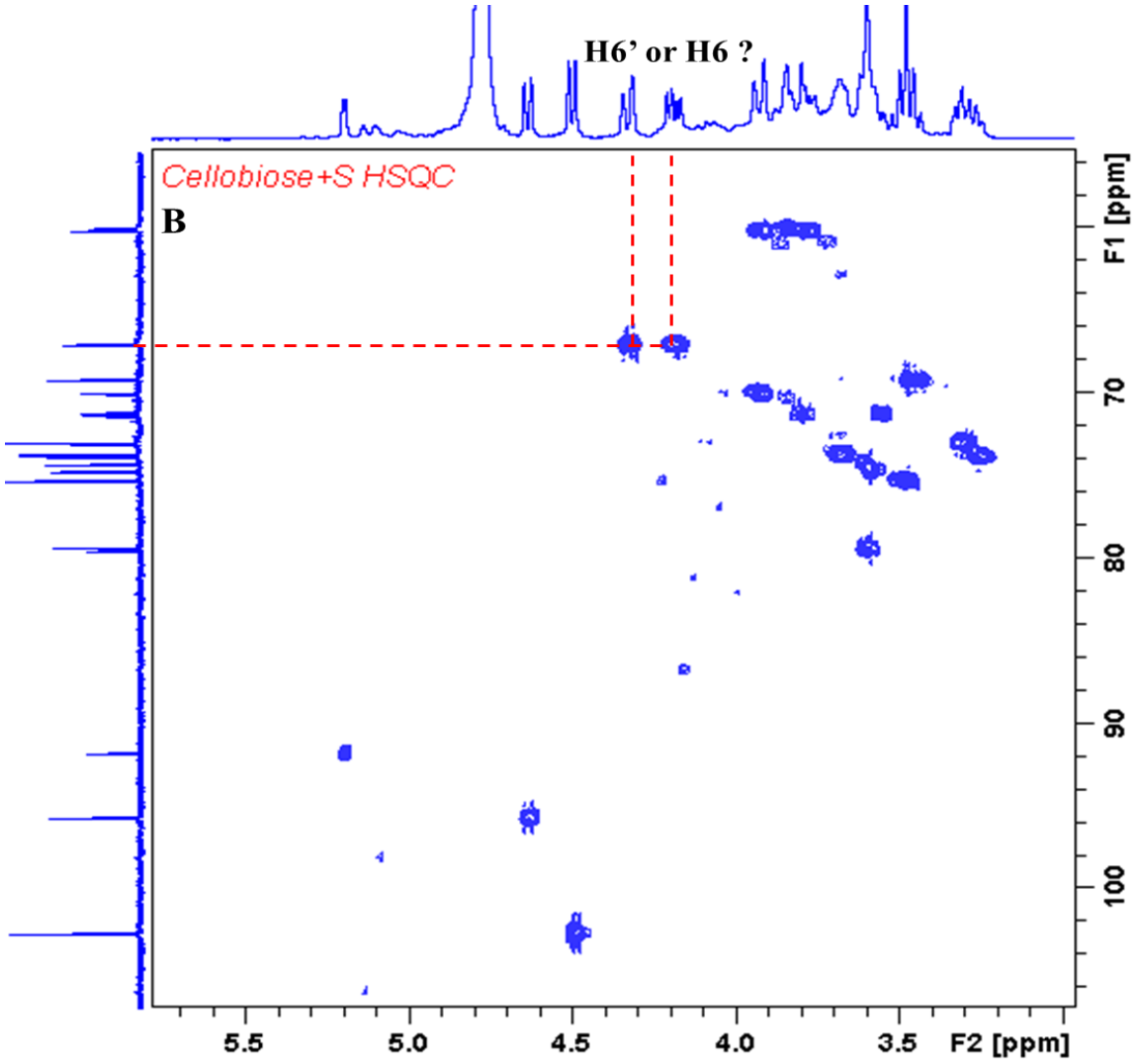
H6' or H6 ?
Cellobiose+S HSQC
B
F1 [ppm]
70
80
90
100
5.5
5.0
4.5
4.0
3.5
F2 [ppm]

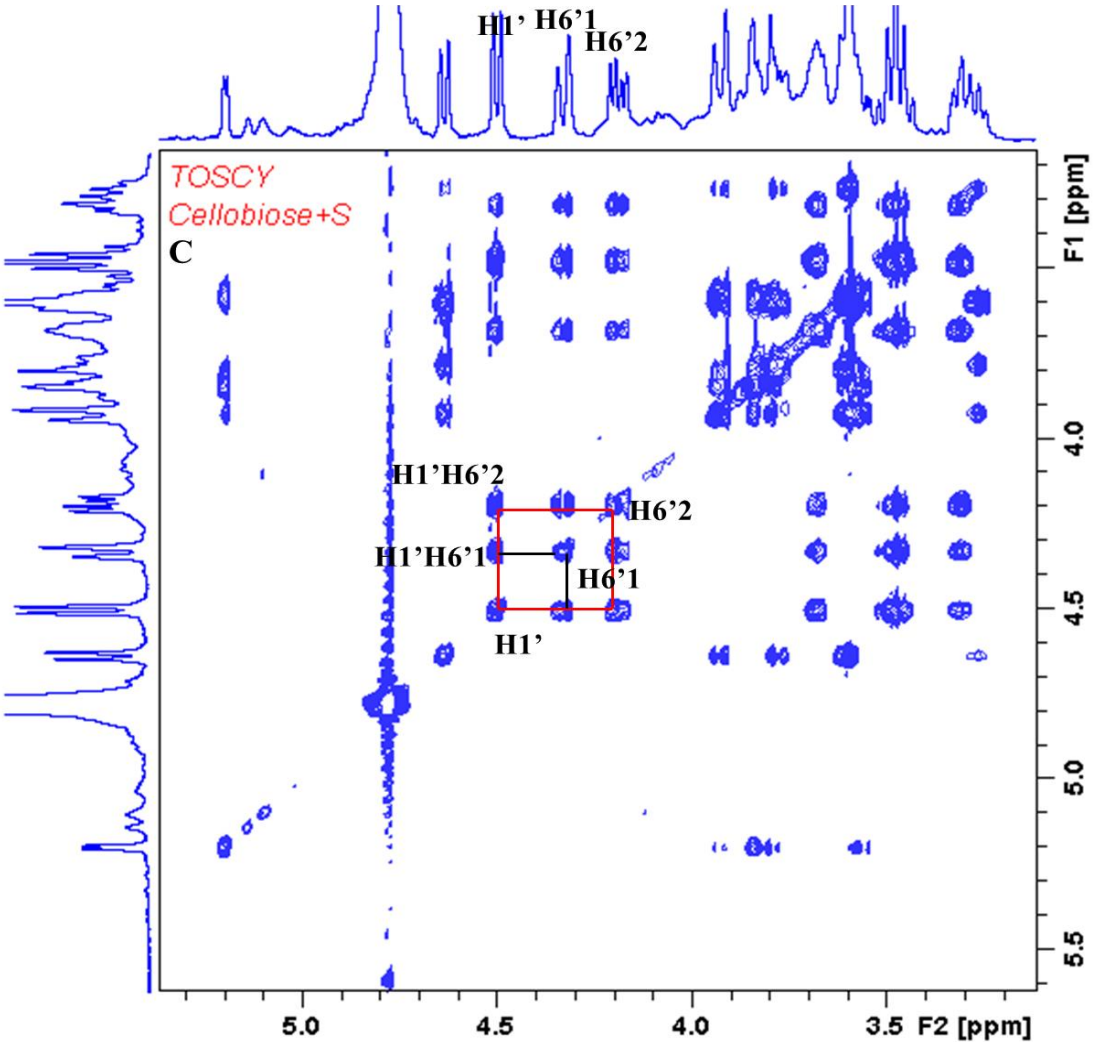

Figure 2.27 ^{13}C and DEPT-135 of S-cellobiose (A), HSQC of S-cellobiose (B), TOSCY of S-cellobiose (C)

4.3.3 Complete ^{1}H and ^{13}C NMR Signal Assignments

Although sulfation position has been finally located, the complete ^{1}H and ^{13}C NMR signals assignments is still meaningful since some of the published data were contradictory (Roslund, Tähtinen et al. 2008). Furthermore, the effect of sulfation on chemical shifts could be investigated according to the assigned peaks before and after modification. Therefore, 1D and 2D NMR were performed to elucidate the assignments (Figure 2.28). The method we used to assign peaks was to combine DQF-COSY, DEPT-135, HSQC, HMBC and TOSCY. The chemical shifts of H' have been analyzed in section 4.3.2, and in turn we could easily assign C1',

C2', C3', C4, C5' and C6' peaks after drawing a vertical and horizontal line in HSQC. Furthermore, we already exactly obtained the chemical shifts of α H1 and β H1, and thus chemical shifts of α H2 (3.55 δ) and β H2 (3.26 δ) could be identified based on the cross peaks in DQF-COSY. In same manner, α H3 (3.80 δ) and β H3 (3.61 δ) was assigned due to the presence of cross peaks. However, α H4 and β H4 were difficult to be directly recognized in DQF-COSY due to overlapped signals. Therefore, it's necessary to combine other 2D NMR results. HMBC (heteromuclear multiple bond correlation) correlates chemical shifts of protons with carbons separated with two or three bonds, in some cases with four bonds (Furihata and Seto 1995). Generally, direct one-bond correlation would be suppressed by setting up the NMR parameters. However, it still could be found in HMBC as two dots, the center of which was the real crossed peak for direct one-bond correlation. Take HMBC of s-cellobiose for example (Figure 2.28 C), two crossed peaks marked in red circles horizontally corresponded to α C1, and no peaks in ^{1}H NMR spectra vertically corresponded to them. However, the center of two symmetrical crossed peaks vertically pointed to the chemical shift of α H1, which indicated a direct one-bond correlation. In other hands, HMBC could also be employed to assign unknown C peaks in ^{13}C NMR spectra. Theoretically, we could find four crossed peaks H1'C2', H1'C3', H1'5' and H1'C4 from the structure of s-cellobiose (Figure 2.28 E). By combination of DQF-COSY and HSQC, we already assigned the chemical shifts of C2', C3' and C5' which at 72.93 δ, 75.19 δ and 73.62 δ, respectively. Therefore, the crossed peak which horizontally corresponded to approximate 80 δ was the correlation of H1' with α, β C4. We could also obtain chemical shifts of α, β H4 based on the carbon-proton cross peaks in HSQC. Additionally, α H4 signal (3.60 δ) displayed a cross peak with a signal at 3.92 δ, which was from α H5. Since C6' signal has been assigned in DEPT-135, we could obtain α, β C6 chemical shift due to its negative signal as well.

Then, α, β H6 signals could be found from HSQC. Finally, β H5 was assigned at 3.57 δ from DQF-COSY. Same approach could be applied to analyze the chemical shifts of cellobiose (Figure 2.29). Finally, the ^{13}C NMR chemical shifts were confirmed by Quantitative ^{13}C NMR (Figure 2.28 F, Figure 2.29 E). Two flowcharts were shown in Figure 2.30 and Figure 2.31, respectively, indicating the process of assignments.

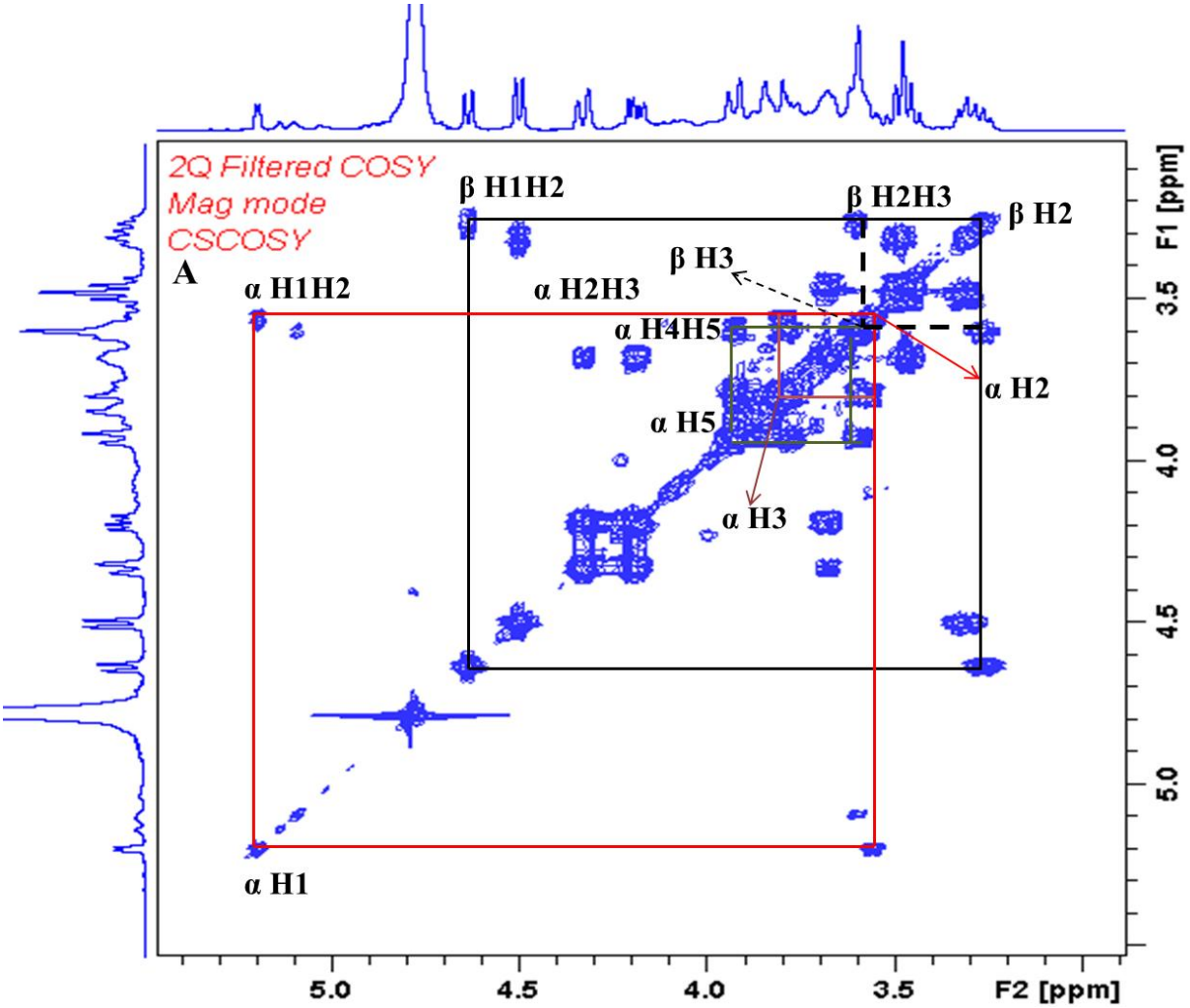

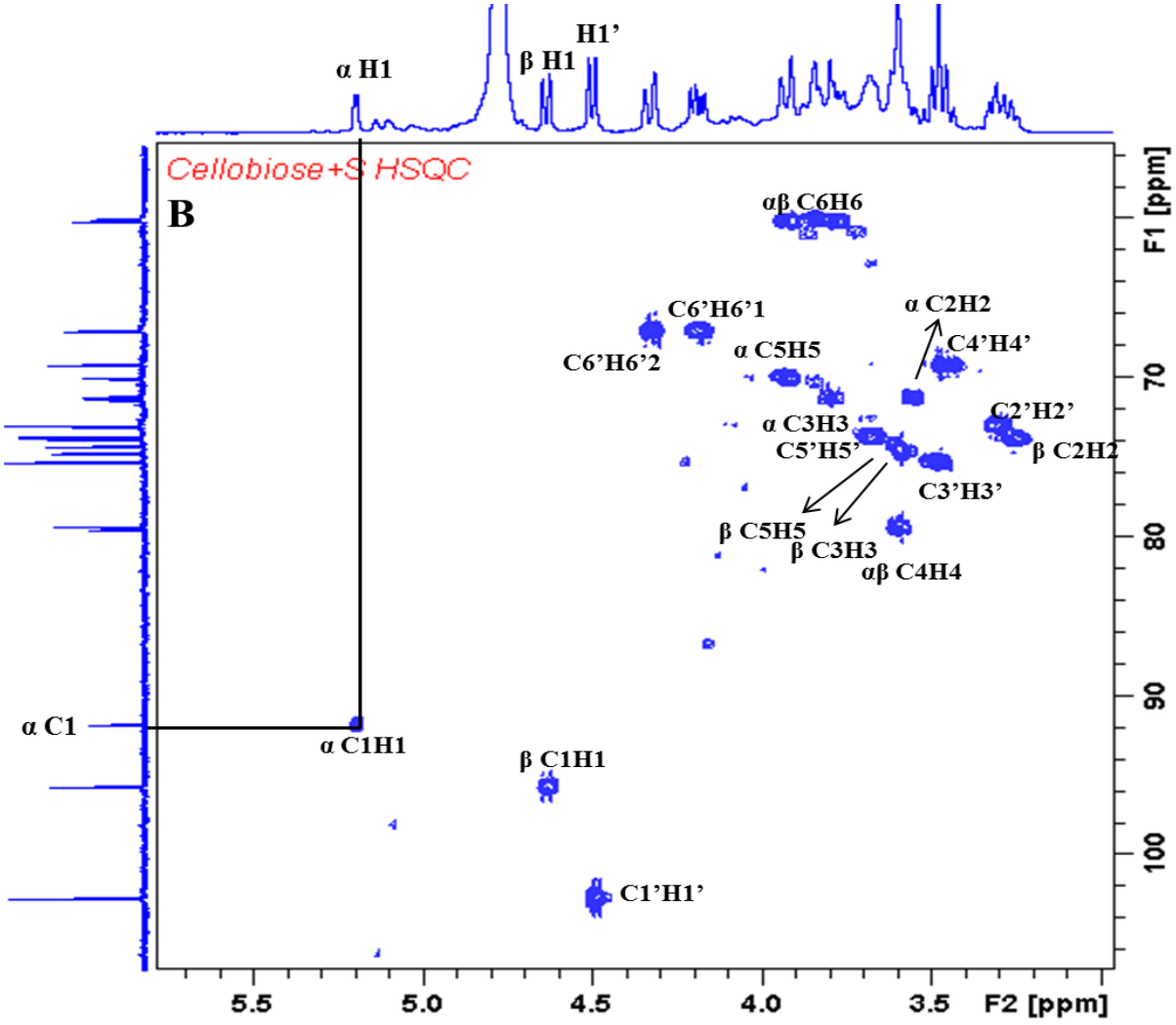
α H1
β H1
H1'
Cellobiose+S HSQC
B
αβ C6H6
C6'H6'1
C6'H6'2
α C5H5
α C2H2
C4'H4'
α C3H3
C5'H5'
C2'H2'
β C2H2
C3'H3'
β C5H5
β C3H3
αβ C4H4
α C1
α C1H1
β C1H1
C1'H1'
F1 [ppm]
70
80
90
100
5.5
5.0
4.5
4.0
3.5
F2 [ppm]

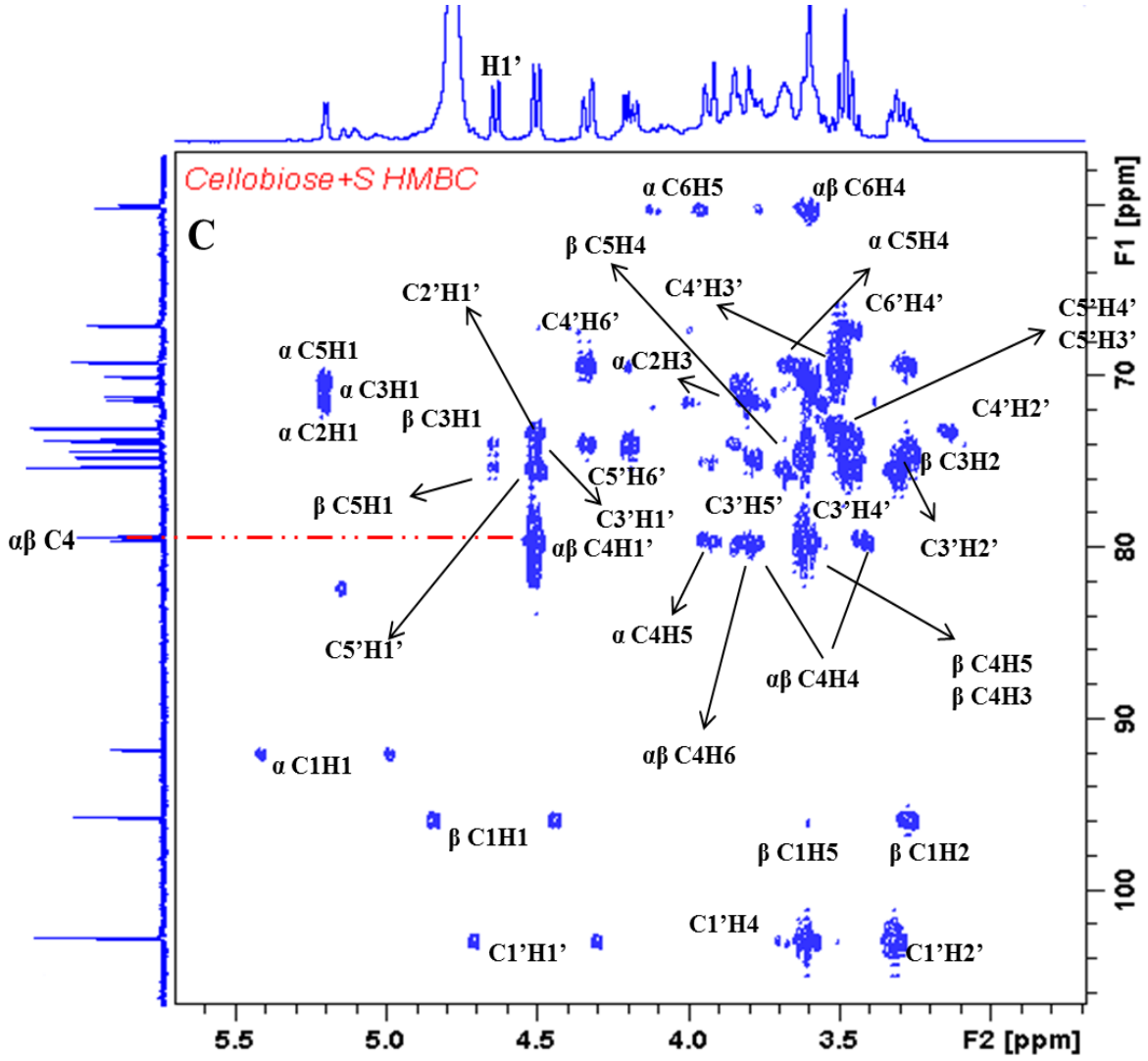
H1'
Cellobiose+S HMBC
C
α C6H5
αβ C6H4
β C5H4
α C5H4
C2'H1'
C4'H3'
C6'H4'
C4'H6'
C5'H4'
C5'H3'
α C5H1
α C3H1
α C2H1
α C2H3
β C3H1
C4'H2'
β C3H2
C5'H6'
β C5H1
C3'H1'
C3'H5'
C3'H4'
αβ C4
αβ C4H1'
C3'H2'
α C4H5
C5'H1'
αβ C4H4
β C4H5
β C4H3
αβ C4H6
α C1H1
β C1H1
β C1H5
β C1H2
C1'H4
C1'H1'
C1'H2'
F1 [ppm]
70
80
90
100
5.5
5.0
4.5
4.0
3.5
F2 [ppm]

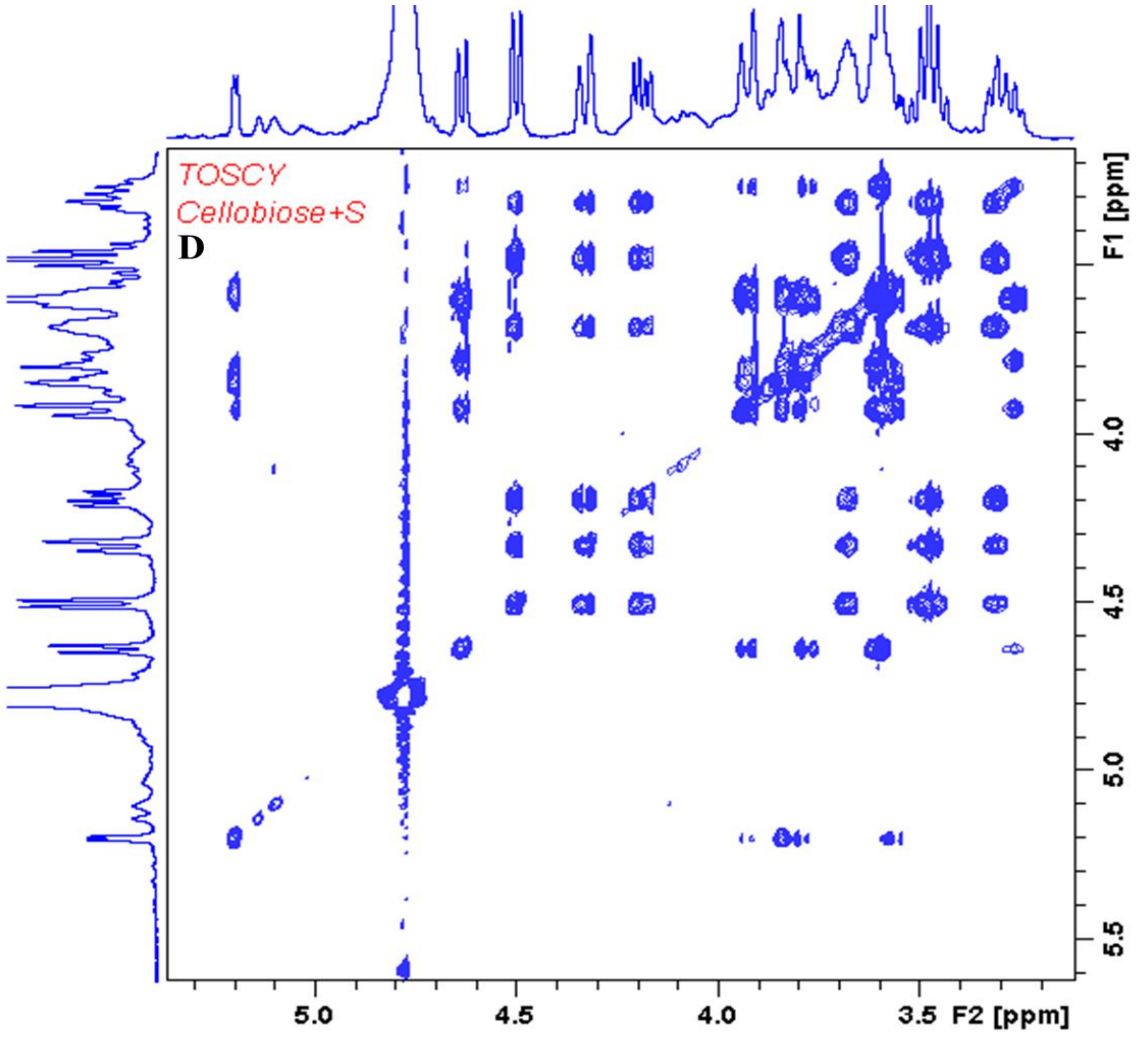
TOSCY
Cellobiose+S
D
F1 [ppm]
4.0
4.5
5.0
5.5
5.0
4.5
4.0
3.5 F2 [ppm]

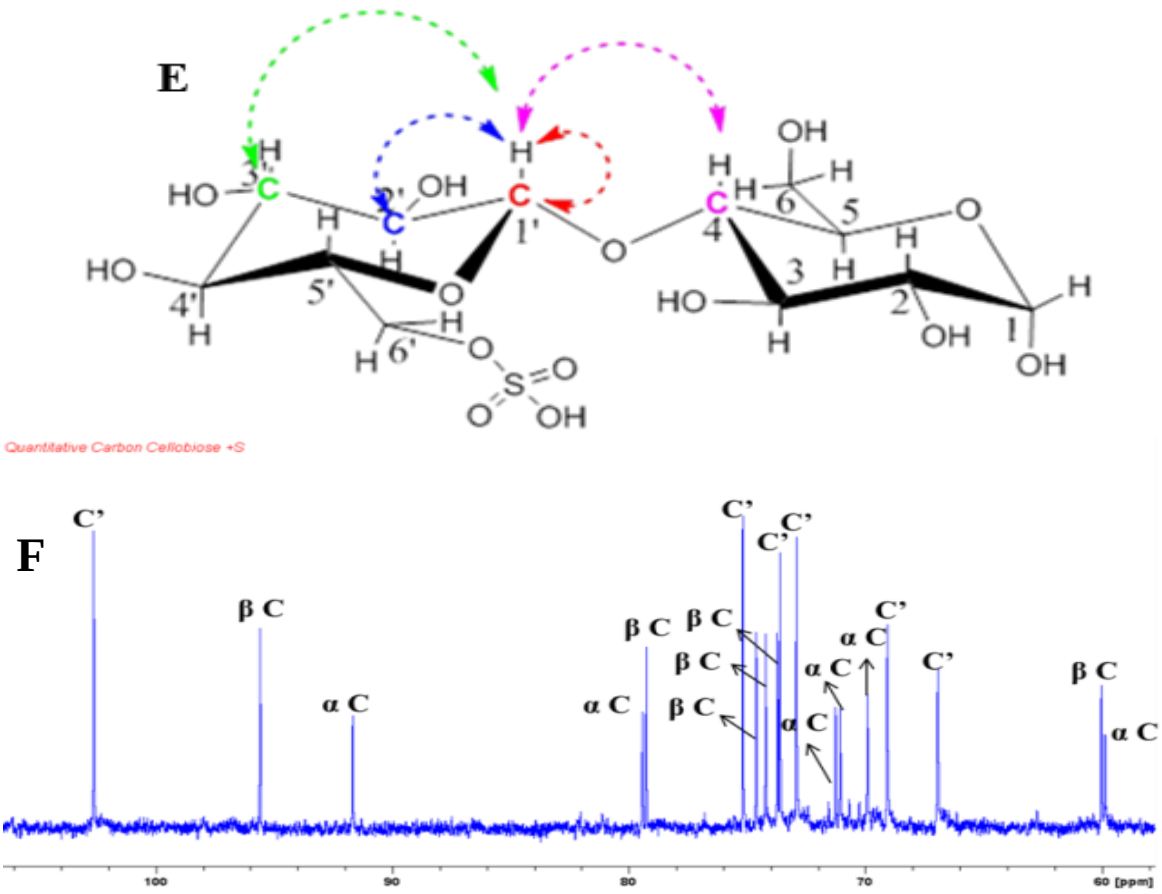

Figure 2.28 HSQC (A), DQF-COSY (B), HMBC (C) and TOSCY (D) of S-cellobiose; Structure of S-cellobiose (E); Quantitative ^{13}C NMR (F)

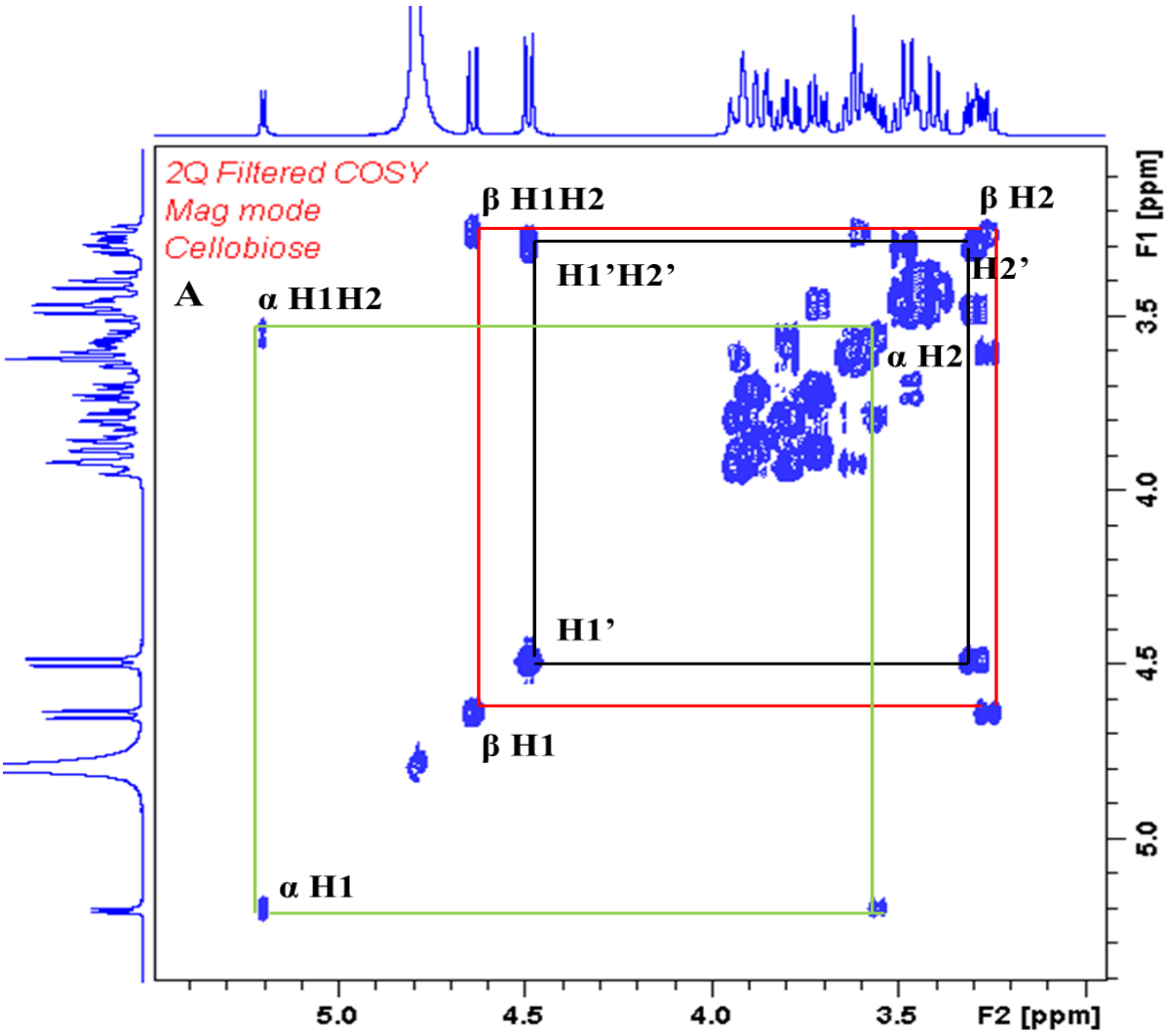
2Q Filtered COSY
Mag mode
Cellobiose
A
β H1H2
β H2
H1'H2'
H2'
α H2
α H1H2
H1'
β H1
α H1
5.0
4.5
4.0
3.5
F2 [ppm]
F1 [ppm]

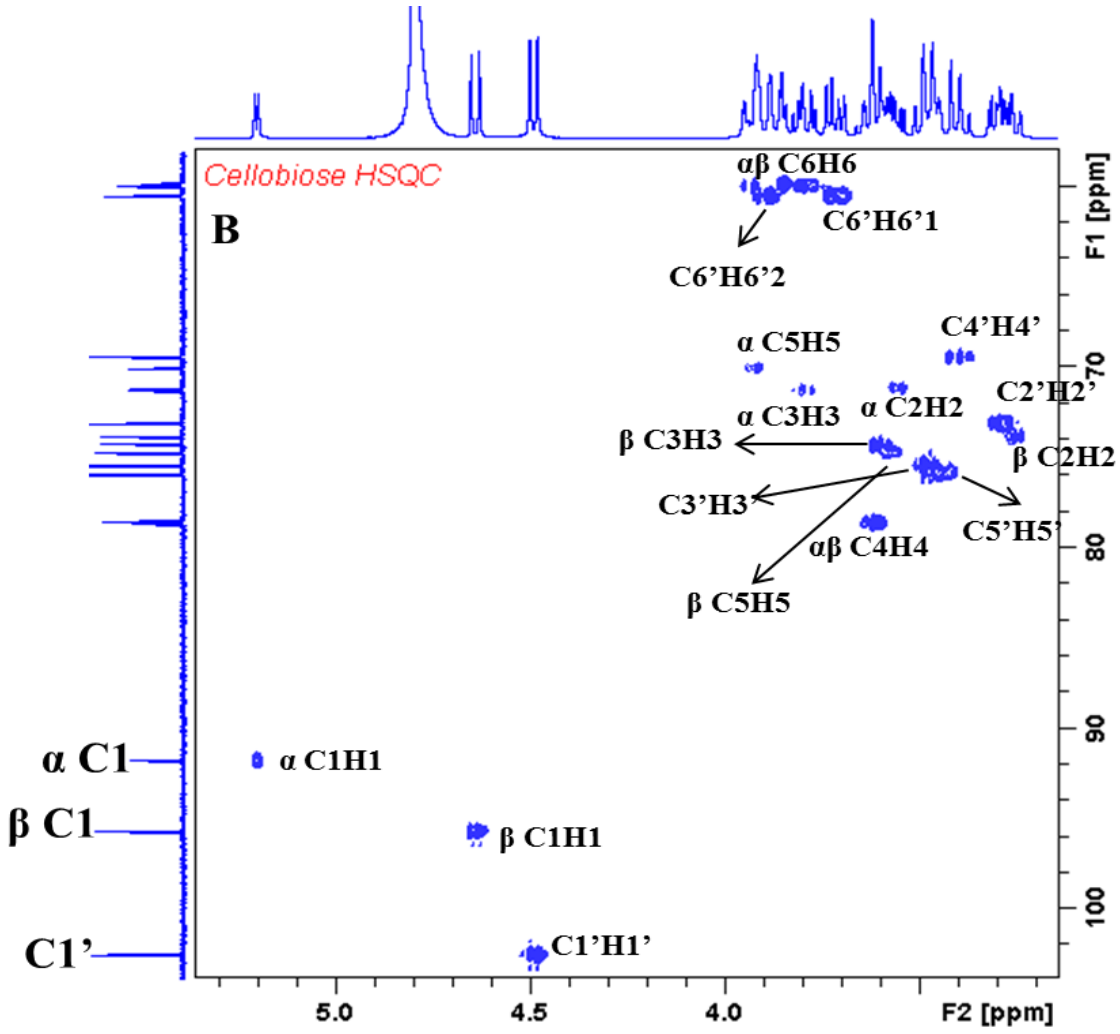
Cellobiose HSQC
B
αβ C6H6
C6'H6'1
C6'H6'2
α C5H5
C4'H4'
α C3H3
α C2H2
C2'H2'
β C3H3
β C2H2
C3'H3
C5'H5'
αβ C4H4
β C5H5
α C1H1
β C1H1
C1'H1'
α C1
β C1
C1'
F1 [ppm]
70
80
90
100
5.0
4.5
4.0
F2 [ppm]

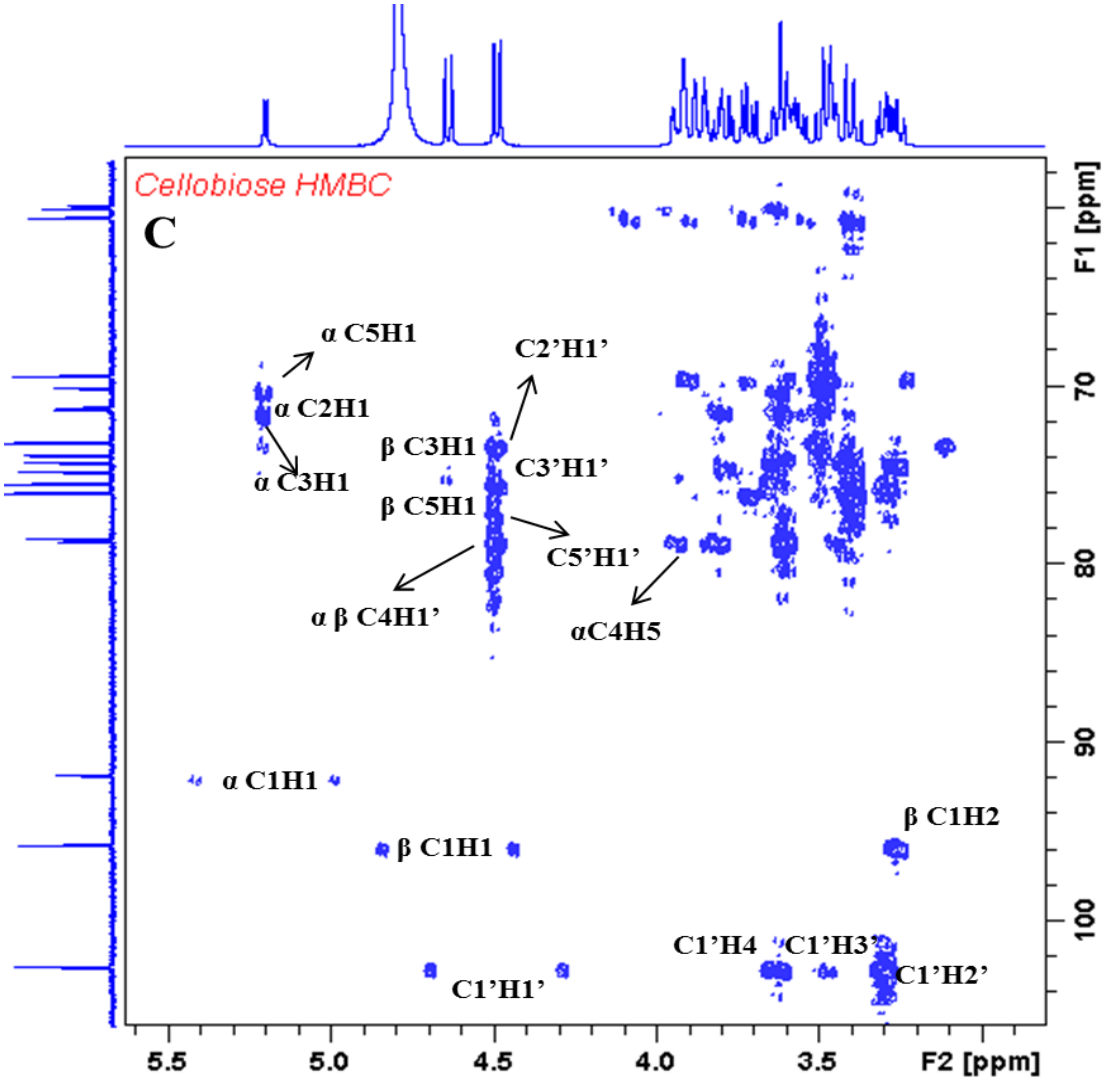
Cellobiose HMBC
C
α C5H1
α C2H1
α C3H1
C2'H1'
β C3H1
C3'H1'
β C5H1
C5'H1'
α β C4H1'
αC4H5
α C1H1
β C1H1
β C1H2
C1'H4
C1'H3'
C1'H2'
C1'H1'
F1 [ppm]
F2 [ppm]
5.5
5.0
4.5
4.0
3.5
70
80
90
100

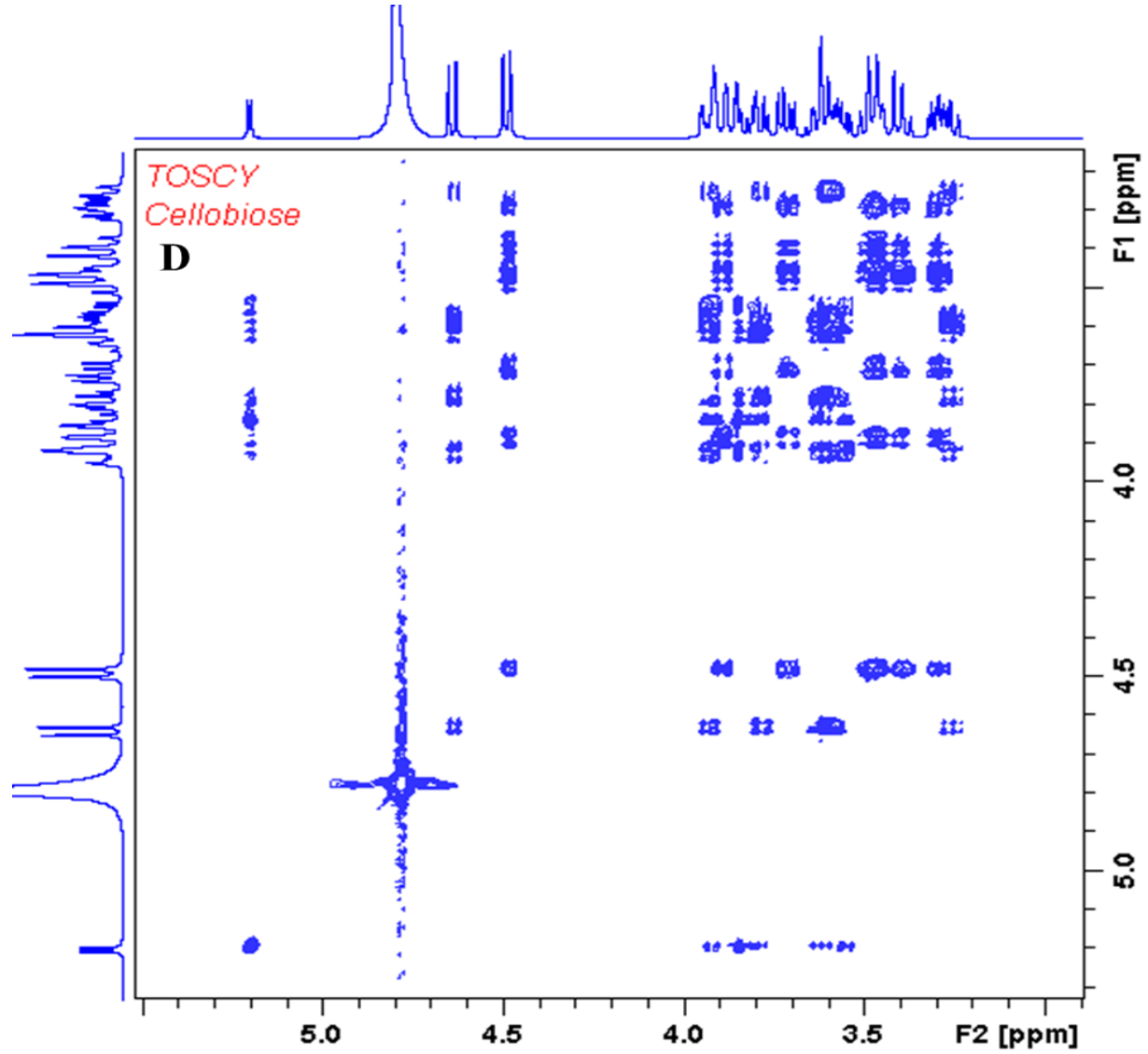

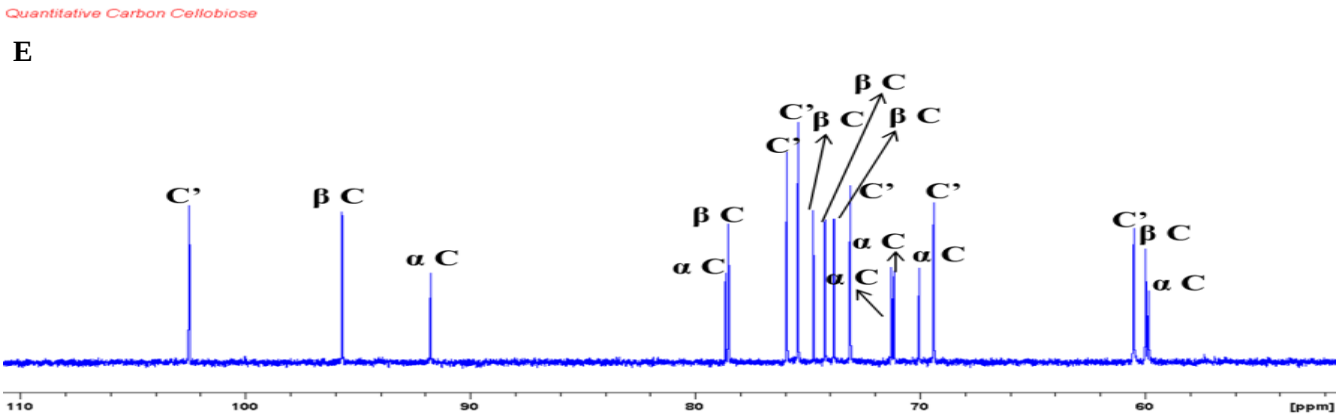

Figure 2.29 DQF-COSY (A), HSQC (B), HMBC (C), TOSCY (D) and Quantitative ^{13}C NMR (E) of Cellobiose

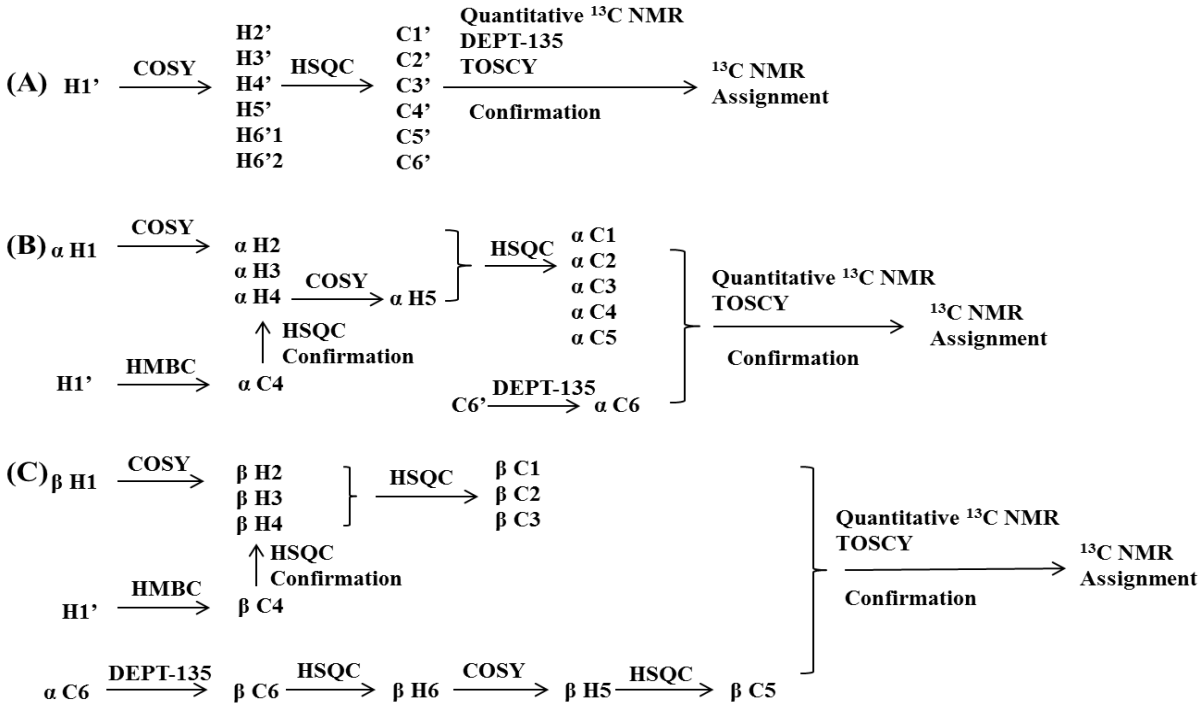

Figure 2.30 Flowchart of ^{13}C NMR Chemical Shifts Assignment of S-cellobiose

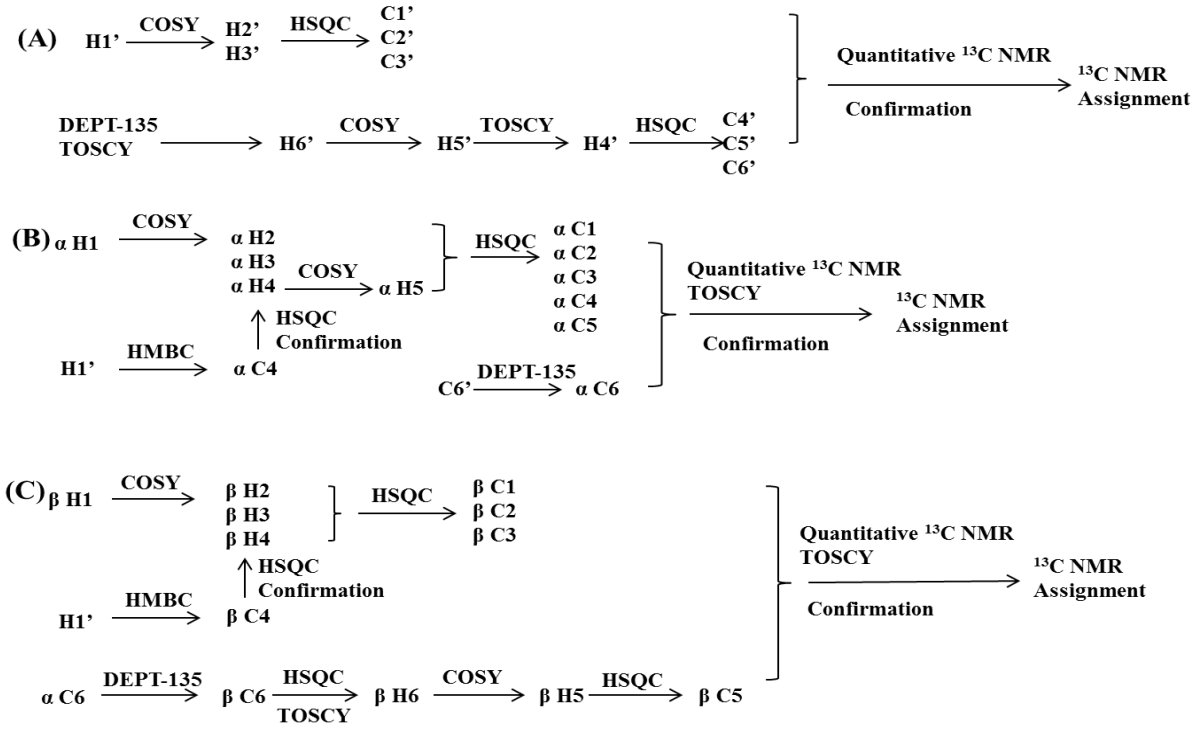

Figure 2.31 Flowchart of ^{13}C NMR Chemical Shifts Assignment of Cellobiose

4.3.4 Discussion and Conclusion of NMR

We have compared chemical shifts between cellobiose and its derivative s-cellobiose to investigate the effect of sulfation on ^{1}H and ^{13}C NMR chemical shifts. The ^{1}H NMR of cellobiose and s-cellobiose were shown in Figure 2.32, and the proton chemical shifts were summarized in Table 2.7. After sulfation occurred on C6', the signals of two proton (H6'1, H6'2) which was bonded to the carbon that directly attached to sulfate groups shifted to downfield by approximate 0.48 and 0.46 δ, respectively. Electron-withdrawing groups would decrease the electron density of protons, which in turn caused a downfield shift. The effect also worked, but not significantly, on the chemical shifts of H4' and H5' with 0.12 and 0.23 δ, respectively. Yamada et al. have presented similar conclusion from ^{1}H NMR characterization of disaccharides prepared from enzyme digestion of chondroitin sulfate and heparin. Signals of protons which directly bound to the O-sulfated carbon and those bound to the neighboring carbon were moved to downfield by 0.4-0.7 and 0.07-0.3 δ, respectively (Yamada, Yoshida et al. 1992). The ^{13}C NMR of cellobiose and s-cellobiose were also compared in Figure 2.33, and summarized in Table 2.8. Three obvious shifts (>0.5 δ) were observed due to sulfated substitution. The signals of α β C4 of s-cellobiose shifted downfield by 0.8 and 0.77 δ, respectively. Another significant downfield shift happened to C6' and the difference was 6.47 δ. This was in accordance with other publications that sulfation would result in a downfield shift of the carbon which directly attached to an electron-withdrawing group (Wang, Niu et al. 2013). However, the signal of C5' shifted upfield by 2.5 δ in contrast to the downfield shifts of H5' in ^{1}H NMR spectra. Similar observation has already been reported that carbon which was indirectly attached to sulfate group would shift upfield (Yang, Gao et al. 2005).

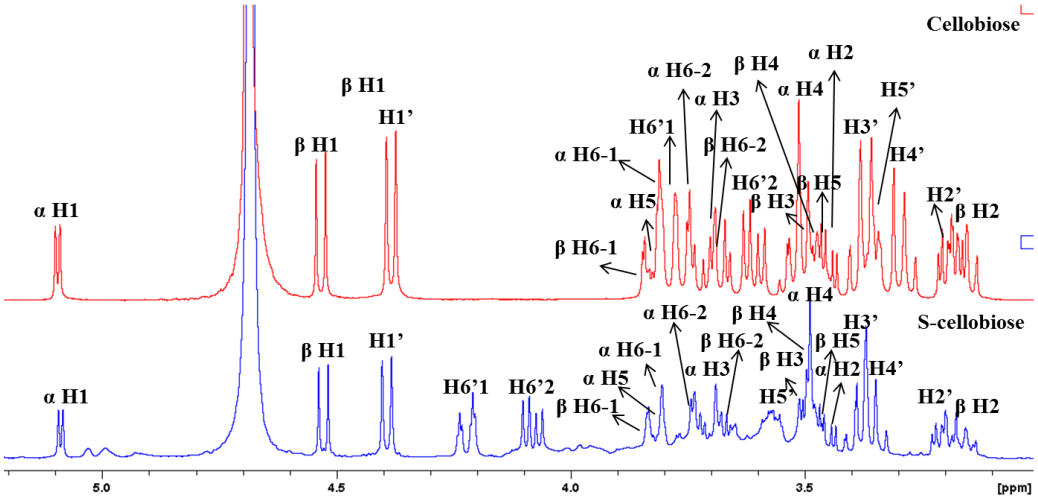

Figure 2.32 Comparison of ^{1}H Chemical Shifts of Cellobiose and S-cellobiose in D_2O

Table 2.7 ^{1}H NMR Chemical Shifts (ppm) of Cellobiose and S-cellobiose in D_2O

Compound	H1	H2	H3	H4	H5	H6-1	H6-2	H1'	H2'	H3'	H4'	H5'	H6'1	H6'2
β-D-Glc6S-(1→4)-α-D-Glc[b]	5.20	3.55	3.80	3.60	3.92	3.91	3.85	4.50	3.30	3.48	3.45	3.68	4.33	4.19
β-D-Glc6S-(1→4)-β-D-Glc	4.63	3.26	3.61	3.60	3.57	3.94	3.77	4.50	3.30	3.48	3.45	3.68	4.33	4.19
β-D-Glc-(1→4)-α-D-Glc[a]	5.20	3.54	3.80	3.61	3.93	3.91	3.84	4.48	3.31	3.48	3.40	3.44	3.88	3.71
β-D-Glc-(1→4)-β-D-Glc	4.63	3.25	3.59	3.58	3.56	3.94	3.79	4.48	3.31	3.48	3.40	3.44	3.88	3.71

a=cellobiose; b=s-cellobiose; Chemical Shifts are Expressed in ppm; Error Range of Chemical Shifts is ± 0.01 ppm

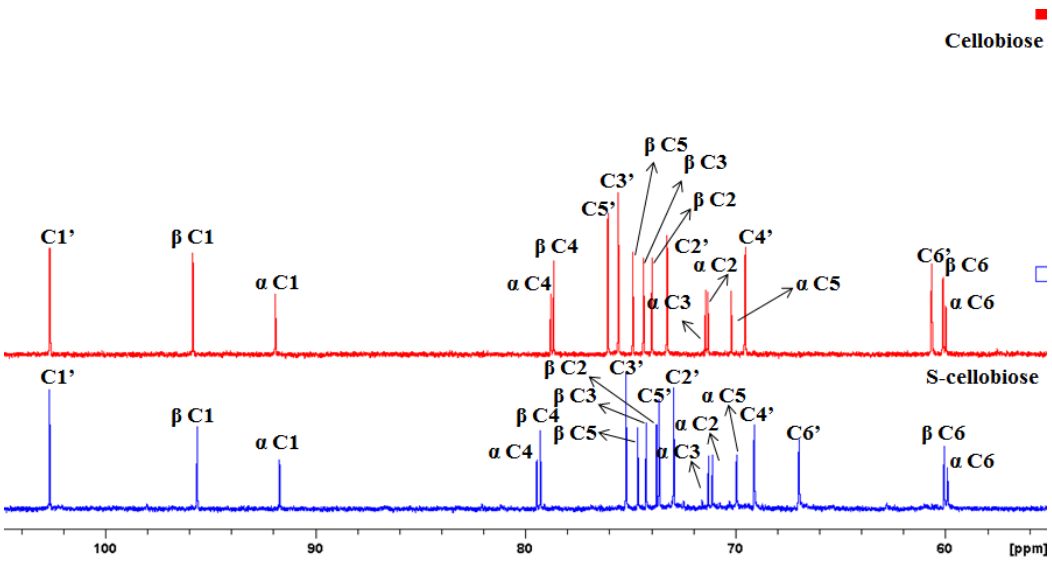

Figure 2.33 Comparison of ^{13}C NMR Chemical Shifts of Cellobiose and S-cellobiose in D_2O

Table 2.8 ^{13}C NMR Chemical Shifts of Cellobiose and S-cellobiose in D_2O

Compound	C1	C2	C3	C4	C5	C6	C1'	C2'	C3'	C4'	C5'	C6'
β-D-Glc6S-(1→4)-α-D-Glc[b]	91.69	71.08	71.27	79.44	69.93	59.89	102.64	72.93	75.19	69.10	73.62	66.98
β-D-Glc6S-(1→4)-β-D-Glc	95.61	73.74	74.23	79.27	74.63	60.04	102.64	72.93	75.19	69.07	73.62	66.95
β-D-Glc-(1→4)-α-D-Glc[a]	91.75	71.15	71.27	78.64	70.04	59.83	102.47	73.10	75.42	69.39	75.92	60.51
β-D-Glc-(1→4)-β-D-Glc	95.68	73.82	74.22	78.5	74.73	59.96	102.49	73.09	75.42	69.38	75.92	60.49

a=cellobiose; b=s-cellobiose; Chemical Shifts are Expressed in ppm;

4.4 Surface Chemistry of CNC-S

The preparation of CNC-S involves a process of selectively hydrolyzing amorphous regions of cellulose fibers, and also introduction of sulfate groups on its surface. Therefore, surface chemistry is important for CNC-S properties and applications. Lin et al. have investigated the effect of sulfation degree on surface chemistry and physical properties of CNC through regulation of reaction conditions (Lin and Dufresne 2014). Although distribution of substitutions of sulfate groups in carbohydrate derivatives is considered to affect their properties, the precise position of sulfate groups on CNC-S has never been investigated. Therefore, in this section, we have first investigated the distribution of sulfate groups on the surface of CNC-S combining with the proposed cellulose model.

4.4.1 Estimation of Surface Sulfate Groups Levels in CNC-S

Several representative models to describe CNC-S have been proposed, which exhibits a rod-like pattern with an either square or rectangular section. According to our XRD results (B_{110} = 4.6 nm, $B_{1\text{-}10}$ = 4.6 nm), as well as previous reports (Elazzouzi-Hafraoui, Nishiyama et al. 2007), a representative cross-section of the crystalline regions of Avicel was proposed in Figure 2.34. 22 glucan chains could be found on the surface of crystal. Considering three hydroxyl groups within one cellobiose faces outside of cellulose according to well-known cellulose I structures, 66

hydroxyl groups are available for sulfation. The number of hydroxyl groups per unit surface area (N_h) on CNC-S can be calculated as 5.78×10^{-3} mmol/m^{-2} based on the following equation:

$$N_h = \frac{N_s}{N_A(2B_{110}L_c + 2B_{1-10}L_c)}$$

Where N_s equals to available hydroxyl groups within one cellobiose on the surface of CNC; N_A is Avogadro's number; B_{110} and B_{1-10} represents the 110 plane and 1-10 plane dimensions; L_c is the length of cellobiose (1.03 nm).

For simplification, CNC was assumed to have square cross sections, and the surface area consequently can be calculated according to the equation:

$$A_{total} = \frac{m_{NCC}A_{single(CNC)}}{\rho_{cellulose}V_{single(CNC)}}$$

$$A_{single(CNC)} = 4WL$$

$$V_{single(CNC)} = W^2L$$

Where A_{total} represents all surface area of CNC; m_{CNC} is the quality of CNC; $\rho_{cellulose}$ is the density of cellulose (1.50 g/cm^3); $A_{single(CNC)}$ and $V_{single(CNC)}$ is the surface area and volume of a single CNC, respectively. W and L equal to width and length of CNC.

The degree of substitution (DS) of surface hydroxyl groups (-OH) can be calculated based on the following equations (Lin and Dufresne 2014):

$$DS = \frac{n_{-oso_3^-}}{n_{surface(OH)}}$$

$$n_{-oso_3^-} = \frac{m_S}{M_S} = \frac{m_{CN}S\%}{M_S}$$

$$n_{surface(-OH)} = N_h A_{total}$$

Where $n_{-oso_3^-}$ and $n_{surface(-OH)}$ represent the mole fraction of sulfate groups and surface hydroxyl groups, respectively; m_s is the sulfur content (g), m_{CN} is the quality of CNC; *S%* is the sulfur percentage obtained from elemental analysis; *Ms* is the molar mass of sulfur.

Based on equations mentioned above, the degree of substitution of surface hydroxyl groups was 11.19 % after sulfuric acid hydrolysis of cellulose, which indicated some hydroxyl groups remained.

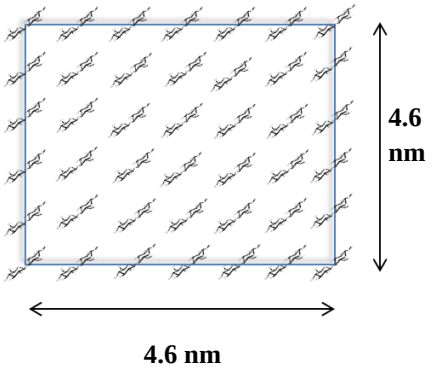

Figure 2.34 Cross-sections of Elementary Crystallites Calculated from Scherrer Equation (Black Bar Represent a Glucan Chain)(Elazzouzi-Hafraoui, Nishiyama et al. 2007)

4.4.2 Determination of Surface Sulfate Groups Position in CNC-S

Zhang et al. have reported C6 position of microcrystalline cellulose (MCC) was easily subject to sulfation in comparison with C2 and C3 position unless using excessive chlorosulfuric acid (Zhang, Brendler et al. 2011). However, the distribution of sulfate groups on CNC prepared by sulfuric acid hydrolysis has never been reported. This subject is particularly interesting due to its potential role in resolving the inconsistent conclusions of effects of sulfate groups on thermal stability (Roman and Winter 2004) (Lin and Dufresne 2014), or explaining the negative effect of sulfate groups on fluorescent labeling of CNC (Abitbol, Palermo et al. 2013). The degree of

substitution of surface hydroxyl groups was 11.19 % which was lower than 33 % (active hydroxyl groups located on C6). Hydroxyl groups on C6 generally display high reactivity in comparison with those of C2 and C3. According to DS, some of hydroxyl groups on C6 remained, and there was less chance for hydroxyl groups on C2 and C3 to be reacted. Therefore, we hypothesized that during the process of CNC preparation, hydroxyls groups on C6 was sulfated similar to TEMPO-mediated oxidation (Okita, Saito et al. 2010).

In order to confirm our hypothesis, we used commercial enzymes (cellulase) for the degradation of CNC-S (0.1 g). The enzymatic hydrolysis reaction was incubated at 50 °C with shaking at 150 rpm for five days with high enzyme loading. Cellobiose sulfate (7.9 mg), β-D-Glc6S-(1→4)-α or β-D-Glc, was collected and characterized. The sulfur percentage was calculated as 0.61 % which is similar to 0.69 % from elemental analysis. No products with substitution on hydroxyl groups of C2 or C3 were found. In Figure 2.35 A, cellulase hydrolysis mechanism indicated that cellobiose sulfate was released from CBH which could process one cellulose chain in an energetically preferred conformation into their catalytic domain and slide unidirectionally on cellulose surface (Igarashi, Uchihashi et al. 2011). Therefore, we believed that hydroxyl groups from the surface cellulose chain which were buried inside the cellulose were unavailable for sulfation (Figure 2.35 B). Summarily, CNC preparation under the conditions used in this thesis (64% w/v, 45°C, 1h) mainly involveed a sulfation reaction between acid and C6 hydroxyl groups rather than those of C2 and/or C3 exposed on the entire surfaces of cellulose crystals. From this observation, we suggest that process to remove the sulfate groups was necessary for further CNC modification since some of reactive hydroxyl groups at C6 were substituted.

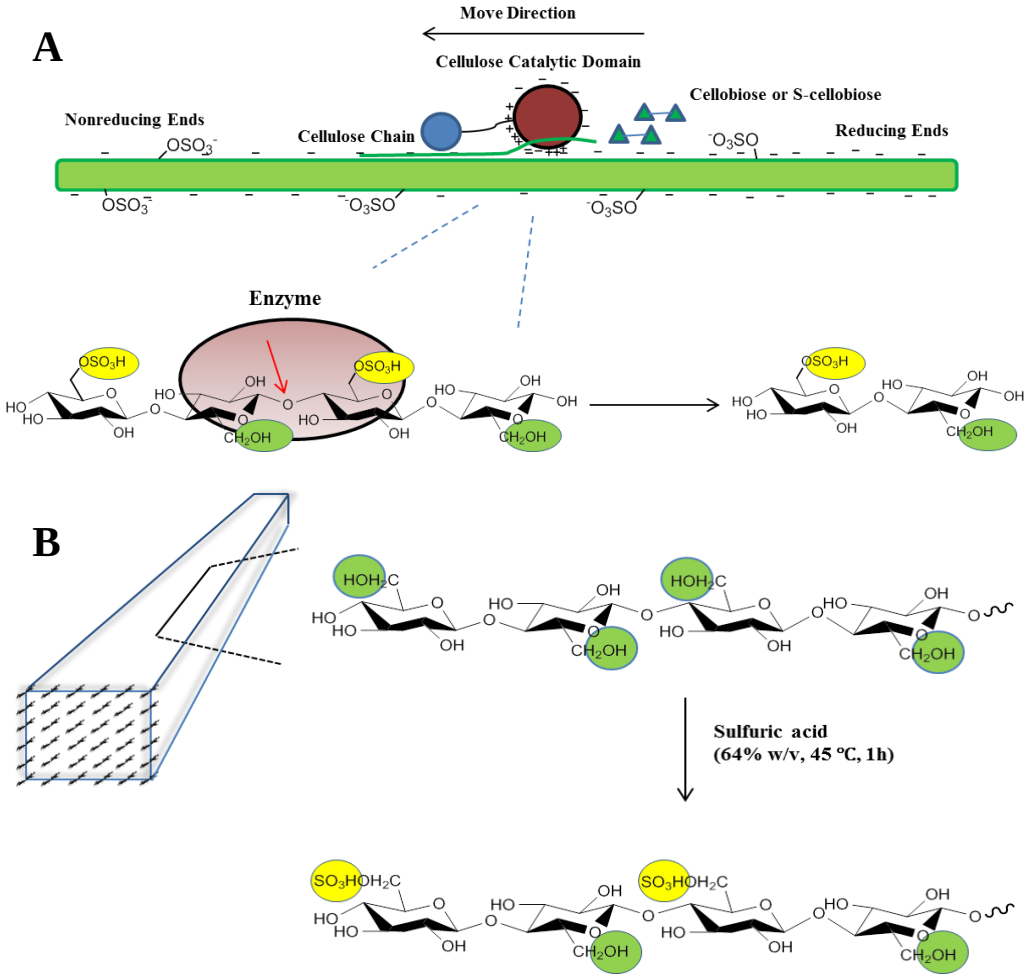

Figure 2.35 Potential Mechanisms of Sulfation of CNC and Enzymatic Hydrolysis of CNC-S (Divne, Ståhlberg et al. 1998; Habibi, Lucia et al. 2010; Kurašin and Väljamäe 2011; Baptista, Ferreira et al. 2013)

Conclusion

In this thesis, firstly, cellulose nanocrystals (CNC) were successfully prepared by hydrolysis of sulfuric acid and hydrochloric acid, respectively. The chemical and physical characteristics of CNC, such as surface charge, crystallinity, dispersion and dimension, were investigated. Furthermore, we have studied the effect of sulfate groups of CNC-S on cellulase adsorption and enzymatic hydrolysis. Sulfate groups on CNC-S could promote the enzyme adsorption, but surprisingly inhibited enzymatic hydrolysis of cellulose substrates. Electrostatic interaction between cellulase and charged substrates was demonstrated by the effects of pH and ionic strength on enzyme adsorption.

Analysis of enzymatic hydrolysate of CNC-S showed there was a new compound except for glucose in HPLC. We applied LC-MS and NMR to elucidate its structure. It's a cellobiose sulfate, and one sulfate group bound to C6'-O of nonreducing end of cellobiose. Considering the CBH hydrolysis mechanism, the presence of cellobiose sulfate indicated that sulfated cellulose chain could be hydrolyzed by CBH. Furthermore, cellulase desorption experiments indicated that there was a strong irreversible binding between enzyme and CNC-S. This irreversible binding probably resulted in lower hydrolysis yield of CNC-S.

Additionally, one surface property of CNC-S, substitution pattern of sulfate groups, was investigated by analyzing the structure of cellobiose sulfate combining with cellulose model. We believed that hydroxyl groups of C6 of cellulose chain showed highest reactivity during the process of CNC preparation. It was first time to present a structural picture of CNC-S with sulfated modification of hydroxyl groups of C6. Furthermore, hydroxyl groups of C6 were

alternatively exposed at the surface crystal and those faced inside cellulose crystal were unavailable to be sulfated.

Reference

Abitbol, T., E. Kloser, et al. (2013). "Estimation of the Surface Sulfur Content of Cellulose Nanocrystals Prepared by Sulfuric Acid Hydrolysis." Cellulose **20**(2): 785-794.

Abitbol, T., A. Palermo, et al. (2013). "Fluorescent Labeling and Characterization of Cellulose Nanocrystals with Varying Charge Contents." Biomacromolecules **14**(9): 3278-3284.

Agrawal, P. K. (1992). "NMR Spectroscopy in the Structural Elucidation of Oligosaccharides and Glycosides." Phytochemistry **31**(10): 3307-3330.

Ahola, S., X. Turon, et al. (2008). "Enzymatic Hydrolysis of Native Cellulose Nanofibrils and Other Cellulose Model Films: Effect of Surface Structure." Langmuir **24**(20): 11592-11599.

Araki, J. and S. Kuga (2001). "Effect of Trace Electrolyte on Liquid Crystal Type of Cellulose Microcrystals." Langmuir **17**(15): 4493-4496.

Araki, J., M. Wada, et al. (2000). "Steric Stabilization of a Cellulose Microcrystal Suspension by Poly(ethylene glycol) Grafting." Langmuir **17**(1): 21-27.

Araki, J., M. Wada, et al. (1998). "Flow properties of microcrystalline cellulose suspension prepared by acid treatment of native cellulose." Colloids and Surfaces A: Physicochemical and Engineering Aspects **142**(1): 75-82.

Astbury, W. and M. Davies (1944). "Structure of Cellulose." Nature **154**: 84.

Atalla, R. H. and D. L. Vanderhart (1984). "Native Cellulose: A Composite of Two Distinct Crystalline Forms." Science **223**(4633): 283-285.

Auad, M. L., V. S. Contos, et al. (2008). "Characterization of Nanocellulose- Reinforced Shape Memory Polyurethanes." Polymer International **57**(4): 651-659.

Balbach, J., V. Forge, et al. (1995). "Following Protein Folding in Real Time using NMR Spectroscopy." Nature Structural & Molecular Biology **2**(10): 865-870.

Baptista, A., I. Ferreira, et al. (2013). "Cellulose-based bioelectronic devices." Cellulose-Medical, Pharmaceutical and Electronic Applications: InTech.

Beck-Candanedo, S., M. Roman, et al. (2005). "Effect of Reaction Conditions on the Properties and Behavior of Wood Cellulose Nanocrystal Suspensions." Biomacromolecules **6**(2): 1048-1054.

Bhardwaj, N. K., S. Kumar, et al. (2004). "Effects of Processing on Zeta Potential and Cationic Demand of Kraft Pulps." Colloids and Surfaces A: Physicochemical and Engineering Aspects **246**(1): 121-125.

Bisaria, V. S. and T. K. Ghose (1981). "Biodegradation of Cellulosic Materials: Substrates, Microorganisms, Enzymes and Products." Enzyme and Microbial Technology **3**(2): 90-104.

Bodin, A., L. Ahrenstedt, et al. (2007). "Modification of Nanocellulose with a Xyloglucan–RGD Conjugate Enhances Adhesion and Proliferation of Endothelial Cells: Implications for Tissue Engineering." Biomacromolecules **8**(12): 3697-3704.

Claesson, P. M., E. Blomberg, et al. (1995). "Protein Interactions at Solid Surfaces." Advances in Colloid and Interface Science **57**: 161-227.

Dasari, R. and R. Eric Berson (2007). "The Effect of Particle Size on Hydrolysis Reaction Rates and Rheological Properties in Cellulosic Slurries." Applied Biochemistry and Biotechnology **137-140**(1-12): 289-299.

De Souza Lima, M. M., J. T. Wong, et al. (2002). "Translational and Rotational Dynamics of Rodlike Cellulose Whiskers." Langmuir **19**(1): 24-29.

Dehnad, D., H. Mirzaei, et al. (2014). "Thermal and Antimicrobial Properties of Chitosan–nanocellulose Films for Extending Shelf Life of Ground Meat." Carbohydrate Polymers **109**(0): 148-154.

Deyrup, S. T., L. E. Eckman, et al. (2011). "2D NMR-spectroscopic Screening Reveals Polyketides in Ladybugs." Proceedings of the National Academy of Sciences **108**(24): 9753-9758.

Divne, C., J. Ståhlberg, et al. (1998). "High-resolution Crystal Structures Reveal How a Cellulose Chain is Bound in the 50 Å Long Tunnel of Cellobiohydrolase I from< i> Trichoderma reesei</i>." Journal of molecular biology **275**(2): 309-325.

Dong, X., J.-F. Revol, et al. (1998). "Effect of Microcrystallite Preparation Conditions on the Formation of Colloid Crystals of Cellulose." Cellulose **5**(1): 19-32.

Drake, E. N. and C. E. Brown (1977). "Application of NMR to Biochemical Kinetics. A laboratory Experiment in Physical Biochemistry." Journal of Chemical Education **54**(2): 124.

Drzaic, P. S. (1995). Liquid Crystal Dispersions, World Scientific.

Duus, J. Ø., C. H. Gotfredsen, et al. (2000). "Carbohydrate Structural Determination by NMR Spectroscopy: Modern Methods and Limitations†." Chemical Reviews **100**(12): 4589-4614.

Elazzouzi-Hafraoui, S., Y. Nishiyama, et al. (2007). "The Shape and Size Distribution of Crystalline Nanoparticles Prepared by Acid Hydrolysis of Native Cellulose." Biomacromolecules **9**(1): 57-65.

Fan, M., D. Dai, et al. (2012). "Fourier Transform Infrared Spectroscopy for Natural Fibres." Fourier Transform–Materials Analysis. intech.

Fox, J. M., S. E. Levine, et al. (2011). "Initial- and Processive-Cut Products Reveal Cellobiohydrolase Rate Limitations and the Role of Companion Enzymes." Biochemistry **51**(1): 442-452.

Furihata, K. and H. Seto (1995). "Decoupled HMBC (D-HMBC), an Improved Technique of HMBC." Tetrahedron letters **36**(16): 2817-2820.

Garcia-Galan, C., Á. Berenguer-Murcia, et al. (2011). "Potential of Different Enzyme Immobilization Strategies to Improve Enzyme Performance." Advanced Synthesis & Catalysis **353**(16): 2885-2904.

Gilkes, N. R., B. Henrissat, et al. (1991). "Domains in Microbial Beta-1, 4-glycanases: Sequence Conservation, Function, and Enzyme Families." Microbiological Reviews **55**(2): 303-315.

Goyal, A., B. Ghosh, et al. (1991). "Characteristics of Fungal Cellulases." Bioresource Technology **36**(1): 37-50.

Graf, J., P. H. Nguyen, et al. (2007). "Structure and Dynamics of the Homologous Series of Alanine Peptides: A Joint Molecular Dynamics/NMR Study." Journal of the American Chemical Society **129**(5): 1179-1189.

Grundke, K., T. Bogumil, et al. (1996). "Liquid-fluid Contact Angle Measurements on Hydrophilic Cellulosic Materials." Colloids and Surfaces A: Physicochemical and Engineering Aspects **116**(1): 79-91.

Gu, J., J. M. Catchmark, et al. (2013). "Quantification of Cellulose Nanowhiskers Sulfate Esterification Levels." Carbohydrate polymers **92**(2): 1809-1816.

Guo, Y. and P. Wu (2008). "Investigation of the Hydrogen-bond Structure of Cellulose Diacetate by Two-dimensional Infrared Correlation Spectroscopy." Carbohydrate Polymers **74**(3): 509-513.

Gurst, J. E. (1991). "NMR and the Structure of D-glucose." Journal of Chemical Education **68**(12): 1003.

Habibi, Y. (2014). "Key advances in the chemical modification of nanocelluloses." Chemical Society Reviews **43**(5): 1519-1542.

Habibi, Y., L. A. Lucia, et al. (2010). "Cellulose Nanocrystals: Chemistry, Self-Assembly, and Applications." Chemical Reviews **110**(6): 3479-3500.

Hajduk, P. J., R. P. Meadows, et al. (1999). "NMR-based Screening in Drug Discovery." Quarterly Reviews of Biophysics **32**(03): 211-240.

Hall, M., P. Bansal, et al. (2010). "Cellulose Crystallinity – A Key Predictor of the Enzymatic Hydrolysis Rate." FEBS Journal **277**(6): 1571-1582.

Harvey, D. J. (2012). "Analysis of Carbohydrates and Glycoconjugates by Matrix-assisted Laser Desorption/ionization Mass Spectrometry: An Update for 2007–2008." Mass Spectrometry Reviews **31**(2): 183-311.

Haupt, B., T. Neumann, et al. (2005). "Activity of Enzymes Immobilized in Colloidal Spherical Polyelectrolyte Brushes." Biomacromolecules **6**(2): 948-955.

Haupt, B., T. Neumann, et al. (2005). "Activity of Ezymes Immobilized in Colloidal Spherical Polyelectrolyte Brushes." Biomacromolecules **6**(2): 948-955.

Hsu, T., R. Ladisch, et al. (1980). "Alcohol from Cellulose." chemical intermediates **1203**(3): 3.

Huang, J.-L., C.-J. Li, et al. (2013). "Cellulose Nanocrystals Incorporating Fluorescent Methylcoumarin Groups." ACS Sustainable Chemistry & Engineering **1**(9): 1160-1164.

Igarashi, K., A. Koivula, et al. (2009). "High Speed Atomic Force Microscopy Visualizes Processive Movement of Trichoderma reesei Cellobiohydrolase I on Crystalline Cellulose." Journal of biological chemistry **284**(52): 36186-36190.

Igarashi, K., T. Uchihashi, et al. (2011). "Traffic Jams Reduce Hydrolytic Efficiency of Cellulase on Cellulose Surface." Science **333**(6047): 1279-1282.

Jamal, S., D. Nurizzo, et al. (2004). "X-ray Crystal Structure of a Non-crystalline Cellulose-specific Carbohydrate-binding Module: CBM28." Journal of Molecular Biology **339**(2): 253-258.

Jenkins, J. E., S. Sampath, et al. (2013). "Characterizing the Secondary Protein Structure of Black Widow Dragline Silk Using Solid-State NMR and X-ray Diffraction." Biomacromolecules **14**(10): 3472-3483.

Jiang, F., A. R. Esker, et al. (2010). "Acid-Catalyzed and Solvolytic Desulfation of H2SO4-Hydrolyzed Cellulose Nanocrystals." Langmuir **26**(23): 17919-17925.

Jiang, F. and Y.-L. Hsieh (2013). "Chemically and mechanically isolated nanocellulose and their self-assembled structures." Carbohydrate Polymers **95**(1): 32-40.

Jiang, F., J. D. Kittle, et al. (2013). "Effects of Sulfate Groups on the Adsorption and Activity of Cellulases on Cellulose Substrates." Langmuir **29**(10): 3280-3291.

Kalia, S., B. S. Kaith, et al. (2009). "Pretreatments of natural fibers and their application as reinforcing material in polymer composites—A review." Polymer Engineering & Science **49**(7): 1253-1272.

Karaaslan, M., G. Gao, et al. (2013). "Nanocrystalline Cellulose/β-casein Conjugated Nanoparticles Prepared by Click Chemistry." Cellulose **20**(6): 2655-2665.

Kim, D. W. and Y. G. Hong (2000). "Ionic strength effect on adsorption of cellobiohydrolases I and II on microcrystalline cellulose." Biotechnology Letters **22**(16): 1337-1342.

Kimura, F., T. Kimura, et al. (2005). "Magnetic Alignment of the Chiral Nematic Phase of a Cellulose Microfibril Suspension." Langmuir **21**(5): 2034-2037.

Kleman-Leyer, K. M., M. SiiKa-Aho, et al. (1996). "The Cellulases Endoglucanase I and Cellobiohydrolase II of Trichoderma reesei Act Synergistically To Solubilize Native Cotton Cellulose but Not To Decrease Its Molecular Size." Applied and environmental microbiology **62**(8): 2883-2887.

Klemm, D., F. Kramer, et al. (2011). "Nanocelluloses: A New Family of Nature-Based Materials." Angewandte Chemie International Edition **50**(24): 5438-5466.

Kokot, S., B. Czarnik-Matusewicz, et al. (2002). "Two-dimensional Correlation Spectroscopy and Principal Component Analysis Studies of Temperature-dependent IR Spectra of Cotton–cellulose." Biopolymers **67**(6): 456-469.

Kongruang, S., M. Han, et al. (2004). "Quantitative analysis of cellulose-reducing ends." Applied Biochemistry and Biotechnology **113**(1-3): 213-231.

Kongruang, S., M. J. Han, et al. (2004). Quantitative Analysis of Cellulose-reducing Ends. Proceedings of the Twenty-Fifth Symposium on Biotechnology for Fuels and Chemicals Held May 4–7, 2003, in Breckenridge, CO, Springer.

Kono, H. (2013). "Chemical Shift Assignment of the Complicated Monomers Comprising Cellulose Acetate by Two-dimensional NMR Spectroscopy." Carbohydrate Research **375**(0): 136-144.

Kresge, C., M. Leonowicz, et al. (1992). "Ordered Mesoporous Molecular Sieves Synthesized by a Liquid-crystal Template Mechanism." nature **359**(6397): 710-712.

Kurašin, M. and P. Väljamäe (2011). "Processivity of Cellobiohydrolases Is Limited by the Substrate." Journal of Biological Chemistry **286**(1): 169-177.

Lai, C., M. Tu, et al. (2014). "Remarkable Solvent and Extractable Lignin Effects on Enzymatic Digestibility of Organosolv Pretreated Hardwood." Bioresource Technology **156**(0): 92-99.

Larsson, P. T., E.-L. Hult, et al. (1999). "CP/MAS 13C-NMR Spectroscopy Applied to Structure and Interaction Studies on Cellulose I." Solid State Nuclear Magnetic Resonance **15**(1): 31-40.

Lee, S.-Y., D. J. Mohan, et al. (2009). "Nanocellulose Reinforced PVA Composite Films: Effects of Acid Treatment and Filler Loading." Fibers and Polymers **10**(1): 77-82.

Lewin, M. and L. G. Roldan (1971). "The effect of liquid anhydrous ammonia in the structure and morphology of cotton cellulose." Journal of Polymer Science Part C: Polymer Symposia **36**(1): 213-229.

Li, M., M. Tu, et al. (2012). "Distinct Roles of Residual Xylan and Lignin in Limiting Enzymatic Hydrolysis of Organosolv Pretreated Loblolly Pine and Sweetgum." Journal of Agricultural and Food Chemistry **61**(3): 646-654.

Li, W., Y. Wu, et al. (2014). "Reduction of the Water Wettability of Cellulose Film through Controlled Heterogeneous Modification." ACS Applied Materials & Interfaces **6**(8): 5726-5734.

Liimatainen, H., N. Ezekiel, et al. (2013). "High-Strength Nanocellulose–Talc Hybrid Barrier Films." ACS Applied Materials & Interfaces **5**(24): 13412-13418.

Lin, N. and A. Dufresne (2014). "Surface chemistry, morphological analysis and properties of cellulose nanocrystals with gradiented sulfation degrees." Nanoscale **6**(10): 5384-5393.

Liu, A., W. Hu, et al. (2000). "NMR Detection of Side Chain–side Chain Hydrogen Bonding Interactions in 13C/15N-labeled Proteins." Journal of biomolecular NMR **17**(4): 305-310.

Lu, P. and Y.-L. Hsieh (2010). "Preparation and Properties of Cellulose Nanocrystals: Rods, Spheres, and Network." Carbohydrate Polymers **82**(2): 329-336.

Lu, Y., B. Yang, et al. (2002). "Cellulase adsorption and an evaluation of enzyme recycle during hydrolysis of steam-exploded softwood residues." Applied Biochemistry and Biotechnology **98-100**(1-9): 641-654.

Mansfield, S. D., H. Kim, et al. (2012). "Whole Plant Cell Wall Characterization using Solution-state 2D NMR." Nature protocols **7**(9): 1579-1589.

Mansfield, S. D., C. Mooney, et al. (1999). "Substrate and Enzyme Characteristics that Limit Cellulose Hydrolysis." Biotechnology Progress **15**(5): 804-816.

Martin-Pastor, M. and C. A. Bush (1999). "New Strategy for the Conformational Analysis of Carbohydrates Based on NOE and 13C NMR Coupling Constants. Application to the Flexible Polysaccharide of Streptococcus mitis J22†." Biochemistry **38**(25): 8045-8055.

Mayans, O., M. Scott, et al. (1997). "Two Crystal Structures of Pectin Lyase A from< i> Aspergillus</i> Reveal a pH Driven Conformational Change and Striking Divergence in the Substrate-binding Clefts of Pectin and Pectate Lyases." Structure **5**(5): 677-689.

Medie, F. M., G. J. Davies, et al. (2012). "Genome Analyses Highlight the Different Biological Roles of Cellulases." Nature Reviews Microbiology **10**(3): 227-234.

Meng, Q. and J. Hu (2009). "A Review of Shape Memory Polymer Composites and Blends." Composites Part A: Applied Science and Manufacturing **40**(11): 1661-1672.

Moon, R. J., A. Martini, et al. (2011). "Cellulose Nanomaterials Review: Structure, Properties and Nanocomposites." Chemical Society Reviews **40**(7): 3941-3994.

Morais, J. P. S., M. d. F. Rosa, et al. (2013). "Extraction and Characterization of Nanocellulose Structures from Raw Cotton Linter." Carbohydrate Polymers **91**(1): 229-235.

Morán, J., V. Alvarez, et al. (2008). "Extraction of Cellulose and Preparation of Nanocellulose from Sisal Fibers." Cellulose **15**(1): 149-159.

Mosier, N., C. Wyman, et al. (2005). "Features of Promising Technologies for Pretreatment of Lignocellulosic Biomass." Bioresource Technology **96**(6): 673-686.

Nakagame, S. (2010). "The Influence of Lignin on the Enzymatic Hydrolysis of Pretreated Biomass Substrates."

Nakagame, S., R. P. Chandra, et al. (2011). "Enhancing the Enzymatic Hydrolysis of Lignocellulosic Biomass by Increasing the Carboxylic Acid Content of the Associated Lignin." Biotechnology and Bioengineering **108**(3): 538-548.

Nakagame, S., R. P. Chandra, et al. (2011). "The Influence of Lignin on the Enzymatic Hydrolysis of Pretreated Biomass Substrates." Sustainable production of fuels, chemicals, and fibers from forest biomass: 145-167.

O'Dell, B. (2009). "Investigating the Structural Characteristics of Cellobiose-Water Solutions< em> via Liquid-State Neutron Diffraction."

Ohwoavworhua, F. and T. Adelakun (2007). "Some Physical Characteristics of Microcrystalline Cellulose obtained from Raw Cotton of Cochlospermum planchonii." Tropical Journal of Pharmaceutical Research **4**(2): 501-507.

Okahisa, Y., A. Yoshida, et al. (2009). "Optically Transparent Wood–cellulose Nanocomposite as a Base Substrate for Flexible Organic Light-emitting Diode Displays." Composites Science and Technology **69**(11): 1958-1961.

Okita, Y., T. Saito, et al. (2010). "Entire Surface Oxidation of Various Cellulose Microfibrils by TEMPO-mediated Oxidation." Biomacromolecules **11**(6): 1696-1700.

Okiyama, A., M. Motoki, et al. (1993). "Bacterial cellulose IV. Application to processed foods." Food Hydrocolloids **6**(6): 503-511.

Park, S., J. Baker, et al. (2010). "Cellulose Crystallinity Index: Measurement Techniques and Their Impact on Interpreting Cellulase Performance." Biotechnology for Biofuels **3**(1): 10.

Puls, J. and T. Wood (1991). "The Degradation Pattern of Cellulose by Extracellular Cellulases of Aerobic and Anaerobic Microorganisms." Bioresource technology **36**(1): 15-19.

Rahikainen, J. L., J. D. Evans, et al. (2013). "Cellulase–lignin interactions—The role of carbohydrate-binding module and pH in non-productive binding." Enzyme and Microbial Technology **53**(5): 315-321.

Reinikainen, T., O. Teleman, et al. (1995). "Effects of pH and High Ionic Strength on the Adsorption and Activity of Native and Mutated Cellobiohydrolase I from Trichoderma reesei." Proteins: Structure, Function, and Bioinformatics **22**(4): 392-403.

Roman, M. and W. T. Winter (2004). "Effect of Sulfate Groups from Sulfuric Acid Hydrolysis on the Thermal Degradation Behavior of Bacterial Cellulose." Biomacromolecules **5**(5): 1671-1677.

Roslund, M. U., P. Tähtinen, et al. (2008). "Complete Assignments of the 1H and 13C Chemical Shifts and JH,H Coupling Constants in NMR Spectra of D-glucopyranose and All D-glucopyranosyl-d-glucopyranosides." Carbohydrate Research **343**(1): 101-112.

Rusli, R., K. Shanmuganathan, et al. (2011). "Stress Transfer in Cellulose Nanowhisker Composites—Influence of Whisker Aspect Ratio and Surface Charge." Biomacromolecules **12**(4): 1363-1369.

Saric-Coric, M., K. H. Khayat, et al. (2003). "Performance characteristics of cement grouts made with various combinations of high-range water reducer and cellulose-based viscosity modifier." Cement and Concrete Research **33**(12): 1999-2008.

Segal, L., J. Creely, et al. (1959). "An Empirical Method for Estimating the Degree of Crystallinity of Native Cellulose using the X-ray Diffractometer." Textile Research Journal **29**(10): 786-794.

Shikiya, Y., S. Tomita, et al. (2013). "Arginine Inhibits Adsorption of Proteins on Polystyrene Surface." PLoS ONE **8**(8): e70762.

Sinitsyn, A. P., A. V. Gusakov, et al. (1991). "Effect of Structural and Physico-chemical Features of Cellulosic Substrates on the Efficiency of Enzymatic Hydrolysis." Applied Biochemistry and Biotechnology **30**(1): 43-59.

Svagan, A. J., M. A. Samir, et al. (2008). "Biomimetic Foams of High Mechanical Performance Based on Nanostructured Cell Walls Reinforced by Native Cellulose Nanofibrils." Advanced Materials **20**(7): 1263-1269.

Tantra, R., P. Schulze, et al. (2010). "Effect of Nanoparticle Concentration on Zeta-potential Measurement Results and Reproducibility." Particuology **8**(3): 279-285.

Tu, M., X. Pan, et al. (2009). "Adsorption of Cellulase on Cellulolytic Enzyme Lignin from Lodgepole Pine." Journal of Agricultural and Food Chemistry **57**(17): 7771-7778.

Wang, J., S. Niu, et al. (2013). "Regioselective synthesis of sulfated guar gum: Comparative studies of structure and antioxidant activities." International Journal of Biological Macromolecules **62**(0): 734-740.

Wang, J. and P. Somasundaran (2005). "Adsorption and Conformation of Carboxymethyl Cellulose at Solid–liquid Interfaces Using Spectroscopic, AFM and Allied techniques." Journal of Colloid and Interface Science **291**(1): 75-83.

Wang, Y., W. M. Kalka-Moll, et al. (2000). "Structural Basis of the Abscess-modulating Polysaccharide A2 from Bacteroides Fragilis." Proceedings of the National Academy of Sciences **97**(25): 13478-13483.

Wu, C.-N., T. Saito, et al. (2012). "Ultrastrong and High Gas-Barrier Nanocellulose/Clay-Layered Composites." Biomacromolecules **13**(6): 1927-1932.

Yamada, S., K. Yoshida, et al. (1992). "One- and Two-Dimensional 1H-NMR Characterization of Two Series of Sulfated Disaccharides Prepared from Chondroitin Sulfate and Heparan Sulfate/Heparin by Bacterial Eliminase Digestion." Journal of Biochemistry **112**(4): 440-447.

Yamakawa, N., M. Jiang, et al. (2009). "Identifying the Local Structures Formed during Lithiation of the Conversion Material, Iron Fluoride, in a Li ion Battery: A Solid-state NMR, X-ray diffraction, and Pair Distribution Function Analysis Study." Journal of the American Chemical Society **131**(30): 10525-10536.

Yang, B., Z. Dai, et al. (2011). "Enzymatic Hydrolysis of Cellulosic Biomass." Biofuels **2**(4): 421-450.

Yang, X. B., X. D. Gao, et al. (2005). "Sulfation of a polysaccharide produced by a marine filamentous fungus Phoma herbarum YS4108 alters its antioxidant properties in vitro." Biochimica et Biophysica Acta (BBA) - General Subjects **1725**(1): 120-127.

Yu, Z., H. Jameel, et al. (2013). "Quantification of Bound and Free Enzymes During Enzymatic Hydrolysis and Their Reactivities on Cellulose and Lignocellulose." Bioresource Technology **147**(0): 369-377.

Zhang, D., C. Wang, et al. (2013). "Three Sulphated Polysaccharides Isolated from the Mucilage of Mud Snail, Bullacta exarata philippi: Characterization and Antitumour Activity." Food Chemistry **138**(1): 306-314.

Zhang, K., E. Brendler, et al. (2011). "Synthesis and spectroscopic analysis of cellulose sulfates with regulable total degrees of substitution and sulfation patterns via 13C NMR and FT Raman spectroscopy." Polymer **52**(1): 26-32.

Zhou, Y., C. Fuentes-Hernandez, et al. (2013). "Recyclable Organic Solar Cells on Cellulose Nanocrystal Substrates." Scientific reports 3.